

Aspects of the dynamic behaviour of the human knee joint

Citation for published version (APA):

Dortmans, L. J. M. G. (1988). *Aspects of the dynamic behaviour of the human knee joint*. [Phd Thesis 1 (Research TU/e / Graduation TU/e), Mechanical Engineering]. Technische Universiteit Eindhoven.
<https://doi.org/10.6100/IR297749>

DOI:

[10.6100/IR297749](https://doi.org/10.6100/IR297749)

Document status and date:

Published: 01/01/1988

Document Version:

Publisher's PDF, also known as Version of Record (includes final page, issue and volume numbers)

Please check the document version of this publication:

- A submitted manuscript is the version of the article upon submission and before peer-review. There can be important differences between the submitted version and the official published version of record. People interested in the research are advised to contact the author for the final version of the publication, or visit the DOI to the publisher's website.
- The final author version and the galley proof are versions of the publication after peer review.
- The final published version features the final layout of the paper including the volume, issue and page numbers.

[Link to publication](#)

General rights

Copyright and moral rights for the publications made accessible in the public portal are retained by the authors and/or other copyright owners and it is a condition of accessing publications that users recognise and abide by the legal requirements associated with these rights.

- Users may download and print one copy of any publication from the public portal for the purpose of private study or research.
- You may not further distribute the material or use it for any profit-making activity or commercial gain
- You may freely distribute the URL identifying the publication in the public portal.

If the publication is distributed under the terms of Article 25fa of the Dutch Copyright Act, indicated by the "Taverne" license above, please follow below link for the End User Agreement:

www.tue.nl/taverne

Take down policy

If you believe that this document breaches copyright please contact us at:

openaccess@tue.nl

providing details and we will investigate your claim.

**ASPECTS OF THE DYNAMIC BEHAVIOUR
OF THE HUMAN KNEE JOINT**

Ardi Dortmans

ASPECTS OF THE DYNAMIC BEHAVIOUR OF THE HUMAN KNEE JOINT

PROEFSCHRIFT

ter verkrijging van de graad van doctor
aan de Technische Universiteit Eindhoven,
op gezag van de Rector Magnificus, Prof. Dr. F.N. Hooge,
voor een Commissie aangewezen door het College van Dekanen
in het openbaar te verdedigen op dinsdag 12 januari 1988
te 14.00 uur

door

Leonardus Johannes Maria Genoveva Dortmans

geboren te Eindhoven

Dit proefschrift is goedgekeurd door de promotoren:

Prof. dr. ir. J.D. Janssen

Prof. dr. A. Huson

Co-promotor:

Dr. ir. A.A.H.J. Sauren

**Het onderzoek, beschreven in dit proefschrift, werd gesteund door de
Stichting voor de Technische Wetenschappen (STW).
The research, reported in this thesis, was supported by the Netherlands
Technology Foundation (STW).**

CONTENTS

Abstract

List of symbols

1 Introduction

Preliminaries

1.1 Historical and contemporary perspective

1.2 Scope and purpose

2 Mechanical properties and functions of the human knee joint and its component structures: a literature review

2.1 Global description of the anatomy of the human knee joint

2.2 Mechanical properties and functions of basic anatomical structures

2.2.1 The bony parts

2.2.2 The menisci

2.2.3 The ligamentous structures

2.2.4 The articular cartilage and synovial fluid

2.3 Mechanical characteristics of the human knee joint

2.3.1 Pressure distributions between articulating surfaces

2.3.2 Deformations of ligaments

2.3.3 In vivo experimental results

2.3.4 Post-mortem experimental results

2.4 Mechanical modelling of the human knee joint

2.5 Summary

3 Experimental strategy

3.1 Methodology

3.2 Experimental set-up

3.2.1 Practical considerations

3.2.2 Basic experimental set-up

3.3 A non-linear black box model of the knee joint

3.3.1 A descriptive model for the dynamic behaviour of the tibial component

3.3.2 Practical considerations

3.3.3 A descriptive model for the load transmission through the joint

3.4 Measurement methods

3.4.1 Measurement of the static load on the muscle tendons

3.4.2 Measurement of accelerations on the tibia

3.4.3 Measurement of the transmitted loads

3.4.4 Measurement of the static equilibrium position

- 3.5 A data-acquisition system
 - 3.5.1 The personal computer
 - 3.5.2 The laboratory interface
 - 3.5.3 The measurement control unit
 - 3.5.4 The software package
- 3.6 Summary
- 4 Experiments I: Analysis in the frequency domain
 - 4.1 Description of the experiments
 - 4.2 Recapitulation and interpretation of the transfer functions
 - 4.3 Typical results for random excitation
 - 4.4 Inaccuracies and disturbing factors
 - 4.4.1 Effects of autolysis
 - 4.4.2 Influence of the experimental set-up
 - 4.4.3 Measurement and postprocessing errors
 - 4.5 The static behaviour of the joint: influence of the static load
 - 4.6 The dynamic behaviour of the joint: influence of the dynamic load
 - 4.7 Evaluation of the results obtained for random and sinusoidal excitation
 - 4.8 Summary
- 5 Experiments II: Analysis in the time-domain
 - 5.1 Selection of an excitation technique
 - 5.2 Description of the experiments
 - 5.3 Determination of the best-fitting linear system for step excitation
 - 5.3.1 Theoretical concept for a curve-fit procedure
 - 5.3.2 Application of the curve-fit procedure
 - 5.4 Pre- and post-operative results for step excitation
 - 5.4.1 Resonance frequencies and damping
 - 5.4.2 Vibration modes
 - 5.4.3 Reproducibility of the results
 - 5.5 Discussion of the results
 - 5.6 Summary
- 6 Conclusions and recommendations
 - 6.1 Conclusions
 - 6.2 Recommendations

Appendices A-E

References

Samenvatting

Curriculum vitae

ABSTRACT

The present thesis deals with aspects of the dynamic behaviour of the human knee joint. Emphasis was laid on an experimental strategy to try and find the important characteristics and parameters describing the behaviour of the joint under dynamic loading in post-mortem experiments. A literature review revealed that, although both the (quasi-)static and dynamic behaviour of the joint have been focused on in a number of experimental and theoretical studies, a lack of knowledge exists on 3 important subjects: a proper understanding of the dynamic behaviour of the joint is not provided, the constitutive behaviour of the soft tissues (ligamentous structures, menisci, articular cartilage) is only known to a limited extent and (estimates for) the in vivo loads acting on the joint as a whole or on the individual joint elements are only poorly known. Because of the limited possibilities to analyse the behaviour of the joint in in vivo and in post-mortem experiments, a mathematical model of the human knee joint is indispensable and should be formulated starting from basic knowledge in the behaviour of the joint. For this purpose an experimental strategy is presented intended to result in guidelines (obtained from experiments) for development of such a model. In view of the expected non-linearity of the behaviour of the joint, an approach is proposed to eliminate geometrical non-linearities by considering only small deflections with respect to a static equilibrium position. This linearization procedure also was expected to reduce physical non-linearities. The LLT results in a description of the joint by means of a linear system with system parameters dependent on the static equilibrium position of the joint, the magnitude of the loads exerted on selected muscle tendons to create this equilibrium position and the degree to which damage is brought about to individual joint elements. Important conclusions could be drawn from experiments with random excitation: creation of a stable, static equilibrium position of the joint by means of forces on three muscle tendons is possible, a description of the dynamic behaviour of the joint by means of transfer functions enables to quantify the influence of the static equilibrium position, the magnitude of the loads on the muscle tendons and damaging of joint elements, but the linearization procedure actually fails due to the essential non-linear behaviour of the joint. This non-linearity, however, can be taken into account by introducing a dependence of the system parameters for the best-fitting linear system on the magnitude of the applied load. This strategy has been worked out for step excitation. The effect of damaging the menisci and the anterior cruciate ligament could well be determined. Interpretation of the results is difficult, however, and makes a numerical model of the joint indispensable.

List of symbols

Scalars, vectors, tensors and matrices

- a : scalar
 \bar{a} : complex conjugate
- \underline{a} : column matrix
 \vec{a} : vector
 $\vec{\underline{a}}$: vector column matrix
 \underline{a}^T : transpose of a column matrix
- A : second order tensor
 \underline{A} : scalar matrix
 $\underline{\underline{A}}$: tensor matrix
 $\vec{\underline{A}}$: vector matrix
 \underline{A}^c : conjugate of a tensor
 \underline{A}^{-1} : inverse of a tensor
 \underline{A}^d : diagonal matrix
 \underline{A}^T : transpose of a matrix
 \underline{A}^{-1} : inverse of a matrix
- $\vec{a} \cdot \vec{b}$: dot product of two vectors
 $\underline{A} \cdot \vec{b}$: dot product of a tensor and a vector
 $\underline{A} \cdot \underline{B}$: dot product of two tensors
 $\vec{a} * \vec{b}$: vector product
 $\vec{a} \vec{b}$: dyadic product of two vectors

Special symbols

- I : unit tensor
 \underline{I} : unit matrix
 0 : null tensor
 $\underline{0}$: null matrix
 $\underline{\underline{0}}$: null column matrix

Chapter 1 Introduction

Preliminaries

"Biomechanics is very difficult mechanics". This maxim also refers to the topic of this thesis, as from a mechanical point of view the knee joint is a complicated structure. Like in other joints in the human musculoskeletal system, the complex geometry of the deformable articulating surfaces and the non-linear time-dependent material properties of the constituting anatomical elements result in a mechanical behaviour with physical non-linearities, apart from the geometrical non-linearities due to large relative movements of the articulating bones. Although a number of experimental and theoretical studies have been devoted to the behaviour of the joint under various loading conditions, a proper insight into its mechanical behaviour is not available, nor is there clarity as to the role various joint elements play herein. This especially applies to the behaviour of the joint under dynamic loads, which has been the subject of investigation only for the last two decades in a limited number of studies. From a medical point of view, the need to come to a more accurate insight into the mechanical behaviour of the joint is obvious. A better insight into the pathomechanics of injured or diseased joints will become possible only if knowledge is available on both the anatomy of the joint and the mechanical behaviour of the joint under various loads. Also repair or replacement of joint elements requires knowledge of the function of these elements in order to judge the reliability of surgical procedures and to avoid unforeseen post-operative cumulative damage. The contents of this thesis may be seen as an attempt to elucidate part of the dynamic behaviour of the joint.

Biomechanical engineering has a strong interaction with other technical disciplines which have a more specific background and can provide necessary scientific research tools. For example, developments in the field of dynamics and structural analysis find applications in analyses of the mechanical behaviour of the human body. Besides, these more fundamental disciplines can obtain a stimulating feedback from requirements imposed by biomechanical engineering. Following these remarks it is not surprising that the present study must be considered as being part of a larger framework. This framework is given by a general view on fundamental and biomechanical engineering in the Division of Engineering Fundamentals (WFW) of the Faculty of Mechanical Engineering at the Eindhoven University of Technology (EUT).

It is obvious that this framework provides facilities and boundary conditions for a study on the mechanical behaviour of the human knee joint, which are relevant in judging the scope and purpose of this thesis, as will be depicted in the following sections.

1.1 Historical and contemporary perspective

The mechanical behaviour of the human knee joint has been the subject of investigation in various studies carried out at EUT, since 1976, partly in collaboration with the University of Leiden (RUL), the University of Limburg (RL) and the University of Nijmegen. Wismans (1980) developed a 3-D statically indeterminate knee joint model which allows for numerical simulation of the behaviour of the joint under quasi-static loads. It incorporates a description of the rigid and perfectly smooth (no friction) contact areas of the femoral and tibial articulating surfaces and a representation of ligamentous structures (including parts of the posterior capsule) by means of non-linear elastic springs. The results obtained with this model, probably one of the most advanced models for the human knee joint described in literature, agree fairly well with experimental data found in literature. Further refinements of the model were incorporated in a more general model developed by Dortmans (1983), although these extensions were merely meant to increase the flexibility of the model. For an experimental validation of the numerical model, Hamer (RL) (1982) developed a 3-D loading apparatus, for the measurement of the static kinematics as well as the loads acting on a knee joint specimen in vitro. The practical validation and possible further refinements of Wismans' model were subsequently agreed to be worked out at the University of Nijmegen, using the loading apparatus developed by Hamer.

One of the essential limitations of Wismans' model is the assumption that the contact areas of the tibia and femur can be considered to be rigid. When dynamic loads are acting on the joint, deformations of the cartilage layers, covering the tibia and the femur, and the menisci may play an important role in the force transmission through the joint. If the contact areas are assumed rigid (as in Wismans' model) the location of the contact points is known for a given external load on the articulating bodies. This is not possible when deformations of the contact zones are taken into account. In that case a coupling exists between the location of the contact zones and the kinematics of the bodies which coupling depends on the loads exerted on the bodies. Another important phenomenon not considered in Wismans' model is the damping effect of the joint due to velocity- or time-dependent material properties. In view of these two important limitations it was felt that the next stage in continued research should be devoted to an analysis of the dynamic behaviour of the human knee joint. From a pilot study it was concluded that such an investigation should start with an experimental approach. The reason for this is that in literature only scattered data was found on the dynamic behaviour of the joint as a whole, as well as on the dynamic properties of individual joint elements such as menisci and ligamentous structures. This resulted in the conclusion that development of a structural numerical model can not be started before some essential characteristics of the knee joint under dynamic loading are obtained

from experiments. It was also felt that only after identification of the mechanical role several joint elements play in the dynamic force transmission through the joint, an appropriate selection can be made for the elements to be included in such a model. The need for a structural numerical model is obvious. Such a model allows for manipulation of model parameters which can be used to study the importance of various joint structures, thus reducing the number of experiments to be carried out (which are often laborious and mostly have a limited scope). On the other hand a numerical model may provide guidelines for further experiments to validate the model.

The research done on the human knee joint is interacting with (and is influenced by) other research projects carried out in WFW:

- * research done on the dynamics of multibody systems with non-linear connections (Sol 1983) can provide a theoretical framework for numerical modelling of the knee joint, as the knee joint is a non-linear connection (although far more complicated than those encountered in mechanical structures).
- * random vibrations is an important subject when considering the mechanical behaviour of the joint as any experiment in this field is likely to contain stochastic elements, which must be dealt with properly. Random vibrations also includes a theoretical framework for analysis of linear or linearized systems by means of transfer function- and modal analysis, which has become an important tool to quantify the dynamic behaviour of mechanical systems (van Heck 1984).
- * long term research done on aortic valve prostheses (van Steenhoven (1979), Sauren (1981), van Renterghem (RL) (1983), Rousseau (1985)) has resulted in both experimental and theoretical knowledge with respect to the mechanical behaviour of soft tissues. Also the work of Oomens et al. (1987) on the mechanical behaviour of the skin is important in this context. The behaviour of soft tissues is focused on extensively in research done on the elbow joint. Roddeman (1988) worked on numerical tools (FEM) to be able to deal with inhomogeneous, fibre-reinforced tissues wrinkling under certain loads. Simultaneously Peters (RL) (1987) developed tools for measurement of stress and strain fields in these tissues. It is obvious that insights gained in these studies are valuable when developing a structural model of the knee joint.

The relationship between research done on the knee joint and other (bio)mechanical structures evidently determines the purpose and scope of the present study to some extent. With the perspective given in this section as a background, the scope and purpose of the present study are outlined in section 1.2.

1.2 Scope and purpose

As mentioned in section 1.1 the purpose of the present study can briefly be formulated as to obtain experimental data on the dynamic behaviour of the human knee joint which can be used for formulation and validation of a structural numerical model. The terms "knee joint" and "dynamic behaviour" in this formulation will be elaborated in the sequel to indicate more clearly the purpose of this study, simultaneously marking the scope of the present investigation.

The knee joint is defined as the assembly of biological structures linking the lower and upper leg, which includes parts of the tibia and femur, the patella, the menisci as well as the surrounding capsular and non-capsular ligamentous structures. To study the mechanical behaviour of this system use must be made of post-mortem experiments on joint specimens, as this system can not be isolated in vivo, apart from the lack of possibilities to measure loads acting on the joint in in vivo situations. The use of post-mortem experiments also eliminates the possibility to include natural muscular activity in this investigation. This is a limitation which can not be avoided however. On the other hand it is felt that insight in the dynamic behaviour of the knee joint is essential, to be able to indicate which phenomena should be focused on when analysing the knee joint in in vivo experiments (with muscular activity). Muscle tendons attaching to the joint must be taken into consideration, as they are interwoven with the complex structure of soft tissues connecting the tibia and the femur.

The dynamic behaviour of the joint must in general be expected to be subject to both geometrical and physical non-linearities. Geometrical non-linearities, due to large relative movements between the articulating bones, are relatively easily taken into account in both experiments and theoretical models. Consequently, emphasis can be laid on the physical non-linearities described by important parameters as stiffness and damping characteristics for various loading configurations of the joint. The loads applied will have a non-static component, but at this stage this can not be specified in terms of a frequency range of interest as inertial effects significantly may contribute to a upper relevant frequency which, consequently, must be determined experimentally. On the other hand, available literature data may provide information on the frequency range of interest for in vivo situations, which must be taken into account in the experimental strategy to be developed. Because of the expected non-linear behaviour of the joint, due to load dependent stiffness- and damping characteristics e.g., not only the frequency range of interest must be considered. In fact the entire load and deformation history must be taken into account in this case, including peak loads, shape of the applied loads, initial conditions for kinematical parameters etc.

In summary the present investigation focuses on the time-dependent behaviour of human knee joint, to gain insight into the physical nonlinearities determining the load transmission through the joint. The results obtained may provide a starting point for development of a structural numerical model of the knee joint.

Chapter 2 Mechanical properties and functions of the human knee joint and its component structures: a literature review.

The significance of some of the anatomical structures in the human knee joint for the transmission of both static and dynamic loads has been the subject of a number of experimental and theoretical investigations described in literature.

In this chapter a brief overview is given of commonly accepted ideas about the mechanical characteristics of the human knee joint. First the basic anatomy of the human knee joint will be discussed. In section 2.2 the mechanical properties and functions of some of the basic anatomical structures are summarized. In section 2.3 an overview is presented of the prime mechanical characteristics of the human knee joint as a whole as established from in vivo and in post-mortem experiments. Finally, in section 2.4, certain types of mathematical models used for the description of the mechanical behaviour of the joint are discussed.

2.1 Global description of the anatomy of the human knee joint

The human knee joint forms a spatial link between the femur and the tibia (Fig. 2.1.1). It is the largest synovial joint in the human body, allowing for large relative movements of the articulating femur and tibia. In appendix A a glossary is given of terms generally used to denote the principal motions of the tibia relative to the femur and which will be used throughout the remaining chapters. The anatomical structures the joint consists of, can be divided into two prime groups with respect to their mechanical properties:

* bony parts

- the proximal part of the tibia, including the proximal part of the fibula

- the distal part of the femur

- the patella

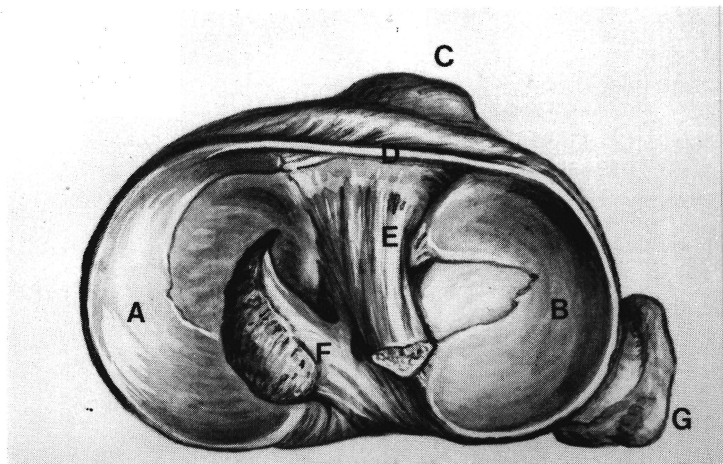
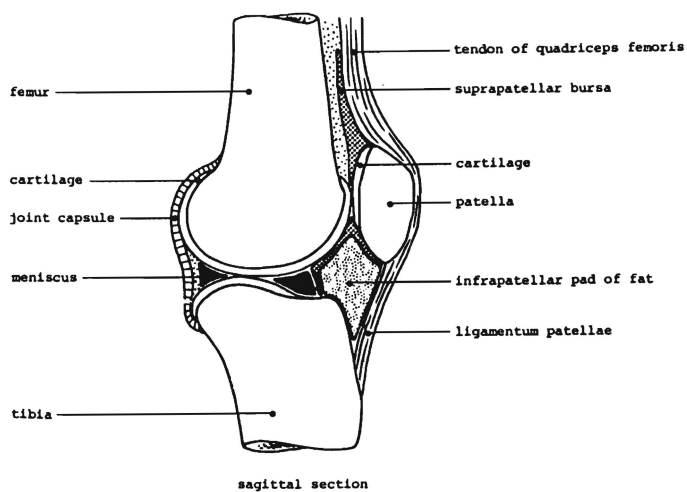
* soft tissues

- fasciae, capsule and ligamentous structures

- menisci

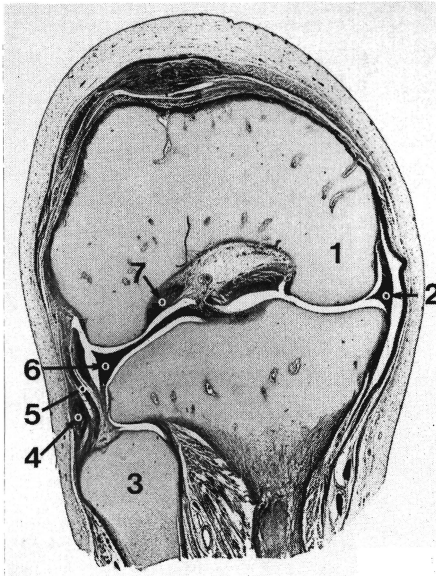
- articular cartilage

- muscle tendons



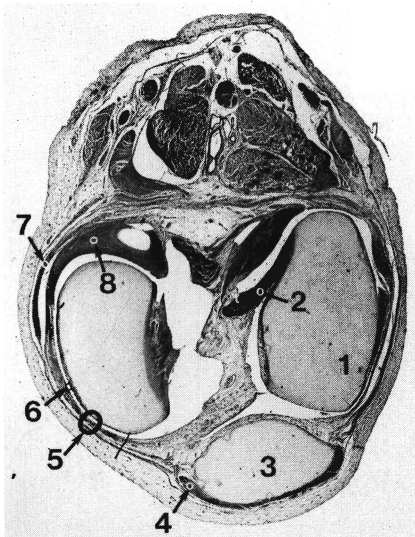
Top view of the tibia of a right knee joint
 A = medial meniscus, D = transverse ligament,
 B = lateral meniscus, E = anterior cruciate ligament,
 C = tibial tuberosity, F = posterior cruciate ligament,
 G = fibula.

Fig. 2.1.1 The human knee joint.



- 1 = medial femoral condyle
- 2 = outer part of medial meniscus attached to the inner layer of the capsule
- 3 = fibula
- 4 = tendon of biceps femoris muscle
- 5 = lateral collateral ligament
- 6 = lateral meniscus (posterior part)
- 7 = femoral insertion of anterior cruciate ligament

Fig. 2.1.2a Cross-section of the knee joint (frontal plane of the tibia with the femur in 90° flexion)



- 1 = lateral femoral condyle
- 2 = femoral insertion of anterior cruciate ligament
- 3 = patella
- 4 = quadriceps tendon
- 5 = multi-layered articular capsule
- 6 = inner layer of fibrous articular capsule
- 7 = medial collateral ligament
- 8 = posterior horn of medial meniscus

Fig. 2.1.2b Cross-section of the knee joint (medio-lateral plane of the femur)

Moreover a small volume of synovial fluid is present in the joint. The bony parts, as compared to the soft tissues, are rigid elements of which the tibia and the femur, and the patella and the femur are articulating in the tibio-femoral and the patello-femoral joint, respectively.

In the joint cavity between the incongruent articulating surfaces of femur and tibia the menisci form a set of two intra-articular (incomplete) rings. The articulating surfaces of the bony parts are covered with a thin layer of articular cartilage which is a soft, porous material. In combination with the articular cartilage, the synovial fluid ensures proper lubrication of the joint (see section 2.2.4).

The bony parts and the menisci are interconnected by a complex structure of soft tissues (Fig. 2.1.2). In anatomical textbooks this structure is divided into intra-capsular ligaments, the multiple layered joint capsule, the extra-capsular ligaments and muscle tendons attaching to the bony parts of the joint.

The intra-capsular ligaments are the anterior cruciate ligament and the posterior cruciate ligament and ligaments connecting the capsule, the menisci, the tibia and the femur.

The joint capsule encloses the joint and consists of 2 layers, the membrana synovialis at the inside and the membrana fibrosa at the outside. The membrana fibrosa is a fibre-reinforced structure, which in itself is a multiple layer with varying thickness, strengthened posteriorly by, e.g., the oblique and arcuate popliteal ligaments. The prime extra-capsular ligaments are the lateral collateral ligament and the patellar ligament, whereas the medial collateral ligament can be seen to be part of the joint capsule. The various muscle tendons attaching to the bony parts of the joint are schematically shown in Fig. 2.1.3.

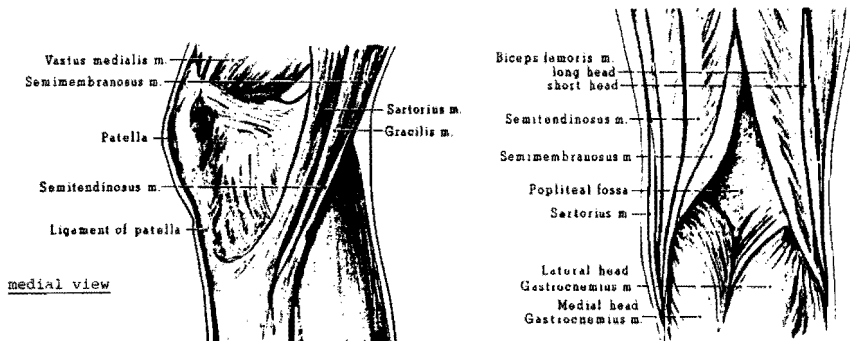


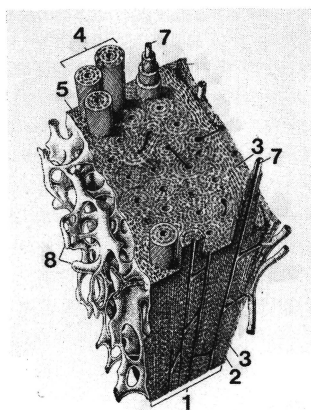
Fig. 2.1.3 Schematic representation of the muscles attaching to the human knee joint.

2.2 Mechanical properties and functions of basic anatomical structures.

In this section the mechanical properties and possible functions of some of the basic anatomical structures mentioned in section 2.1 will be discussed. The bony parts in the joint, the menisci, the ligamentous structures, the articular cartilage and the synovial fluid are successively dealt with.

2.2.1 The bony parts.

The bone material of the bony parts consists of layers of an inorganic phase, mainly calcium and phosphate, and an organic phase, mainly collagen (a fibrillar protein). It occurs basically in two forms, a more massively built and relatively rigid form, the compact bone and a more lightly built and weaker form, the trabecular or spongy bone, which mostly has an outer shell (the cortical bone) of compact bone. Most of the compact bone consists of osteons or Haversian systems (Fig. 2.2.1) which are tubular structures, enclosing a capillary (Haversian canal) used for nutrition. Each osteon is made up of several bone layers whose collagen fibres run parallel and spiral about the axis of the osteon.



- 1 = compact bone with
- 3 = lamellar outer layer
- 4,5 = inner osteonal bone
- 2 = periosteum
- 7 = Haversian canal
- 8 = trabecular bone

Fig. 2.2.1 The structure of compact and trabecular bone (Krstic 1978).

As the bony parts in the human skeleton are of eminent importance for weight bearing and resisting forces due to muscular activity, the behaviour of bone under various mechanical loading and physiological conditions has been the subject of a number of experimental investigations. From these investigations it follows that compact bone and trabecular bone largely differ in apparent stiffness. The apparent stiffness can be seen to depend also slightly upon the strain rate applied which might be due to time-dependent material properties

(Lakes et al. 1979), although Pugh et al.(1973) state that bone can be regarded as purely elastic under physiological loads. Also the material properties of bone tend to be anisotropic which is not surprising in view of its tubular structure (Reilly and Burstein 1975).

When considering the mechanical function of the bony parts in the joint, it will be clear that the tibia and the femur act as load bearing elements, transmitting loads via their incongruent articulating surfaces. Finite Element calculations have shown that the surface load is mainly transmitted by the trabecular bone beneath the cortical bone at the loaded surface to the shaft of the bone (Burstein et al. 1970, Hayes et al. 1978). Besides the trabecular bone may act as an energy absorber as at impulsive loads micro-fractures occur (Ducheyne et al. 1977, Simon et al. 1972).

The patella generally is considered to have the following functions: protection of anatomical structures in the joint cavity, transmission of loads exerted by the musculus quadriceps femoris to the tibia and amplification of the extending moment generated by these loads (Dahhan et al. 1981, van Eijden 1985, van Kampen 1987).

2.2.2 The menisci

Between the tibia and the femur the menisci form a set of two intra-articular discs, partly filling the space between the incongruent contact surfaces of the tibia and femur (Fig. 2.1.1). The medial meniscus tends to be a semi-circular ring with both ends attached to the intercondylar area. At the medial side of the joint the medial meniscus is attached to the deep layer of the medial collateral ligament whereas the posterior part is connected to the capsule. Furthermore, the ligamentum transversum genus connects the medial and the lateral meniscus anteriorly. The lateral meniscus generally has a stronger curvature and resembles more a complete ring than the medial meniscus. Its ends also attach to the intercondylar area.

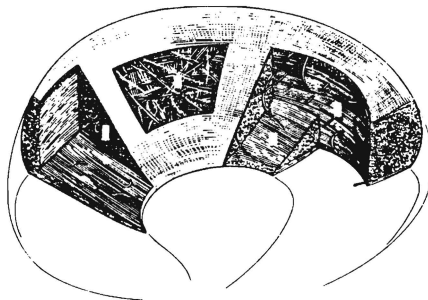


Fig. 2.2.2 The structure of the menisci (Bullough et al. 1970).

The menisci basically consist of fibrous tissue, with collagen fibres embedded in a ground substance of glycosaminoglycans. The collagen fibres are mainly oriented in the circumferential direction, thus causing an anisotropic mechanical behaviour of the menisci (Fig. 2.2.2) (Bullough et al. 1970). The presence of the collagen fibres also appears in the non-linear stress-strain relationship found for menisci specimens under uni-axial tension as shown in Fig. 2.2.3.

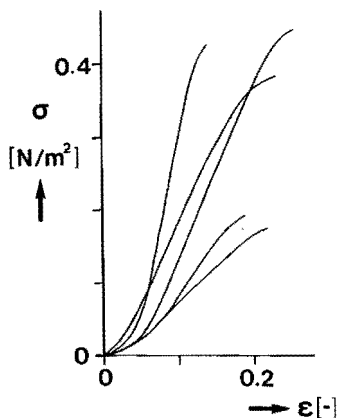


Fig. 2.2.3 Stress-strain characteristics for menisci specimens under uni-axial tension (Uezaki et al. 1979).

A number of mechanical functions are attributed to the menisci. Three of the most important possible functions are:

- * a load bearing function, resulting in a reduction of the stresses in the area of direct bone to bone contact between the tibia and the femur. This function is derived from the observation that the menisci may increase the tibio-femoral contact surface (Krause et al. 1976, Jaspers 1982, Sauren et al. 1984, Walker and Hajek 1972), resulting in a distribution of the loads transmitted.
- * a stabilizing function. A number of post-mortem experimental studies (Hsieh and Walker 1976, Markolf et al. 1976, Wang and Walker 1974) showed the knee joint to have a much less constrained kinematic behaviour after meniscectomy resulting in larger possible relative motions between the femur and the tibia. This also may cause an increased loading of the ligamentous structures.
- * a function in the lubrication of the joint (see section 2.2.4)

2.2.3 The ligamentous structures

In biomechanical literature much attention is paid to the mechanical function of the ligamentous structures attaching to the bony parts in the joint, but only few studies are reported dealing with their mechanical properties. The ligamentous structures generally consist of collagen and elastin fibres embedded in a glycosaminoglycans rich ground substance. The orientation of the fibres varies from one part in the ligamentous structures to another but it is assumed that they are mainly oriented in the direction of the transmitted load. The ligamentous structures show a typical non-linear stress-strain relationship under uni-axial loading (Kennedy et al. 1976, Trent et al. 1976). Experiments on (animal) ligaments have also shown their strain-rate dependent behaviour which could be due to visco-elastic material properties (Woo 1982).

When considering the mechanical function of the ligamentous structures, it must be noticed that, apart from the cruciate ligaments, they can be seen as either separate structures or ligaments (from a classical anatomical point of view) or as a set of layers with local thickenings that could be interpreted as ligaments in a classical sense. In biomechanical literature much attention is paid to the function of ligaments in the classical sense, resulting in partly opposite conclusions (Butler et al. 1980, Hsieh and Walker 1976, Markolf et al. 1976, Markolf et al. 1981, Piziali et al. 1977, Piziali et al. 1980, Seering et al. 1980, Shoemaker and Markolf 1985). This may be caused by rather imperfect experimental techniques, e.g. techniques that do not allow for a precise definition of applied loads and resulting displacements. Also different opinions about the anatomical description of the ligamentous structure analysed may contribute to these opposite conclusions.

Generally accepted primary mechanical functions of some ligamentous structures can be summarized as follows. The anterior and posterior cruciate are important to resist anterior and posterior displacements of the tibia relative to the femur, respectively. The medial and lateral collateral ligament on the other hand delimit exo-endorotation and ad-abduction.

In most studies the function of a knee ligament is derived from experiments where a comparison is made between the behaviour of the joint (under a given external load and relative position and orientation of the femur and tibia) before and after removal or damaging of the ligament studied. Due to the complexity of the joint, this comparison is not necessarily leading to a direct insight into the function of the structure under investigation. After removal or damaging of a particular structure other structures may partly take over its function, depending on the applied load and the relative position and orientation of femur and tibia. This has led to the introduction of secondary and tertiary functions of ligaments, indicating that the function of a ligament is controlled directly by other ligamentous structures. Moreover, the mechanical behaviour of the joint is

strongly influenced by the magnitude of the applied loads, the geometry of the articulating femoral and tibial surfaces and the presence of the menisci. These factors may also influence the results of experiments and thus lead to different opinions about the function of the ligamentous structures considered.

Apart from a force transmitting function also a neurosensory function is proposed for the ligamentous structures (Brand 1986, Schultz et al. 1984), because of the presence of mechanoreceptors. These may provide input for the central nervous system and thereby the ligamentous structures may act as sensors for muscle control.

2.2.4 The articular cartilage and synovial fluid

The human knee joint shows low friction and minimal wear. Two components important for these features are the synovial fluid and articular cartilage.

The human knee joint contains a small volume of synovial fluid (0.2 ml (Wright 1981)), which is dialysed from blood plasma and contains a hyaluronic acid-protein complex. These large molecules cause the synovial fluid to have a viscosity that decreases with increasing shear rate (Radin and Paul 1971).

Articular cartilage is the thin top-layer of the condyles of the femur, the tibia and the patella. For the femoral and tibial condyles the thickness of this layer varies between 2 and 3 mm (Walker and Hajek 1972) and is up to 5 mm for the patella (Dahhan et al. 1981). Cartilage can be seen as a two-phase material with a solid matrix (composed of proteoglycan macromolecules, collagen fibres and bound water) and interstitial water (Fig. 2.2.4) (Mow 1984).

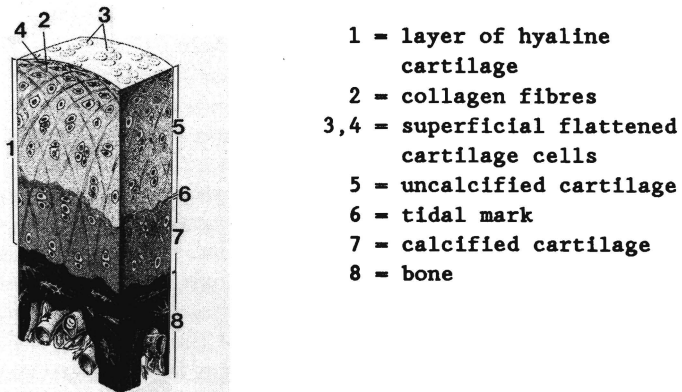


Fig. 2.2.4 The structure of articular cartilage in the knee joint (Krstic 1978).

Upon compressive loading of the cartilage the interstitial water is squeezed out of the permeable matrix causing a decrease in volume. The volume of the cartilage can attain its normal value after removal of the compressive load if enough water is available for resorption. The mechanical behaviour of articular cartilage is currently best described by means of a biphasic poroviscoelastic model (Mak 1986) where the solid matrix is modelled as a viscoelastic continuum. Mixture theories are applied to describe the flow of interstitial fluid in the matrix. Friction between the two phases is included by means of a body force term in the governing equations which depends on the relative velocity of the two phases and the permeability of the matrix. From these models it can be concluded that both the viscoelasticity of the matrix and the interstitial fluid flow are important factors for the time-dependent behaviour of articular cartilage. The biphasic behaviour of articular cartilage is important for two reasons. First the relatively high compliance is of importance for the distribution of joint forces and results in a reduction of stress gradients. Secondly it plays an important role in the lubrication mechanism of the joint.

To explain the low values of the friction coefficients measured for the joint, 0.005-0.02 (Radin and Paul 1972), a number of lubrication mechanisms for different loading configurations have been considered (Armstrong and Mow 1980, Dowson 1967), which partly are adapted from lubrication mechanisms encountered in technical bearings. However, none of them has been shown to occur in *in vivo* situations. Boundary or film lubrication may occur depending on the load exerted on and the relative velocity of the articular surfaces. Boundary lubrication may occur under large static loads. Film lubrication, for example, is likely to occur during the swing phase of the leg during walking and may be supported by the menisci as they may prevent the lubricating fluid to be squeezed out of the contact surfaces. To include the presence of the porous articular cartilage, weeping and boosted lubrication have been proposed as specific lubrication mechanisms for the knee joint. Under weeping lubrication (McCutchen 1967, Sokoloff 1978) a fluid film is generated in the hydrostatically loaded part of the articular cartilage as fluid is squeezed out of the cartilage. This fluid is resorbed in the unloaded part, resulting in a self-maintaining hydrostatic lubrication mechanism. Boosted lubrication (Walker et al. 1968) may occur if the contact surfaces in the joint approach. In this case the large hyaluronic acid-protein molecules cannot escape with the bulk synovial fluid, which is partly squeezed and captured between the loaded part of the articular cartilage and partly squeezed out, thus leaving a viscous hyaluronic gel between the cartilage surfaces in the contact area.

2.3 Mechanical characteristics of the human knee joint.

A number of experimental studies described in literature deal with aspects of the mechanical behaviour in vivo and post-mortem of the knee joint as a whole.

2.3.1 Pressure distributions between articulating surfaces.

To gain insight into the transmission of loads via the articulating surfaces of the knee joint several post-mortem studies have been carried out to measure static pressure distributions or the area of contact between the tibia and femur, the tibia and the menisci or the femur and the menisci. Static contact-area measurement has been done using a casting technique (Walker and Hajek 1972), radio-opaque fluids (Kettelkamp and Jacobs 1972), plastic micro-indentation transducers (Ahmed and Burke 1983) and color-forming, pressure sensitive, photographic films (Fukubayashi and Kurosawa 1980). The latter two techniques also allow for the determination of local contact pressure patterns after appropriate calibration of the transducer. It must be recognized that these transducers do not only reflect normal pressure but also are sensitive to shear stresses which influence their response (Ahmed and Burke 1983). From the before mentioned studies on the tibio-femoral joint under static axial compression the following common phenomena are observed:

- * increase in flexion angle causes a decrease in contact area in both the lateral and medial compartment;
- * increase in flexion angle shifts the contact areas posteriorly. This effect is more dominant in the lateral compartment;
- * the medial meniscus carries more load, primarily due to its larger surface;
- * the menisci are load carrying although their load carrying function depends on the relative position of tibia and femur as well as on the magnitude of applied loads. Posterior displacements of the tibia relative to the femur tend to decrease the load carried by the menisci whereas increasing compressive loads cause a decrease in the fractional load carried by the menisci, possibly caused by increasing bone-to-bone contact;
- * total meniscectomy results in a drastic change in contact pressure distribution patterns (increase in peak pressures, increase in peak pressure areas, increase in pressure gradients).

2.3.2 Deformations of ligaments

Measurement of deformations of ligaments in situ is of prime importance to study their behaviour under loading of the knee joint. Although a number of qualitative descriptions of ligament behaviour can be found (Brantigan and Voshell 1941, Girgis et al. 1975), quantitative information about ligament deformations is rare, especially for in situ situations.

Direct static ligament-force measurement in post-mortem experiments was carried out by Lewis et al. (1982) using a buckle transducer. The static ligament forces measured for various joint configurations and joint loads typically reached values up to 60 N. This technique however only gives information on the forces transmitted by part of the ligament considered and consequently the total force transmitted is unknown.

Another technique used to obtain information about static ligament-behaviour in post-mortem experiments is stereoröntgenphotogrammetry (van Dijk et al. 1979, Huiskes et al. 1984). The 3-D position of markers implanted near the insertion areas of ligaments is reconstructed from X-ray's for various loading configurations of the joint. These positions are then used to calculate distances between the markers, giving an indication for ligament length patterns, and to calculate the spatial orientation of ligaments. These data, however, do not provide information about the actual deformations in ligaments and their relation with transmitted loads, as a constitutive relation relating length patterns to transmitted loads is not available. Especially this concerns an initial, unloaded, configuration of the ligaments.

2.3.3 In vivo experimental results

The experimental determination of loads acting on the knee joint in vivo is of interest for both mathematical modelling and in post-mortem experiments. Experiments to obtain the 3-D forces and moments working on the tibia and the femur at the level of the knee joint in vivo are not described in literature. This is not surprising because of the ethical problems involved. Indirect measures for these loads are found from vibration studies which also result in an indication of the attenuation of vibrations through the knee joint. Voloshin and Wosk (1983) and Wosk and Voloshin (1981) have carried out a number of in vivo experiments in which accelerometers were attached to the skin near the tibial tuberosity and the medial femoral condyle by means of elastic strips, in an attempt to measure accelerations of the underlying bone. Although this procedure is sensitive to the dynamic behaviour of the skin and underlying soft tissue (Nokes et al. 1984, Ziegert and Lewis 1979), use of low mass transducers in combination with an adequate pre-load yields a negligible effect of these structures (Cornelissen et al. 1986, Nokes et al. 1984). Voloshin and Wosk showed that vibrations, induced upon heel strike during bare-footed

walking and transmitted to the tibia, can be absorbed in the knee joint resulting in a decrease in vibration amplitudes at the femur of about 30 % (Fig. 2.3.1).

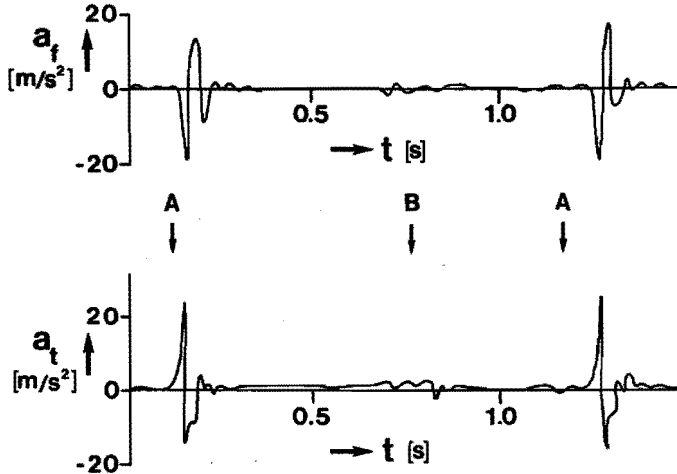


Fig. 2.3.1 Accelerations measured by Voloshin and Wosk (1983) during level walking. The upper trace results from the medial condyle of the femur, the lower trace from the tibial tuberosity (right leg). A and B correspond to a heel strike of the right and left leg, respectively.

Meniscectomy leads to a reduction of this shock absorbing capacity by 20 % which may lead to the supposition that the menisci are important for shock absorption. From the recorded signals it was concluded that the accelerations have a major frequency component in the range of 25-35 Hz. They also remark (without specification) that the measured signals reveal changes in the frequency components. Whether this is due to non-linearities cannot be examined as a change of the frequency contents of the accelerations can also be caused by a change of the frequency contents of the load exerted on the foot. Using a 3-D force platform these loads can be measured (Antonsson and Mamm 1985, Dickinson et al. 1985). A curve for the vertical reaction force on the foot during walking is depicted in Fig. 2.3.2, resulting in the indication that for this activity the relevant frequency range is limited to 100 Hz. It must be emphasized that the shape of the force pattern is sensitive to parameters as walking speed, the kind of walking surface, the type of shoes worn during experiments and the individual walking style.

Loads acting on the knee joint due to muscular activity cannot be measured directly. The importance of these loads is indicated, however, by results obtained by Markolf et al. (1978), who observed a clear increase of whole joint stiffness in vivo under muscle contraction (up to 400%). Whether this increase is due to changes in the

load dependent stiffness properties of joint elements or to an increase of the stiffness of the muscle tendons cannot be assured.

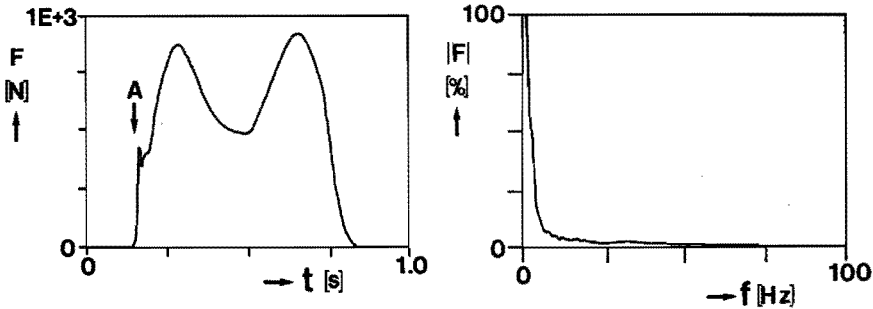


Fig. 2.3.2 Time and frequency domain representation for the vertical reaction force measured under the foot during the stance phase. A denotes heel strike. The picture on the right gives the amplitude of the fouriertransform of the picture on the left expressed as the percentage of the maximum amplitude (Antonsson and Mann 1985).

In a number of experiments the dynamic behaviour of the leg under mechanically exerted dynamic loads is studied and described quantitatively by means of a one-degree-of-freedom linear mass-spring-damper system. Crowninshield et al. (1976b) and Pope et al. (1976) applied small sinusoidal loads to the foot and used measured data to calculate the relationship between the exerted load and the velocity of the foot in the frequency range of 0 to 10 Hz. The resulting stiffness and damping coefficients for ad-abduction and exo-endorotation depend on the static knee joint flexion angle and static medio-lateral displacements of the foot, thus indicating non-linear dynamic behaviour. Resonance frequencies found are typically in the range of 2 to 7 Hz. A similar strategy was employed by Moffat et al. (1969) to study forced flexion-extension movements. Again influence on the stiffness and damping coefficients by the static knee joint flexion angle was observed. Also an increase of voluntary muscle contraction showed to increase the stiffness and damping coefficients found.

2.3.4 Post-mortem experimental results

Various post-mortem experimental studies are reported in literature, describing aspects of the behaviour of the knee joint under static or dynamic loads. Usually these experiments are meant to determine the mechanical behaviour of the knee joint as a whole or to determine the influence of certain anatomical structures upon this behaviour. Static experiments generally lead to a non-linear relation between an applied load and a resulting relevant kinematic parameter, e.g. a

relation between an exo-endo rotation torque applied to the tibia and the resulting exo-endo rotation of the tibia (Fig. 2.3.3).

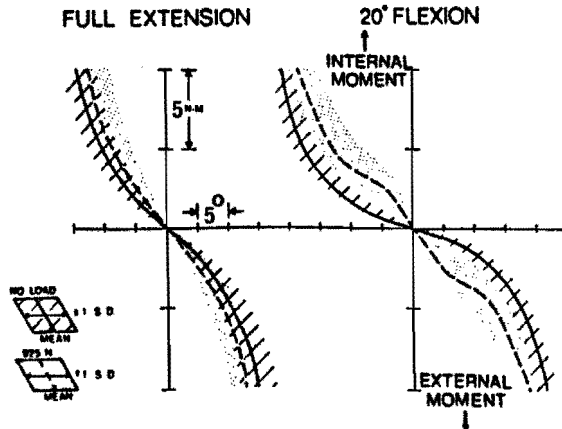


Fig. 2.3.3 Relation between the exo-endo torque and the exo-endo rotation of the tibia for two flexion angles of the joint and an axial load of 0 and 925 N (Markolf et al. 1981).

Apart from biological variability, the results obtained are also influenced by exerted loads as well as joint movements in other directions. As a consequence the full 3-D static behaviour of the joint can only be described by a set of non-linear equations relating applied loads and measured kinematical parameters. No experimental procedure has been applied so far to determine this relationship completely, which is not surprising in view of the experimental difficulties involved.

Some post-mortem experimental studies deal with the behaviour of the knee joint under dynamic loads. Radin and Paul (1971) state that the subchondral bone is an important structural component for shock absorption in the knee joint, whereas articular cartilage and the menisci are less important in this context. This last phenomenon is also reported by Chu et al. (1986), who found an increase of about 20% in the accelerations measured on the tibia under impulsive loading after removal of the menisci and abrasion of the articular cartilage.

2.4 Mechanical modelling of the human knee joint

A number of mechanical models described in literature are employed to analyse aspects of the mechanical behaviour of the knee joint. Mathematical models that describe the knee joint as an isolated mechanical

system are found in different degrees of complexity. Crowninshield et al. (1976a) developed a purely kinematic model to calculate ligament length patterns during motion of the femur relative to the tibia, which subsequently were used to determine the contribution of the ligaments to the stiffness properties of the joint. Simplifications in modelling can lead to statically determinate models, which can be used to calculate forces in joint structures and/or contact forces using the equilibrium equations only (Johnson et al. 1981, Morrison 1968, Wongchaisuwat et al. 1984). To obtain kinematical parameters, contact forces and ligament forces for a given external load, statically indeterminate models are employed (Andriachi et al. 1983, Moeinzadeh et al. 1983, Wismans et al. 1980). These models include a description of the articular surfaces and constitutive relationships for non-linear elastic springs representing ligamentous structures which are either measured or suitably chosen.

A number of mathematical models have been developed to describe the behaviour of the leg as a whole. Generally, in these models the knee joint is reduced to a simple connection between the tibia and the femur. Morrison (1968) used a hinge element to model the knee joint, although he included forces arising from ligamentous structures. In combination with the use of hinge elements for the ankle and the hip joint, assumed activity of a number of muscles (based on measured EMG signals), measured kinematical data and ground reaction forces Morrison arrived at a statically determinate set of equations for muscle forces, joint reaction forces and forces in ligamentous structures. For normal walking this resulted in a maximum compressive contact force on the tibial-femoral joint of about 4 times body weight.

Using a similar simplification of the joints in the leg, but including a large number of muscles, Seireg and Arvikar (1975) formulated an indeterminate set of equations for muscle forces and joint reaction forces, which was solved by minimizing a weighted sum of the forces in the model. From this approach it followed that for normal walking the maximum compressive force working on the knee joint is about 7 times body weight.

2.5 Summary

In this chapter the anatomy and some elementary aspects of the mechanical behaviour of the human knee joint have been discussed. From literature data it can be concluded that little knowledge is available on the dynamic force transmission through the joint, neither from experiments nor from experimentally verified mathematical models. Considering the basic joint structures, the bony parts (considered as a continuous structure) are best known with respect to their mechanical properties, but these are largely unknown for the

soft tissues. This especially applies for 2- and 3-dimensional loading configurations as both experimental techniques and a theoretical framework to analyse the mechanical behaviour of the soft tissues are not developed yet, although 2-dimensional strain field analysis for soft tissues comes within reach by developments in the field of digital image processing (Peters 1987). The poor knowledge with respect to the mechanical properties of the joint elements is also reflected in the available mathematical models as the bony parts are generally modelled as rigid bodies, whereas soft tissues are usually represented as elastic, uni-axial force transmitting elements. The dynamic force transmission through the joint has gained some attention, resulting in the indication that the joint may act as a non-linear shock-absorber or damping-element between the upper- and lower leg. However, it is neither experimentally nor theoretically investigated in detail how these characteristics are influenced by the external loads acting on the joint, the kinematical behaviour of the joint and the presence and mechanical properties of individual joint elements.

Chapter 3 Experimental strategy

From chapter 2 it was concluded that in literature only little data is available on the dynamic force transmission through the human knee joint. Therefore it was decided to start an explorative experimental investigation into the mechanical characteristics of the knee joint under dynamic loading. In this chapter an overview is given of the experimental strategy applied. In section 3.1 the methodology handled for the experiments is discussed. In section 3.2 some guidelines for the development of an experimental set-up are derived from the methodology discussed in section 3.1, resulting in a basic experimental set-up. Section 3.3 deals with a simple dynamic model of the knee joint to elucidate the experimental approach and to indicate which mechanical parameters should be measured to assess the basic dynamic characteristics of the joint. Section 3.4 deals with measurement methods applied to obtain analog signals used to quantify the dynamic behaviour of the joint. Finally in section 3.5 a data-acquisition system is discussed that allows for digitization of the analog signals.

3.1 Methodology

Because of the limited amount of experimental data and validated models for the dynamic behaviour of the human knee joint it was felt that an attempt had to be made to gain more insight into the behaviour of the joint by means of experiments. From a methodological and practical point of view a combined experimental-theoretical approach is favourable, as insights gained from experiments may lead to refinements in the initial theoretical model, possibly resulting in guidelines for further experiments. This iterative process will ultimately yield an experimentally validated numerical model. In the present study an initial structural theoretical model is not provided. Besides little information on the dynamic behaviour of the joint was found in literature which can be used as a guideline for development of an experimental method to study the behaviour of the joint. This causes the need for an experimental approach that is as general as possible in order to be able to fulfill demands imposed by a theoretical model developed at a later stage. To avoid a waste of efforts the experimental set-up must be suitable for a number of experiments requiring only minor modifications, irrespective of an initially chosen experimental method to quantify the dynamic behaviour of the joint.

Bearing in mind these considerations it was decided to start an explorative experimental investigation into the mechanical characteristics of the human knee joint under dynamic loading. It should be recognized that in general the dynamic behaviour of the joint must be described by means of relationships between:

- * loads exerted on the joint (loads due to muscular activity, loads transmitted by the femur and the tibia and loads due to gravitational effects);
- * the 3-dimensional position and orientation of the tibia relative to the femur;
- * deformations of and stress distributions in the joint elements which are related by their individual constitutive behaviour.

All these quantities will in general be time-dependent and interacting non-linearly. In an explorative experimental investigation the dynamic behaviour described above is much too complicated to deal with due to a lack of experimental techniques to quantify all parameters and quantities governing the relationships mentioned. Therefore some restrictions will have to be made.

In post-mortem experiments a choice must be made for loads applied to the knee joint specimen. Of course it is advisable to apply loads encountered in vivo, but these loads are only known to a limited extent. Global information is available for joint loads (e.g. during walking) but detailed information on intensity, duration and the frequency contents of these loads is not available. In striving at the realization of physiological loads, dynamic loads exerted by muscles should also be taken into account, which is impossible in post-mortem experiments. This lack of knowledge of physiological loads is a major disadvantage in such experiments. However, part of this disadvantage can be relieved because of the possibilities to vary magnitude, direction and shape of the applied loads in a range marked by data found in literature for in vivo joint loads. The experimental results obtained can be used for formulation and validation of a numerical model describing the dynamic behaviour of the joint, which then can be verified using data from in vivo experiments.

From this point of view the necessity for application of physiological loads vanishes, and loads applied to the knee joint can be chosen such that the development of experimental techniques for quantification of its dynamic behaviour can be given prime attention. Furthermore, the applied loads can be chosen such that the experimental results can be compressed in a manageable number of parameters. The need for such a choice arises from the expectation that the joint behaves as a non-linear system with load- and time-dependent stiffness and damping characteristics. Applying loads such that, apart from physical non-linearities, also geometrical non-linearities are involved due to large changes in position and orientation of the tibia relative to the femur, will considerably increase the difficulties in finding parameters describing the dynamic behaviour.

From these considerations it was concluded that a local linearization technique (LLT) may yield an appropriate experimental procedure. The LLT basically consists of two steps. The first step involves the creation of a stable, static equilibrium position of the joint by means of a static load exerted on the joint. To include one important effect of muscular activity this static load can also be used to generate a compressive pre-load, which may have considerable effect on the transmission of dynamic forces through the joint. The second step in the LLT is the application of dynamic loads such that only relatively small changes in the joint configuration will occur. It is assumed that these changes are small enough to obtain a dynamic behaviour that corresponds to the behaviour of a linear system with constant mass, damping and stiffness characteristics. These characteristics may depend on the static equilibrium position and the static load exerted, but it is essential that they are constant for a certain range of the magnitude of the applied dynamic loads, which must be determined experimentally.

This approach is attractive because an experimental tool is available for the analysis of linear systems, yielding a limited number of parameters for a full description of their dynamic behaviour. This so-called modal analysis technique results in a number of vibration modes and corresponding stiffness and damping values, which can be determined by a system identification technique either in the frequency- or the time-domain (Bendat and Piersol 1980, Natke 1983). As these modal parameters can also be determined for a given numerical model of the joint, they provide an easy means for quantification of the experimental results and validation of the numerical model. These modal parameters may also be used to formulate a numerical model of the joint as they give an insight into its essential static and dynamic characteristics. The experimental procedure described above must be carried out for a number of static load levels and different static equilibria of the joint to investigate the influence of these parameters.

It must be realized that this approach may fail for two reasons. First it is possible that the behaviour of the joint is essentially non-linear such that non-linearities arising from non-linear damping or non-linear static load-displacement characteristics cannot be linearized. On forehand this is not expected to occur as the friction in the knee joint is found to be very small (section. 2.2.4) and as a LLT has been applied by Crowninshield et al. (1976b), Moffat et al. (1969) and Pope et al. (1976) to describe joint behaviour without giving indications for possible failure. Also a similar procedure has successfully been applied by van Heck (1984) to determine the strongly non-linear stiffness and damping characteristics of the contact zone found between slideways of machine-tools. Secondly, generally handled measurement techniques provide a threshold for the minimal magnitude of dynamic loads to be applied as below this threshold the signal-to-noise ratio considerably decreases. This finite measurement accuracy

may make it impossible to apply the small dynamic loads required to allow for the local linearization. Because of the lack of knowledge of the dynamic behaviour of the joint, at this juncture it is not possible to judge whether these disturbing factors will play a role. Consequently it is decided to start with the experimental procedure described above bearing in mind the possible reasons for failure mentioned.

Under the assumption that the LLT provides a means to quantify the dynamic behaviour of the intact joint, the next step in the experimental strategy can be considered. The experimental results obtained for the intact joint will depend on the loads exerted, the 3-D static equilibrium position and on the role of the different joint elements. To obtain an indication of their mechanical function from experiments, an experimental tool must be found to clarify their contribution to the whole joint dynamic behaviour. It is clear that, in the ideal case, their role should be determined by direct measurement of the deformations and stress-distributions in the individual joint elements, which generally will be of a 3-D nature. If possible at all, measurement of these quantities requires complex experimental techniques. As a consequence another method will be employed that is expected to give indirect measures for the mechanical function of the different joint elements. The basic idea is that if the joint elements play a role, deliberate damaging of a particular joint element in situ must have effect on the dynamic behaviour of the joint as a whole as was indicated in section 2.3. This effect will result in changes in vibration modes and stiffness and damping characteristics and thus can be quantified.

To elucidate the use of the modal analysis technique in section 3.3 a simple, black box, dynamic model of the knee joint is discussed. Before doing so some aspects are considered in section 3.2 that allow for a simplification of a general model of the joint.

3.2 Experimental set-up

In this section a basic experimental set-up will be discussed which was developed to do experiments on knee joint specimens according to the methodology discussed in section 3.1.

3.2.1 Practical considerations

The methodology discussed in section 3.1 needs to be considered on some important points to obtain guidelines for development of an experimental set-up. First a choice must be made for a method to apply the static load and an indication must be given for the magnitude and direction of the static load to be applied to the knee joint specimen. Secondly the frequency range of interest used for analysis

of the dynamic behaviour of the joint must be specified, as this imposes demands on the dynamic behaviour of the experimental set-up.

In general some mechanical device must be attached to the joint to exert the static load. In selecting a device two boundary conditions need to be taken into account:

- * it must be possible to apply the static load independently of the magnitude, direction and shape of the dynamic load;
- * the device used may not impose any constraints on the dynamic behaviour of the joint.

The first condition arises from the consideration that it must follow from experiments which type of dynamic load is preferable to study the dynamic behaviour of the joint. Application of random, sinusoidal, step- or impuls-like dynamic loads generally will require the use of different excitation techniques. For example, random or sinusoidal loads can be exerted by an electromechanical or hydraulic excitator, but these devices are not well suited to exert step- or impuls-like loads, although both can be used to exert static loads. Use of a different apparatus to apply the dynamic load, therefore also may result in the necessity to select a different method to apply the static load. Thus it seems not sensible to select a device that generates both the static and the dynamic load. The second condition is obvious, because imposing constraints will yield an artificial dynamic behaviour (e.g. due to a limitation of the number of degrees of freedom of the specimen imposed by the dynamic characteristics of the load generating device).

To realize a simple solution for a static load generating device it is assumed that a stable static equilibrium position of the joint can be created by exerting static forces via a limited number of tendinous muscle attachments on the joint. This assumption follows from the observation that in vivo muscle forces play an important role in maintaining a stable equilibrium position of the joint.

At this point it must be emphasized that the method discussed to apply the static load is not an attempt to simulate muscle forces. It is merely a technical solution to be able to control the static equilibrium position of the joint, in which use is made of some elementary biomechanical considerations to assure stability of the static equilibrium position.

When selecting muscle tendons to carry the static load, also the necessity for clamping the knee joint specimen at a particular point must be considered. Clamping the joint at its femoral or tibial side is allowed as only the relative motion of the femur and the tibia is important for the dynamic behaviour of the joint. When the upper part of the tibia is clamped, only those muscle tendons that have a connection to the femur can be selected. The insertions of the musculus gastrocnemius may be used, but other tendons are not available.

Regarding their location with respect to the joint, it is not realistic to expect that a stable equilibrium position of the joint can be created by exerting static forces via these muscle tendons only. Clamping the lower part of the femur seems a better solution, as a number of muscle tendons attach to the upper part of the tibia. For a start the tendons of the musculus rectus femoris, the musculus biceps femoris and the musculus semitendinosus are selected and will be loaded with static forces \vec{f}_r , \vec{f}_b and \vec{f}_s , respectively (Fig. 3.2.1).

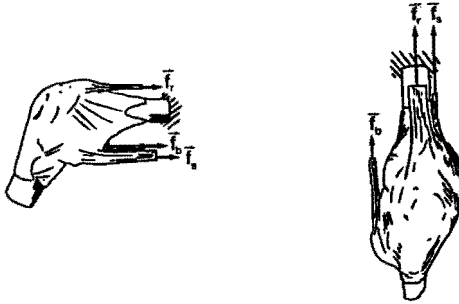


Fig. 3.2.1 Forces \vec{f}_r , \vec{f}_b and \vec{f}_s acting on the musculus rectus femoris, musculus biceps femoris and musculus semitendinosus to create a stable static equilibrium position.

As these static loads will be used to control the static equilibrium position of the joint as well as to exert a static compressive preload, the direction of the forces \vec{f}_r , \vec{f}_b and \vec{f}_s and their magnitude are important parameters. It is assumed that the direction of these forces can be chosen to be approximately parallel to the longitudinal axis of the femur, irrespective of the static equilibrium position of the joint. This assumption is derived from the observation that in vivo the muscle tendons show a similar orientation with respect to the joint. To obtain an indication for the maximal static load to be carried by the individual muscle tendons, values for the compressive static load working on the femur given in literature are considered. From the biomechanical models discussed in chapter 2 it follows that this load depends on the position and orientation of the tibia relative to the femur and on the specific activity being analysed (walking, running, jumping etc.). The maximal values reported vary from 4 to 8 times bodyweight, which yields an averaged maximal compressive load of about 4500 N. This load cannot directly be translated into loads acting on the muscle tendons due to a possible load bearing function of the ligamentous structures and menisci e.g.. However, a rough measure can be found if it is assumed that the compressive load is equal to the sum of the loads carried by the muscle tendons. This results in a maximal load of approximately |

1500 N to be carried by each muscle tendon. Whether the individual muscle tendons can carry this load must be established in experiments.

As to the frequency range within which the dynamic behaviour of the joint has to be analysed, use must be made of data available in literature as discussed in chapter 2. Using the data given by Voloshin and Wosk (1983), Wosk and Voloshin (1981) and Antonsson and Mann (1985), an upper relevant frequency of 100 Hz can be assumed. This upper frequency limit is important for several experimental aspects:

- * first it imposes requirements on the dynamic behaviour of the experimental set-up. As the knee joint and the experimental set-up are coupled mechanical systems, the dynamic behaviour of the experimental set-up may not result in disturbing components in the signals measured to quantify the dynamic behaviour of the joint. In general this requires an experimental set-up that has sufficiently low or high resonance frequencies such that it can be considered to be rigid in the frequency range of interest. This aspect will be analysed further in chapter 4 as the dynamic behaviour of the experimental set-up must be compared to the measured dynamic behaviour of the knee joint to assure that the experimental set-up does not play a disturbing role;
- * secondly the upper frequency limit imposes demands on the selected transducers. They must have a dynamic behaviour that does not result in disturbing components in the signals measured (section 3.4);
- * finally the upper frequency limit must be taken into account when selecting a data-acquisition system for digitization of the analog signals (section 3.5).

Also the lower frequency limit must be taken into consideration as this limit is also of importance for the selection of transducers. For example, if the lower frequency limit would turn out to be less than 5 Hz, use of piezo-electric transducers is prohibited as charge-leakage will result in poor measurement accuracy. At this juncture the lower frequency limit is unknown and consequently must be determined by experiments.

3.2.2 Basic experimental set-up

Given the guidelines discussed in the previous section, a basic experimental set-up was assembled (Fig. 3.2.2). A rectangular concrete block A with a steel plate (B) rigidly attached to its upper plane constitutes the basis of this set-up. A rectangular steel block (C) is welded on the steel plate at one of its short sides and a

grate (M) with 8 vertical slots at the other. A clamping flange (E) is mounted on a 3-D piezo-electric force platform (G) and this unit is attached to block C (Fig. 3.2.3). The purpose of the force platform (G) will be elucidated in sections 3.3 and 3.4.

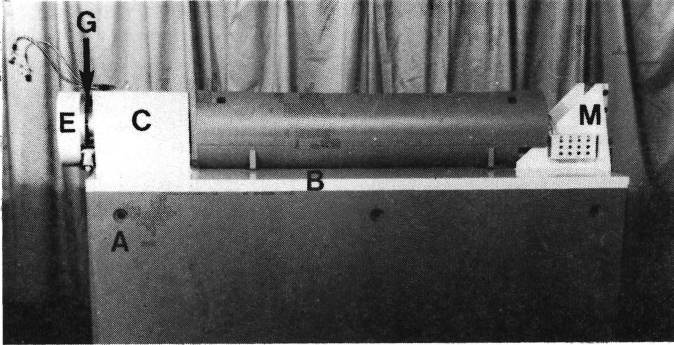


Fig. 3.2.2 Foundation of the experimental set-up (see text).

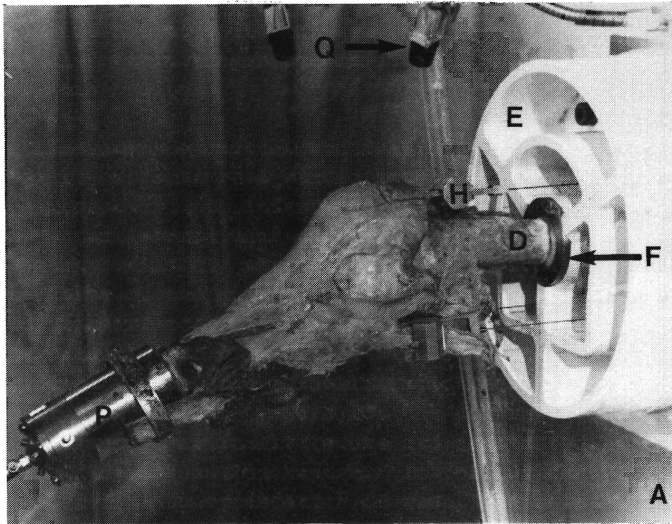


Fig. 3.2.3 A knee joint specimen clamped at the femur (see text).

The combined mass of the set-up discussed so far is approximately 3500 kg. To avoid disturbance by environmental vibrations the set-up is mounted on an isolated floor. This type of foundation is required

to assure that resonance phenomena do not disturb the signals measured to study the behaviour of the knee joint specimen. The stiffness of the foundation is typically 10^{11} N/m whereas the force platform has a typical stiffness of 10^9 N/m. As will be illustrated in chapter 4 these values are well above the stiffness of the knee joint specimen (typically 10^5 N/m). A detailed description of the joint specimen is given in chapter 4.

The proximal part of the femur (D) is - with use of a rapidly curing polymer (Fastacryl) - fixed in a stainless steel cylinder (F) and subsequently mounted into the clamping flange (E). Static forces on the muscle tendons are generated with the use of bracing wires (Fig. 3.2.4).

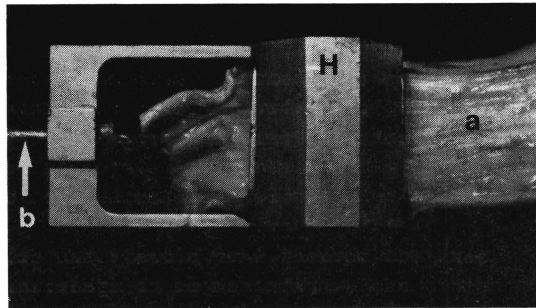


Fig. 3.2.4 A muscle tendon a clamped in the tendon clamp H, b is the bracing wire connected to clamp H.

The reasons for this are as follows:

- * use of bracing wires with sufficiently low longitudinal stiffness assures the dynamic behaviour of the load generating device to be of little influence on the dynamic behaviour of the joint, as in this case no artificial stiffness and damping are introduced. Furthermore, the bending and torsional stiffness can be neglected compared to the longitudinal stiffness;
- * if the stiffness characteristics of the wires should not be negligibly small compared to the 3-D stiffness characteristics of the joint, they can relatively easily be taken into account in a numerical model and hence their influence can be incorporated.

As the stiffness characteristics of the joint are unknown at this stage, the bracing wires are initially chosen to have the following properties: diameter 1.0 mm, length 1.5 m, elastic modulus 210 GPa and yield strength 2 GPa, which yields a longitudinal stiffness k_1 of approximately 110 N/mm. It is assumed that this stiffness value is

sufficiently low, to keep fluctuations in the static load transmitted by the wires as small as possible during dynamic loading of the joint.

The bracing wires are attached to the muscle tendons by means of self-tightening aluminium clamps (H). Each clamp has a mass of 0.026 kg and is capable of transmitting loads up to 1500 N. The mass of the clamps was minimized to obtain a sufficiently high resonance frequency f_r for longitudinal vibrations of the mass-spring system formed by the clamp and the bracing wire. The values for the stiffness of the bracing wire and the mass of the clamp given above yield a value for f_r of approximately 229 Hz, which is well beyond the upper frequency limit of 100 Hz for analysis of the dynamic behaviour of the joint. The bracing wires pass through holes in the clamping flange (E), force platform (G) and block C and are connected to a stud-and-nut combination (N), placed in one of the slots of grate (M) (Fig. 3.2.5).

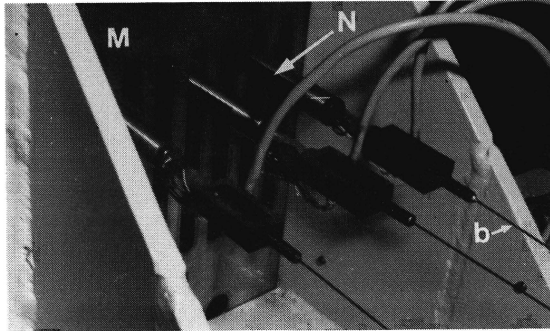


Fig. 3.2.5 The location of the stud-and-nut combinations N in the slots of grate M, b is a bracing wire connected to such a stud-and-nut combination.

The magnitude of the tensile force in the wire is adjusted by turning the nut. The direction of the tensile force on a particular muscle tendon can be changed within certain limits by changing the place on grate M of the corresponding stud-and-nut combination. These changes, however, have only little influence on the direction of the wire due to its length and are primarily meant to avoid contact between the wire and its surroundings, as this contact may disturb the force transmission through the wire due to friction.

The distal part of the tibia is - identical to the proximal part of the femur - fixed in a stainless steel cylinder (P). The distal part of the fibula is tightly secured to this cylinder using a steel strip, as otherwise the connection between the tibia and the fibula falls for the magnitude of the force on the tendon of musculus biceps femoris applied in the experiments. The cylinder P is also meant to provide a fixed location to apply the dynamic load to the tibia.

Finally, two sprinklers (Q) are mounted on top of block C to allow of a continuous moistening of the knee joint specimen with Ringer's solution.

3.3 A non-linear black box model of the knee joint

The experimental approach discussed in the previous sections can be elucidated by means of a simplified, black box, model of the knee joint. Especially the use of the LLT and modal analysis for quantification of the dynamic behaviour of the knee joint specimen in the experimental set-up will be illustrated. Of course this model only applies if the LLT is valid and will yield a set of coupled linear differential equations. The nature of the model is essentially determined by some assumptions concerning the loads exerted on the tibia and the femur by the remainder of the joint structures. The resulting equations can readily be used to consider some practical consequences for the application of modal analysis. Another purpose of the model is to indicate which parameters are to be measured to quantify the basic dynamic behaviour of the knee joint specimen. Subsequent paragraphs in this section are devoted to

- * a descriptive model for the dynamic behaviour of the knee joint expressed in parameters to be measured on the tibia
- * a relation between the loads exerted on the tibia, the loads transmitted to the femur and the kinematics of the tibia.

3.3.1 A descriptive model for the dynamic behaviour of the tibial component

To formulate a simple model describing the (expected) behaviour of the knee joint in the experimental set-up discussed in section 3.2, the configuration given in Fig. 3.3.1 is considered.

It is assumed that the tibia and the femur behave as rigid bodies, while the latter is clamped. In the model the knee joint is seen as a massless connection and a tibial and femoral component. This connection represents the remainder of the joint structures (ligaments, menisci, articular cartilage etc.). Due to its presence loads will be exerted on the tibia and femur, non-linearly depending on the position and orientation of the tibia relative to the femur. In general these internal loads of the joint are given by the constitutive relation of the connection and are denoted with a vector column $\vec{L}_j^T = [\vec{F}_j \quad \vec{m}_j]$ which contains the force \vec{F}_j and the moment \vec{m}_j with respect to a certain reference point on the tibia. The moment \vec{m}_j will consist of external moments (torques) and a internal moments due to forces exerted by the connection with a finite leverarm with respect to the chosen reference point. This constitutive relation can formally be

written as $\dot{\underline{I}}_j = \dot{\underline{I}}_j(\underline{k}, t)$ with \underline{k} as 6×1 matrix containing the 6 mutually independent kinematic parameters describing the kinematics of the tibia with respect to a reference coordinate system (translations and rotations). Using a massless connection seems allowed as the mass of the ligaments, menisci etc. can be neglected in comparison with the mass of the tibia.

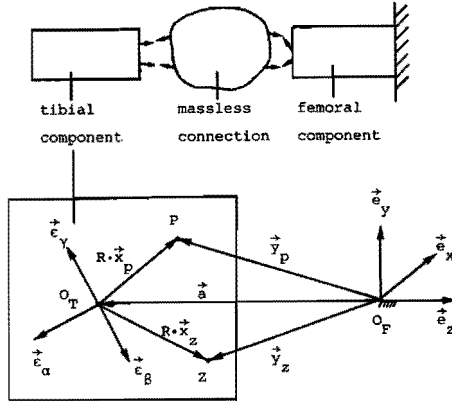


Fig. 3.3.1 The prime elements for the dynamic model of the knee joint and the vectors used to describe the kinematics of the tibial component (see text).

In the model external loads can be exerted on the tibia. The presence of the bracing wires is taken into account by the assumption that the static load exerted on the wires results in a static load exerted on the tibia. Besides a dynamic external load can be applied to the tibia, which does not influence the static equilibrium position, however.

In the sequel the relations describing the dynamic behaviour of the tibia will be formulated and elaborated in case only small deflections from a static equilibrium position occur.

To describe the kinematics of the tibia two body fixed vector bases are introduced as depicted in appendix A. The position and orientation of the tibia with respect to the femur can then be described by means of the translation vector \vec{a} and the proper orthogonal rotation tensor R .

The equations of motion for the tibia are given by the Newton-Euler laws

$$\dot{\vec{I}}_T = \dot{\vec{p}} \tag{3.3.1}$$

$$\dot{\vec{m}}_T = \dot{\vec{d}} - m_T \dot{\vec{y}}_Z * \dot{\vec{a}} \tag{3.3.2}$$

Here \vec{f}_T is the resultant force and \vec{m}_T the resultant moment with respect to O_T working on the tibia, whereas \vec{p} and \vec{d} are the absolute momentum and angular momentum of the tibia with respect to O_P . It should be noted that relation (3.3.2) represents the equilibrium of moments working on the tibia with respect to point O_T . As O_T in general does not coincide with the center of gravity Z of the tibia the second term on the right-hand side of equation (3.3.2) must be included. The reason for this formulation will be made clear later. As it is assumed that the LLT applies, initially a static equilibrium position is provided characterized by the kinematical parameters \vec{a}_0 and R_0 .

To elaborate relations (3.3.1) and (3.3.2) first the momentum vectors \vec{p} and \vec{d} are considered. In general these can be written as

$$\vec{p} = m_T \dot{\vec{y}}_Z \quad (3.3.3)$$

$$\vec{d} = m_T (R \cdot \vec{x}_Z) * \dot{\vec{a}} + J_T \cdot \vec{\omega} \quad (3.3.4)$$

\vec{y}_Z is the momentary position vector with respect to O_P of the center of gravity Z of the tibia with reference position vector \vec{x}_Z with respect to O_T . m_T is the mass of the tibia and J_T the momentary symmetric inertia tensor of the tibia with respect to O_T . $\vec{\omega}$ is the axial vector of the skew-symmetric tensor $\hat{R} \cdot R^C$, which describes the angular velocity of the tibia with respect to the femur. As the momentary position vector \vec{y}_P with respect to O_P of an arbitrary point P on the tibia with reference position vector \vec{x}_P with respect to O_T is given by

$$\vec{y}_P = \vec{a} + R \cdot \vec{x}_P \quad (3.3.5)$$

it holds

$$\vec{y}_Z = \vec{a} + R \cdot \vec{x}_Z \quad (3.3.6)$$

$$\dot{\vec{y}}_Z = \dot{\vec{a}} + \vec{\omega} * (R \cdot \vec{x}_Z) \quad (3.3.7)$$

In case of small deflections from an initial equilibrium position relations (3.3.3) and (3.3.4) can be linearized. In this case R can be written as

$$R = R_0 + \Delta R = (I + \Delta R \cdot R_0^C) \cdot R_0 \quad (3.3.8)$$

From the orthogonality condition $R \cdot R^C = I$ it follows

$$R_0 \cdot R_0^C + \Delta R \cdot R_0^C + R_0 \cdot \Delta R^C + \Delta R \cdot \Delta R^C = I \quad (3.3.9)$$

Neglecting the quadratic term $\Delta R \cdot \Delta R^C$ in relation (3.3.9) and using the identity $R_O \cdot R_O^C = I$ one can readily verify that the tensor $\Delta R \cdot R_O^C$ is skew-symmetric and therefore has an axial vector $\vec{\pi}$ such that

$$\Delta R \cdot R_O^C \cdot \vec{v} = \vec{\pi} * \vec{v} \quad \text{for all } \vec{v} \quad (3.3.10)$$

In this case the axial vector $\vec{\omega}$ of the tensor $\dot{R} \cdot R^C$ satisfies

$$\vec{\omega} = \dot{\vec{\pi}} \quad (3.3.11)$$

The vector $\vec{\pi}$ characterizes the small changes in the relative orientation of the tibia and the femur. The translation vector \vec{a} will also be subjected to small changes, denoted with \vec{c} so that

$$\vec{a} = \vec{a}_O + \vec{c} \quad (3.3.12)$$

$$\dot{\vec{a}} = \dot{\vec{c}} \quad (3.3.13)$$

With relations (3.3.6) through (3.3.13) relations (3.3.3) and (3.3.4) can be linearized, neglecting non-linear terms containing $\vec{\pi}$, \vec{c} and their first time derivatives. This yields

$$\vec{p} = m_T (\dot{\vec{c}} - X_Z \cdot \dot{\vec{\pi}}) \quad (3.3.14)$$

$$\vec{d} = m_T X_Z \cdot \dot{\vec{c}} + J_{T_O} \cdot \dot{\vec{\pi}} \quad (3.3.15)$$

with

$$X_p \cdot \vec{v} = (R_O \cdot \vec{x}_p) * \vec{v} \quad \text{for all } \vec{v} \text{ and } p \quad (3.3.16)$$

and J_{T_O} representing the symmetric inertia tensor of the tibia with respect to O_T in the static equilibrium position.

The linearization applied also results in a neglection of the term $m_T \dot{\vec{y}}_Z * \dot{\vec{a}}$ in relation (3.3.2), as this term only contains non-linear terms in $\dot{\vec{c}}$ and $\dot{\vec{\pi}}$.

To obtain the resultant force \vec{f}_T and moment \vec{m}_T , loads are introduced as schematically given in Fig. 3.3.2.

The static forces exerted on the bracing wires will result in a static force \vec{f}_{wO} and a static moment \vec{m}_{wO} with respect to O_T (which may consist of both external and internal moments).

A dynamic external load is applied at point E of the tibia with reference position vector \vec{x}_e with respect to O_T . It is assumed that this load consists of a force \vec{f}_e and a torque \vec{t}_e , resulting in a moment \vec{m}_e with respect to O_T acting on the tibia

$$\vec{m}_e = \vec{t}_e + (R \cdot \vec{x}_e) * \vec{f}_e \quad (3.3.17)$$

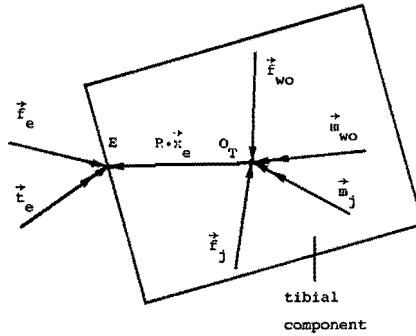


Fig. 3.3.2 Loads working on the tibial component of the knee joint (see text).

Linearization of relation (3.3.17) yields

$$\vec{m}_e = \vec{t}_e + X_e \cdot \vec{f}_e \quad (3.3.18)$$

where it is assumed that no static force or torque is exerted in point E to create the static equilibrium position. In this linearization process also terms containing products of \vec{f}_e and $\vec{\pi}$ are neglected because these terms would result in follower moments and consequently to a non-linear model.

To account for the force \vec{f}_j and moment \vec{m}_j with respect to O_T due to the massless connection, representing joint elements as ligamentous structures, menisci etc., a rigorous assumption is made. It is assumed that its presence results in a static force \vec{f}_{j0} and moment \vec{m}_{j0} with respect to O_T and a contribution which depends linearly on the changes in the position and orientation of the tibia with respect to the femur and their first time derivatives

$$\vec{f}_j = \vec{f}_{j0} - K_1 \cdot \vec{c} - K_2 \cdot \vec{\pi} - B_1 \cdot \dot{\vec{c}} - B_2 \cdot \dot{\vec{\pi}} \quad (3.3.19)$$

$$\vec{m}_j = \vec{m}_{j0} - K_3 \cdot \vec{c} - K_4 \cdot \vec{\pi} - B_3 \cdot \dot{\vec{c}} - B_4 \cdot \dot{\vec{\pi}} \quad (3.3.20)$$

K_1 through K_4 and B_1 through B_4 can be seen to represent stiffness and damping properties respectively. These tensors are not necessarily symmetric, but they are independent of time. Also they generally will depend on the static equilibrium position and the static force \vec{f}_{wo} and moment \vec{m}_{wo} . In relations (3.3.19) and (3.3.20) inertial effects have been neglected which seems valid due to the low mass of the joint elements compared to the mass of the tibia. Consequently relations (3.3.19) and (3.3.20) may be thought of as the resultant force and moment obtained from a massless connection between tibia and femur, which may be modelled as a 3-D spring-damper system or by

means of a Finite Element model. In the sequel it is assumed that no limitation of the number of degrees of freedom of the tibia arises from the presence of the joint elements mentioned. This is not essential for coming considerations as a reduced number of degrees of freedom can always be taken into account by a suitable transformation between dependent and independent kinematic parameters.

With the use of the loads introduced above, the equations of motion for the tibia can now be written as

$$m_T(\ddot{\vec{c}} - X_z \cdot \ddot{\vec{\pi}}) = \vec{f}_e + \vec{f}_{j0} + \vec{f}_{wo} + \\ - K_1 \cdot \dot{\vec{c}} - K_2 \cdot \dot{\vec{\pi}} - B_1 \cdot \dot{\vec{c}} - B_2 \cdot \dot{\vec{\pi}} \quad (3.3.21)$$

$$m_T X_z \cdot \ddot{\vec{c}} + J_{To} \cdot \ddot{\vec{\pi}} = \vec{t}_e + X_e \cdot \vec{f}_e + \vec{m}_{j0} + \vec{m}_{wo} + \\ - K_3 \cdot \dot{\vec{c}} - K_4 \cdot \dot{\vec{\pi}} - B_3 \cdot \dot{\vec{c}} - B_4 \cdot \dot{\vec{\pi}} \quad (3.3.22)$$

To satisfy the static equilibrium the following relations must hold

$$\vec{f}_{j0} + \vec{f}_{wo} = \vec{0} \quad (3.3.23)$$

$$\vec{m}_{j0} + \vec{m}_{wo} = \vec{0} \quad (3.3.24)$$

After substitution of relations (3.3.23) and (3.3.24) relations (3.3.21) and (3.3.22) can be written as a set of 6 coupled linear second-order differential equations:

$$\underline{M} \cdot \ddot{\underline{u}} + \underline{B} \cdot \dot{\underline{u}} + \underline{K} \cdot \underline{u} = \underline{G} \cdot \underline{f}_e \quad (3.3.25)$$

where the following tensor matrices and vector columns have been introduced

$$\underline{M} = \begin{vmatrix} m_T I & -m_T X_z \\ m_T X_z & J_{To} \end{vmatrix}; \underline{B} = \begin{vmatrix} B_1 & B_2 \\ B_3 & B_4 \end{vmatrix}; \underline{K} = \begin{vmatrix} K_1 & K_2 \\ K_3 & K_4 \end{vmatrix} \\ \underline{G} = \begin{vmatrix} I & 0 \\ X_e & I \end{vmatrix}; \underline{u} = \begin{vmatrix} \vec{c} \\ \vec{\pi} \end{vmatrix} \quad \text{and} \quad \underline{f}_e = \begin{vmatrix} \vec{f}_e \\ \vec{t}_e \end{vmatrix} \quad (3.3.26)$$

Relation (3.3.25) gives 6 second-order vector differential equations for the unknown components of the column \underline{u} in case of a given external load \underline{f}_e . However the damping and stiffness coefficients are not yet known and must be determined experimentally. A method to obtain these characteristics is given by application of modal analysis. To illustrate this, equation (3.3.25) is transformed into a matrix differential equation by representation of all vector- and tensor

quantities with respect to the inertial vector base \vec{e} which is connected to the femur

$$\underline{M} \ddot{\underline{u}} + \underline{B} \dot{\underline{u}} + \underline{K} \underline{u} = \underline{G} \underline{l}_e \quad (3.3.27)$$

\underline{M} , \underline{B} , \underline{K} and \underline{G} are 6*6 scalar matrices, whereas \underline{u} and \underline{l}_e are 6*1 scalar matrices. The matrices \underline{B} and \underline{K} will in general be non-symmetric, while \underline{M} is symmetric. In appendix B it is shown that relation (3.3.27) can be solved for the Fourier transform $\underline{u}(f)$ of the column \underline{u} , using the so-called transfer function matrix $\underline{H}(f)$ and the Fourier transform $\underline{l}_e(f)$ of the column \underline{l}_e

$$\underline{u}(f) = \underline{H}(f) \underline{G} \underline{l}_e(f) \quad (3.3.28)$$

with

$$\underline{x}(f) = \lim_{\alpha \rightarrow 0} \int_{-\infty}^{+\infty} \underline{x}(t) \exp(-\alpha|t|) \exp(-2\pi jft) dt \quad (3.3.29)$$

as the generalised Fourier transform of an arbitrary signal $\underline{x}(t)$, which must be handled to be able to deal with sinusoidal signals e.g..

The transfer function matrix $\underline{H}(f)$ can be written as a function of a set of modal parameters called poles s_k and residues \underline{A}_k ($k=1\dots 6$) where each pole s_1 and residue matrix \underline{A}_1 correspond to a particular vibration mode of the freely vibrating system. Of course the number of relevant vibration modes may be taken to be $N_m \leq 6$ as the number of vibration modes in the frequency interval of interest.

At this point the choice for the location of O_T may be considered. The derivation given above results in a set of residues which represent the displacements of the tibia for a particular vibration mode with respect to O_T . The location of O_T influences the numerical values of these residues. However, if the residues are known for a certain location of O_T the residues for another location of O_T can easily be determined as the tibia is assumed to behave as a rigid body. In this case a simple coordinate transformation has to be applied to calculate the residues corresponding to the changed location of O_T . This means that the location of O_T can be chosen such that it is useful for practical purposes. For example, O_T can be chosen to coincide with point E. In this case the matrices \underline{K}_e and \underline{G}_e are reduced to a null- and identity-matrix, respectively, which yields a simplification of relation (3.3.28) (this convenience will be used in section 3.3.2)

The modal parameters are system parameters and do not depend upon the loads \underline{l}_e or the displacements \underline{u} , which must be verified by experiments, although they can be a function of the parameters describing the static equilibrium position. For an undercritically damped system it holds

$$\underline{H}(f) = \sum_{k=1}^{N_m} \frac{\underline{A}_k}{2\pi jf - s_k} + \frac{\underline{\bar{A}}_k}{2\pi jf - \bar{s}_k} \quad (3.3.30)$$

The poles s_k can be written as a function of the dimensionless damping ξ_k and the undamped resonance angular velocity ω_{ok}

$$s_k = -\xi_k \omega_{ok} + j\omega_{ok} \sqrt{1 - \xi_k^2} \quad (3.3.31)$$

As for all relevant transfer function matrices introduced in this chapter, the characteristic shape of an element of such a matrix will be discussed in chapter 4.

An essential problem is caused by the need of some form of numerical postprocessing to extract the relevant parameters from the measured signals \underline{y} and \underline{l}_e . Here two basic parameter estimation techniques are available, which will be denoted as a time-domain technique and a frequency-domain technique, respectively.

First the time-domain technique will be considered. It is obvious that relation (3.3.28) can be transformed to the time-domain using an inverse Fourier transformation

$$\underline{y} = \int_0^{\infty} \underline{H}(t-\tau) \underline{G} \underline{l}_e(\tau) d\tau \quad (3.3.32)$$

with $\underline{H}(t)$ as the inverse Fourier transform of the transfer function matrix $\underline{H}(f)$, commonly denoted as the impulse response matrix of the system. Using measured columns \underline{y} and \underline{l}_e , the components of the matrix $\underline{H}(t)$ can be obtained from a (non-linear) curve fit. For an arbitrary excitation \underline{l}_e this yields a cumbersome procedure due to the need to evaluate the integral in relation (3.3.32). However, for certain types of signals relation (3.3.32) can be solved to obtain an explicit (non-linear) expression for \underline{y} as a function of time and the unknown parameters describing the matrix $\underline{H}(t)$. Impulse or sinusoidal excitation are examples of signals well suited for this purpose. However, such an approach was not taken into consideration as an efficient tool is available to determine the transfer function matrix $\underline{H}(f)$ directly.

The frequency-domain technique considered uses relation (3.3.28) as a starting point. The transfer function matrix $\underline{H}(f)$ can be obtained from calculated Fourier transforms $\underline{y}(f)$ and $\underline{l}_e(f)$. Subsequently a (non-linear) curve fit can be applied to extract the unknown system parameters describing the matrix $\underline{H}(f)$ (Mergeay 1980). To reduce the influence of measurement errors and errors due to non-linearity, usually the matrix $\underline{H}(f)$ is not determined from the Fourier transforms $\underline{y}(f)$ and $\underline{l}_e(f)$ but from estimates for the cross- and autopower spectra of the components of the column matrices \underline{y} and \underline{l}_e (Bendat and Piersol 1980). Spectral analysis has become increasingly important in engineering practice since developments in the field of computer technology and digital signal processing allow for an efficient

determination of these power spectra by means of the Fast Fourier Transform algorithm. In section 3.3.2 further attention will be paid to how for this case the transfer function matrix $\underline{H}(f)$ can be obtained.

3.3.2 Practical considerations

Relation (3.3.28) shows that the components of \underline{y} and \underline{l}_e must be measured to determine the behaviour of the joint. In the sequel it will be shown that some simplification can be obtained by a proper design of the measurements. Such a strategy is generally applied when modal analysis is carried out and results in experiments in which only linear displacements and forces are measured, avoiding measurement of angular displacements and torques.

Considering the components of the column \underline{y} it is seen that these consist of the translation vector \vec{c} and the rotation vector $\vec{\pi}$. As measurement of translations is easier accomplished than measurement of rotations, a method can be employed which avoids direct measurement of the latter (Angeles 1987, Padgaonkar et al. 1975). Under the assumption that the tibia behaves as a rigid body the linearized displacement vector of an arbitrary point P on the tibia is found from relation (3.3.5)

$$\Delta \vec{y}_p = \vec{y}_p - \vec{y}_{po} = \vec{c} - \underline{X}_p \cdot \vec{\pi} \quad (3.3.33)$$

Using a uni-axial displacement transducer the component of $\Delta \vec{y}_p$ along a line with momentary unit direction vector $\underline{R} \cdot \vec{n}_p$ can be measured, resulting in a signal s_p

$$s_p = \vec{n}_p \cdot \underline{R}^c \cdot \Delta \vec{y}_p = \vec{n}_p \cdot \underline{R}^c \cdot (\vec{c} - \underline{X}_p \cdot \vec{\pi}) \quad (3.3.34)$$

Linearization of relation (3.3.34) yields

$$s_p = \vec{n}_p \cdot \underline{R}_o^c \cdot (\vec{c} - \underline{X}_p \cdot \vec{\pi}) \quad (3.3.35)$$

Substitution of the identity

$$-\vec{n}_p \cdot \underline{R}_o^c \cdot \underline{X}_p \cdot \vec{\pi} = \vec{n}_p \cdot \underline{R}_o^c \cdot (\vec{\pi} * (\underline{R}_o \cdot \vec{x}_p)) = (\vec{x}_p * \vec{n}_p) \cdot \underline{R}_o^c \cdot \vec{\pi} \quad (3.3.36)$$

in relation (3.3.35) yields

$$s_p = \vec{n}_p \cdot \underline{R}_o^c \cdot \vec{c} + (\vec{x}_p * \vec{n}_p) \cdot \underline{R}_o^c \cdot \vec{\pi} \quad (3.3.37)$$

From relation (3.3.37) it follows that the signal s_p results in one equation for the unknown vectors \vec{c} and $\vec{\pi}$. As depicted in appendix C the vectors \vec{c} and $\vec{\pi}$ can be determined from 6 such signals, measured on different points and in different directions.

Within the possibilities available it was decided to use 6 piezo-electric accelerometers to measure 6 signals \bar{s}_1 through \bar{s}_6 which for the linearized case considered are related to the vectors \vec{c} and $\vec{\pi}$ by

$$\bar{s}_p = \vec{n}_p \cdot R_O^C \cdot \vec{c} + (\vec{x}_p * \vec{n}_p) \cdot R_O^C \cdot \vec{\pi} \quad (3.3.38)$$

A disadvantage of the piezo-electric accelerometers used is that vibrations below approximately 5 Hz can not be measured due to charge-leakage. As a consequence the relevant frequency range for the measurements must be starting above 5 Hz. In chapters 4 and 5 it will be shown that this condition is met for the experiments carried out. The derivation in appendix C can now identically be used to determine the vectors \vec{c} and $\vec{\pi}$ from the 6 signals measured, provided a suitable choice is made for the locations \vec{x}_p and directions \vec{n}_p of the accelerometers. This results in the following relation derived in appendix C

$$\underline{A} \cdot \begin{vmatrix} R_O^C \cdot \vec{c} \\ R_O^C \cdot \vec{\pi} \end{vmatrix} = \sum_{p=1}^6 \begin{vmatrix} \bar{s}_p \vec{n}_p \\ \bar{s}_p \vec{x}_p * \vec{n}_p \end{vmatrix} \quad (3.3.39)$$

with

$$\underline{A} = \sum_{p=1}^6 \begin{vmatrix} \vec{n}_p \vec{n}_p & \vec{n}_p (\vec{x}_p * \vec{n}_p) \\ (\vec{x}_p * \vec{n}_p) \vec{n}_p & (\vec{x}_p * \vec{n}_p) (\vec{x}_p * \vec{n}_p) \end{vmatrix} \quad (3.3.40)$$

The choice for the locations \vec{x}_p and directions \vec{n}_p has to be such that the tensor matrix \underline{A} is regular. Moreover this choice has to be made in such a way that the signals contain sufficient information to determine all relevant vibration modes. This can be achieved by a proper alignment of the transducers with respect to the spatial orientation of the vibration modes of the tibia.

The kinematics of the tibia can now be described by means of the vectors \vec{c} and $\vec{\pi}$ but also by means of the 6 signals \bar{s}_p . As relation (3.3.39) gives a linear set of equations for \vec{c} and $\vec{\pi}$, in general there exists a bijective linear relationship between these two descriptions, which can be expressed by

$$\vec{s} = \underline{H} \cdot \begin{vmatrix} R_O^C \cdot \vec{c} \\ R_O^C \cdot \vec{\pi} \end{vmatrix} \quad (3.3.41)$$

with

$$\underline{\underline{z}}^T = [s_1 \ s_2 \ s_3 \ s_4 \ s_5 \ s_6] \quad (3.3.42)$$

and $\underline{\underline{\Psi}}$ as a 6×2 vector matrix (see appendix C). So far it has been assumed that the displacements $\underline{\underline{z}}$ can be obtained from the measured accelerations. This can either be done using a numerical integration in the time-domain or by integration in the frequency domain as the Fourier transform $\underline{\underline{z}}(f)$ of the column $\underline{\underline{z}}$ is given by

$$\underline{\underline{z}}(f) = -4\pi^2 f^2 \underline{\underline{z}} \quad (3.3.43)$$

Hence it follows that integration in the frequency domain easily can be carried out.

Written in matrix representation with respect to vector base $\underline{\underline{z}}$ equation (3.3.41) yields

$$\underline{\underline{z}} = \underline{\underline{\Psi}} \underline{\underline{R}}_{06}^T \underline{\underline{u}} \quad (3.3.44)$$

with

$$\underline{\underline{R}}_{06} = \begin{vmatrix} \underline{\underline{R}}_0 & \underline{\underline{0}} \\ \underline{\underline{0}} & \underline{\underline{R}}_0 \end{vmatrix} \quad (3.3.45)$$

and $\underline{\underline{\Psi}}$ as the 6×6 non-singular matrix representation of $\underline{\underline{\Psi}}$. The orthogonal matrix $\underline{\underline{R}}_{06}$ can be used to define a transfer function matrix $\underline{\underline{H}}_0(f)$, which is obtained if all vector and tensor quantities in relation (3.3.25) are represented with respect to vector base $\underline{\underline{z}}_0$ which is given by $\underline{\underline{z}}_0^T = \underline{\underline{R}}_0 \cdot \underline{\underline{z}}^T$

$$\underline{\underline{H}}_0(f) = \underline{\underline{R}}_{06}^T \underline{\underline{H}}(f) \underline{\underline{R}}_{06} \quad (3.3.46)$$

The poles of the transfer function matrices $\underline{\underline{H}}_0(f)$ and $\underline{\underline{H}}(f)$ are identical, but the residues $\underline{\underline{A}}_{k0}$ and $\underline{\underline{A}}_k$ are related by

$$\underline{\underline{A}}_{k0} = \underline{\underline{R}}_{06}^T \underline{\underline{A}}_k \underline{\underline{R}}_{06} \quad (3.3.47)$$

The residue matrices $\underline{\underline{A}}_{k0}$ represent vibration modes with respect to the static equilibrium position and therefore are useful to visualize motions of the tibia and to compare vibrations of the tibia for different static equilibria as they represent displacements of the tibia with respect to a vector base attached to the tibia. This is easily verified by defining a column $\underline{\underline{u}}_0$ as

$$\underline{\underline{u}}_0 = \underline{\underline{z}}_0 \cdot \underline{\underline{u}} = \underline{\underline{R}}_{06}^T \underline{\underline{u}} \quad (3.3.48)$$

and substitution of relation (3.3.48) in relation (3.3.28)

$$\underline{\underline{u}}_0(f) = \underline{\underline{H}}_0(f) \underline{\underline{G}}_0 \underline{\underline{z}}_{e0}(f) \quad (3.3.49)$$

with \underline{G}_O and \underline{l}_{eO} as the matrix representations with respect to the vector base $\underline{\hat{e}}_O$ of the tensor matrix \underline{G} and the load vector \underline{l}_e , respectively.

A further transfer function matrix $\underline{H}_\psi(f)$ may be defined by

$$\underline{H}_\psi(f) = \underline{\Psi} \underline{H}_O(f) \underline{\Psi}^T = \underline{\Psi} \underline{R}_{O6}^T \underline{H}(f) \underline{R}_{O6} \underline{\Psi}^T \quad (3.3.50)$$

which relates the displacements \underline{g} to the loads \underline{l}_ψ

$$\underline{g}(f) = \underline{H}_\psi(f) \underline{l}_\psi(f) \quad (3.3.51)$$

with

$$\underline{l}_\psi(f) = \underline{\Psi}^{-T} \underline{G}_O \underline{l}_{eO} \quad (3.3.52)$$

By the coordinate transformation with the non-orthogonal matrix $\underline{\Psi}$, the original degrees of freedom stored in the column \underline{u}_O are replaced with the degrees of freedom stored in the column \underline{g} , which is allowed as this means no loss of information due to the regularity of the matrix $\underline{\Psi}$. The residues $\underline{A}_{\psi k}$ now can be interpreted as being related to the modal displacements of the tibia in the measurement direction of a particular transducer, located at a particular point of the tibia. It applies that

$$\underline{A}_{\psi k} = \underline{\Psi} \underline{A}_{kO} \underline{\Psi}^T \quad (3.3.53)$$

The load column \underline{l}_ψ can easily be determined as $\underline{\Psi}$ follows from the position and orientation of the accelerometers with respect to the tibia, \underline{G}_O depends on the location where the external load acts on the tibia and \underline{l}_{eO} must be determined by measurement of the external load applied. It is obvious that if $\underline{H}_\psi(f)$ can be determined, the transfer function matrix $\underline{H}(f)$ can be determined according to relation (3.3.50) as the matrices $\underline{\Psi}$ and \underline{R}_O are regular.

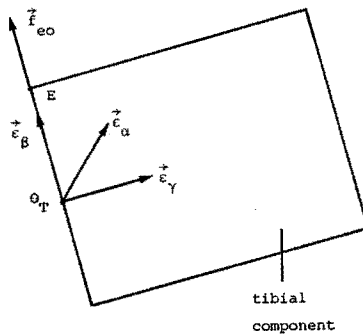


Fig. 3.3.3 Application of a force \vec{F}_{eO} along a line with unit direction vector \vec{n}_{eO} , which coincides with \vec{e}_β in this configuration.

Now suppose that a force $\underline{f}_{eo} = f_e \underline{n}_{eo}$ is exerted on the tibia such that its unit direction \underline{n}_{eo} coincides with one of the coordinate axes of the vector base connected to the tibia (Fig. 3.3.3).

In this case \underline{x}_{eo} (the column matrix representing the position of point E with respect to the vector base $\underline{\hat{x}}$) can be written as

$$\underline{x}_{eo} = \lambda_e \underline{n}_{eo} \quad (3.3.54)$$

where λ_e determines the exact position of point E. It then holds that

$$\underline{l}_{eo}(f) = \begin{vmatrix} \underline{n}_{eo} \\ \underline{\rho} \end{vmatrix} f_e(f) \quad (3.3.55)$$

$$\underline{G}_o \underline{l}_{eo} = \underline{l}_{eo} \quad (3.3.56)$$

or

$$\underline{l}_{\psi}(f) = \underline{\Psi}^{-T} \underline{l}_{eo}(f) \quad (3.3.57)$$

With the chosen location and orientation of the accelerometers (appendix C) it follows

$$\underline{\Psi}^{-T} = \begin{vmatrix} 1 & 0 & 0 & 0 & -1/z_5 & 0 \\ 0 & 1 & 0 & 1/z_5 & 0 & 0 \\ 0 & 0 & 1 & 0 & 0 & 0 \\ 0 & 0 & 0 & 0 & 1/z_5 & 1/y_5 \\ 0 & 0 & 0 & 0 & 0 & -1/y_5 \\ 0 & 0 & 0 & -1/z_5 & 0 & 0 \end{vmatrix} \quad (3.3.58)$$

where y_5 and z_5 determine the location of the accelerometers with respect to O_T (appendix C). Substitution of relation (3.3.58) into relation (3.3.57) yields a simple expression for $\underline{l}_{\psi}(f)$

$$\underline{l}_{\psi}(f) = \begin{vmatrix} \underline{n}_{eo} \\ \underline{\rho} \end{vmatrix} f_e(f) \quad (3.3.59)$$

Relation (3.3.59) in combination with relation (3.3.51) yields

$$\underline{g}(f) = \underline{H}_{\psi}(f) \begin{vmatrix} \underline{n}_{eo} \\ \underline{\rho} \end{vmatrix} f_e(f) \quad (3.3.60)$$

Relation (3.3.60) reveals that for an experiment in which \underline{n}_{eo} coincides with coordinate axis j ($j=1,2,3$) of the vector base connected to the tibia, a component $s_i(f)$ ($i=1,2,3,4,5,6$) of the column matrix $\underline{g}(f)$ is given by

$$s_i(f) = H_{\psi,ij}(f) f_e(f) \quad (j=1,2,3) \quad (3.3.61)$$

If this approach is applied, two points should be considered:

- * it must be assured that this excitation technique shows all relevant vibration modes in the frequency range of interest. As no torques are taken into consideration vibration modes, which only are excited when a torque is exerted, may not have a component in the signals measured and therefore may falsely be omitted. To verify that this does not occur additional experiments are necessary in which a force is exerted that does not coincide with one of the coordinate axes. For all experiments done on the knee joint specimens described in chapters 4 and 5, it turned out that such experiments yielded no additional resonance phenomena.
- * care must be taken that no torques or forces with a leverarm with respect to O_T are exerted on the tibia as otherwise the description given above is not valid. This must be taken into consideration when selecting a method to apply the dynamic force.

The calculation of the elements $H_{\psi,ij}(f)$ according to relation (3.3.61) can now efficiently be done by means of spectral analysis. As this computational process is essentially straightforward, it is not discussed in detail. In appendix D an overview is given of the essential steps involved, which results in the following expression

$$H_{\psi,ij}(f) = - \frac{S_{\ddot{s}_i f_e}(f)}{S_{f_e f_e}(f)} \frac{1}{4\pi^2 f^2} \quad (j=1,2,3) \quad (3.3.62)$$

Here $S_{\ddot{s}_i f_e}(f)$ is the cross power spectrum of the signals \ddot{s}_i and f_e , and $S_{f_e f_e}(f)$ is the autopower spectrum of the dynamic force f_e . These spectra are calculated, in an averaging process to reduce the influence of measurement errors and errors due to non-linearity, from the measured signals by means of a Discrete Fourier Transformation. The coherence function $\gamma_{\psi,ij}^2(f)$ (introduced in appendix D) is an important measure to judge whether measurement errors or errors due to non-linearity play a significant role and is given by

$$\gamma_{\psi,ij}^2(f) = \frac{S_{\ddot{s}_i f_e}(f) S_{\ddot{s}_i f_e}(f)}{S_{\ddot{s}_i \ddot{s}_i}(f) S_{f_e f_e}(f)} \quad (3.3.63)$$

with $S_{\ddot{s}_i \ddot{s}_i}(f)$ as the autopower spectrum of the measured acceleration \ddot{s}_i . For an ideal measurement the coherence function is 1 in the frequency range of interest. If the coherence function deviates from 1, measurement errors or errors due to non-linearity play a role although no distinction can be made between the influence of the separate error sources (of course it is assumed that the magnitude of the signals is well above the lower limit below which a particular

transducer fails to respond, as otherwise an additional error source is introduced). To be able to analyse the influence of non-linearity the magnitude of the dynamic force exerted on the tibia must be varied. If changes in this magnitude result in significant changes in the transfer functions found, non-linearity is likely to play a role. In this case the system considered cannot be seen as a linear system and application of transfer function analysis is questionable. It is hereby assumed that the frequency contents of the dynamic force f_e is such that its autopower spectrum is not zero in the frequency range of interest. For sinusoidal excitation e.g., $S_{f_e f_e}(f)$ is zero except for a particular frequency. In this case only limited information can be obtained about the transfer functions $H_{\psi, ij}(f)$ unless a large number of experiments is carried out with varying frequency of the sinusoidal force. Such an excitation technique was not taken into consideration. Excitation signals which cover a broader frequency range are impact and random excitation, as theoretically their autopower spectrum can be adjusted such that it is constant in the frequency range of interest. Impact excitation has the disadvantages that the magnitude of the load is difficult to control and that non-linearities are rapidly introduced due to the high peak-load. Random excitation is relatively easily applied by means of a shaker and the frequency contents can easily be controlled as a random signal can be generated digitally. It was therefore decided to use a random signal for excitation of the tibia.

In summary it can be stated that the dynamic behaviour of the tibia (considered as a rigid body) can be investigated by varying

- * the static equilibrium position with respect to the femur
- * the static load exerted on the muscle tendons
- * the point of application, direction and magnitude of the external loads applied to the tibia

To quantify the dynamic behaviour of the tibia the following parameters must be measured

- * the kinematic parameters describing the static equilibrium position
- * the forces on the bracing wires
- * the signals from at least 6 accelerometers
- * the dynamic load exerted on the tibia

3.3.3 A descriptive model for the load transmission through the joint

In sections 3.3.1 and 3.3.2 emphasis was laid on how the dynamic characteristics of the tibia can be obtained by measurement of loads exerted on and accelerations of the tibia. Another important aspect of the force transmission through the joint is found in the loads transmitted to the femur. To arrive at an expression for these loads Fig. 3.3.4 is considered.

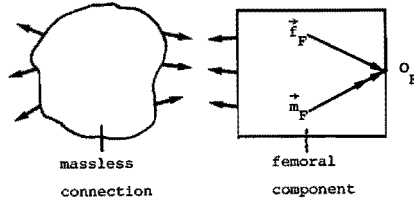


Fig. 3.3.4 Interactions between the femoral component and the massless connection resulting in a transmitted force and moment.

In paragraph 3.3.1 it was assumed that the load exerted on the tibia by the joint elements results in a force \vec{F}_j and a moment \vec{m}_j which only depend upon damping and stiffness characteristics and briefly can be written as

$$\vec{F}_j = \underline{K}_j \cdot \vec{u} + \underline{B}_j \cdot \dot{\vec{u}} \quad (3.3.64)$$

In relation (3.3.64) inertial effects are neglected. This also implies that the forces and moments exerted on the femur are a function of \vec{u} and $\dot{\vec{u}}$ only. As the femur is considered as a space-fixed, rigid body the load exerted on the femur can be measured in terms of a force \vec{F}_F and a moment \vec{m}_F with respect to O_F . These transmitted loads can then be written as

$$\begin{pmatrix} \vec{F}_F \\ \vec{m}_F \end{pmatrix} = \begin{pmatrix} \underline{S}_F \\ \underline{D}_F \end{pmatrix} \cdot \begin{pmatrix} \vec{u} \\ \dot{\vec{u}} \end{pmatrix} \quad (3.3.65)$$

where \underline{S}_F and \underline{D}_F represent stiffness and damping properties. Of course \underline{S}_F and \underline{D}_F are related to the tensor matrices \underline{K}_j and \underline{B}_j in relation (3.3.64) but this relationship is not known yet. Relation (3.3.65) results in a transfer function matrix $\underline{H}_F(f)$ if all vector- and tensor quantities are represented with respect to the fixed vector base \vec{e}

$$\underline{x}_F(f) = \underline{H}_F(f) \underline{u}(f) \quad (3.3.66)$$

$$\underline{H}_F(f) = \underline{S}_F(f) + 2\pi j f \underline{D}_F(f) \quad (3.3.67)$$

The elements of the transfer function matrix $\underline{H}_F(f)$ can be determined from measured components of the columns \underline{x}_F and \underline{u} .

Measurement of the transmitted forces and moments can provide valuable information as they are related to the kinematical parameters of the tibia by stiffness and damping characteristics only and because they do not depend upon inertial effects (if the description given above is valid). Furthermore, they may give useful information for validation of a structural numerical model.

Using relation (3.3.28) a relation can be laid between the loads exerted on the tibia and the loads transmitted to the femur

$$\underline{x}_F(f) = \underline{H}_{F1}(f) \underline{G} \underline{l}_e(f) \quad (3.3.68)$$

with

$$\underline{H}_{F1}(f) = \underline{H}_F(f) \underline{H}(f) \quad (3.3.69)$$

Finally, using relations (3.3.55) and (3.3.56) relation (3.3.68) can be written as

$$\underline{x}_F(f) = \underline{H}_{F1} \underline{R}_{06} \underline{G}_0 \underline{l}_{e0}(f) = \underline{H}_{F1,0}(f) \begin{vmatrix} \underline{H}_{e0} \\ \underline{g} \end{vmatrix} \underline{f}_e(f) \quad (3.3.70)$$

with

$$\underline{H}_{F1,0}(f) = \underline{H}_{F1}(f) \underline{R}_{06} \quad (3.3.71)$$

3.4 Measurement methods

In section 3.3 a number of parameters are indicated that must be measured to quantify the dynamic behaviour of the knee joint. In this section a number of transducers are discussed which are applied in all experiments described in chapters 4 and 5.

3.4.1 Measurement of the static load on the muscle tendons

To measure the static load on the bracing wires strain-gauges are glued to each stud of the stud-and-nut combinations described in section 3.2. Compensation for bending moments and temperature is included using 4 strain-gauges in a Wheatstone-bridge. The uni-axial force transducers thus obtained were calibrated for axial forces from

0 to 1500 N, showing a relative overall accuracy of approximately 1%. To monitor the forces during measurements a LED-display is available.

3.4.2 Measurement of accelerations on the tibia

As depicted in section 3.3.2, 6 accelerometers are applied to determine the kinematical behaviour of the tibia. The accelerometers can be mounted on the stainless steel cylinder P which is casted around the distal part of the tibia (see section 3.2). Fig. 3.4.1 shows the spatial orientation of the accelerometers for a particular joint specimen.

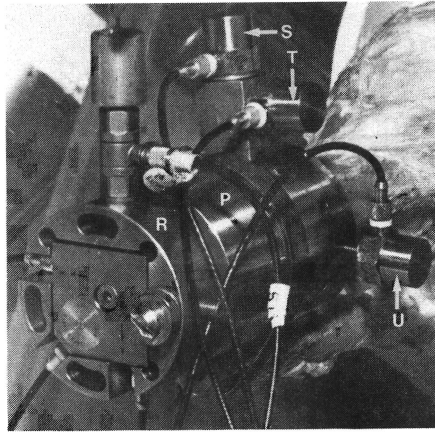


Fig. 3.4.1 Accelerometers mounted on the tibia.

A tri-axial accelerometer (Brüel & Kjaer type 4321) is mounted in a brass housing (R) which is bolted to the bottom plane of the cylinder P. Three uni-axial accelerometers S, T and U (Brüel & Kjaer type 4367) are mounted on the surface of the cylinder P. This set-up corresponds to that described in appendix C. The 6 signals from the accelerometers are led to charge-amplifiers (Kistler type 5007) resulting in 6 analog signals. For the coordinates y_5 and z_5 describing the location of the accelerometers S, T and U it holds:

$$y_5 = 0.035 \text{ m}, z_5 = 0.06 \text{ m}.$$

3.4.3 Measurement of transmitted loads

To measure the forces and moments transmitted to the femur, a 3-D piezo-electric force platform is included in the basic experimental set-up discussed in section 3.2. As commercially available platforms were not suited due to the need to pass the bracing wires through the platform, a force platform was specially developed for this purpose with assistance of Kistler A.G., Switzerland. The platform is shown in detail in Fig. 3.4.2.

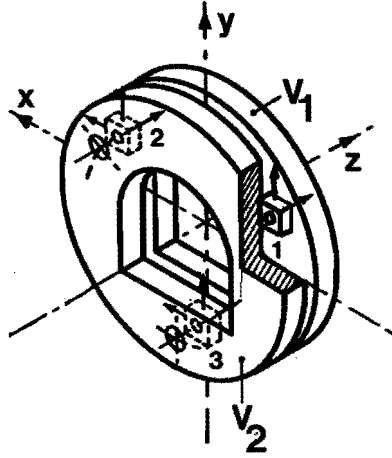


Fig. 3.4.2 The piezo electric force platform.

It basically consists of two circular plates with an asymmetric opening to pass the bracing wires. Plate V_1 is bolted to block C of the experimental set-up, whereas plate V_2 acts as a rigid foundation for clamping flange E. Between these two plates three 3-D loadcells (Kistler type 9251) are mounted under an axial preload of 5000 N. Each loadcell k produces signals s_{kx} , s_{ky} and s_{kz} , which represent forces along the x-, y- and z-axis of the loadcell, respectively. The external force and moment with respect to the center O_F of the platform can now be obtained from:

$$\mathbf{f}_p^T = [f_{px} \ f_{py} \ f_{pz}] \text{ and } \mathbf{m}_p^T = [m_{px} \ m_{py} \ m_{pz}] \quad (3.4.1)$$

with

$$f_{px} = s_{1x} + s_{2x} + s_{3x} \quad (3.4.2)$$

$$f_{py} = s_{1y} + s_{2y} + s_{3y} \quad (3.4.3)$$

$$f_{pz} = s_{1z} + s_{2z} + s_{3z} \quad (3.4.4)$$

$$m_{px} = r_p ((s_{1z} + s_{2z}) \frac{1}{2} - s_{3z}) \quad (3.4.5)$$

$$m_{py} = r_p ((s_{1z} - s_{2z}) \frac{\sqrt{3}}{2}) \quad (3.4.6)$$

$$m_{pz} = r_p (s_{3x} - (s_{1x} + s_{2x}) \frac{1}{2} + (s_{2y} - s_{1y}) \frac{\sqrt{3}}{2}) \quad (3.4.7)$$

Here r_p is the radius of the circle the loadcells are placed on ($r_p = 0.09$ m).

The determination of the forces \underline{f}_p and moments \underline{m}_p according to relations (3.4.2) through (3.4.7) is carried out by analog summing amplifiers which are incorporated in the Kistler electronic unit type 9807. The output of this unit consist of 6 analog signals representing the components of \underline{f}_p and \underline{m}_p .

The platform was calibrated by Kistler A.G. for forces s_{kx} and s_{ky} from 0 to 2500 N and a force s_{kz} from 0 to 5000 N. The overall relative accuracy was found to be better than 1.5% which includes errors due to non-linearity and cross-talk between the different signals.

3.4.4 Measurement of the static equilibrium position

In section 3.1 it was discussed that the static equilibrium position of the joint should be measured as it is expected to determine in a non-linear way the dynamic behaviour of the joint. The static equilibrium position must be quantified by means of the 6 mutually independent kinematic parameters describing the components of the translation vector \vec{a}_0 and the rotation tensor R_0 with respect to the inertial vector base \vec{e} connected to the femur. Accurate measurement of these parameters requires a rather complex measuring system. As the present investigation focuses on the dynamic characteristics of the knee joint, it was decided to select a simple method to get an indication about the static equilibrium position of the joint.

Making use of a goniometer the orientation of the tibia with respect to the femur can be measured, whereas the translations of the tibia can be measured by means of a ruler. Of course such a measurement technique has only limited accuracy ($\pm 2^\circ$ for the rotations and ± 1 mm for the translations), but it provides an easy tool for measurement of the static equilibrium position. It allows of frequently monitoring, with some accuracy, changes in the static equilibrium position. Furthermore this technique can provide an indication for the required accuracy of a more sophisticated measurement technique. For example, if a different dynamic behaviour of the joint is found for changes in static equilibrium position which are within the accuracy of the method discussed above, it is obvious that another measurement technique with a far better accuracy should be selected. On the other hand, if drastic changes in the static equilibrium position do not result in significant changes in the dynamic behaviour of the joint the accuracy of another measurement technique does not need to exceed the values given above.

3.5 A data-acquisition system

Using the measurement methods discussed in the previous section, the dynamic behaviour of the knee joint is quantified by means of a number of analog signals. To allow for digitization of these signals and storage of the digitized signals a data-acquisition system (DAS) is indispensable. Furthermore, some tool for numerical postprocessing

will be necessary, e.g. to calculate the transfer function between two signals which subsequently can be used for determination of the modal parameters, as was indicated in section 3.3.

For this purpose a DAS was developed, based on an IBM Personal Computer and a commercially available laboratory interface (TECMAR Labmaster) (Fig. 3.5.1).

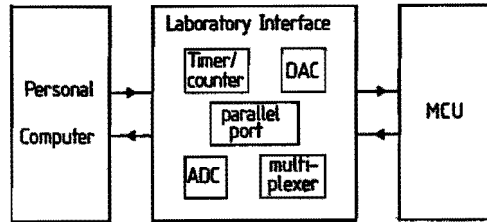


Fig. 3.5.1 Hardware for the data-acquisition system.

This basic hardware is expanded with a 16 channel measurement control unit (MCU) and a software package that allows for software control of the laboratory interface and the MCU. Besides the software package provides a tool for implementation of postprocessing of the digitized signals. To cope with the limited storage capacity of the PC, additionally use is made of a tape-streamer (IRWIN type 310) to back-up the measured data. Finally a connection is available to a PRIME 750 mini-computer for off-line number crunching and extended graphic and plotting facilities.

The following paragraphs in this section are used to discuss the prime elements of the DAS mentioned in more detail.

3.5.1 The personal computer

The Personal Computer acts as a central controller for measurements and allows for storage and postprocessing of the digitized signals. It is a standard IBM PC-XT with an INTEL 8088 CPU (4.77 MHz clock) equipped with an INTEL 8087 numerical coprocessor, 640 Kb RAM, an IBM Color Graphics Adapter, a 10 Mb hard disk and a 360 Kb floppy unit. The operating system used is Micro-Soft DOS 3.20.

3.5.2 The laboratory interface

The TECMAR Labmaster serving as an interface between PC and experimental set-up provides the following standard features:

- * a 12 bit Analog to Digital Converter (ADC) which is installed in a 2-complements mode with an input range of -5 to +5 Volt. Its maximum conversion rate is 30 KHz;

- * two 12 bit Digital to Analog Converter's (DAC) which are installed in a 2-complements mode with an output range of -10 to + 10 Volt;
- * a timer/counter chip with 5 individually programmable 16 bit counters which can be used to count external events or to generate blockwaves with a specified frequency;
- * an INTEL 8255 Programmable Parallel Port I.C. (PPI) with 24 I/O lines which can be used for control of external devices;
- * a 16 channel multiplexer enabling to select one of the 16 single ended analog inputs to be connected to the ADC.

The laboratory interface is plugged in in one of the available slots of the PC and is installed in a memory-mapped mode, thus allowing for software control of the board by means of memory read and write commands from or to the 16 memory locations (bytes) the board occupies.

3.5.3 The measurement control unit

Although the laboratory interface is suited to be directly used for digitization of the analog signals, a measurement control unit (MCU) was developed, essentially to allow for improving the accuracy of the digitized signals and to include a possibility for simultaneous measurement of all signals. The MCU contains 16 channels which each are built up as shown in Fig. 3.5.2.

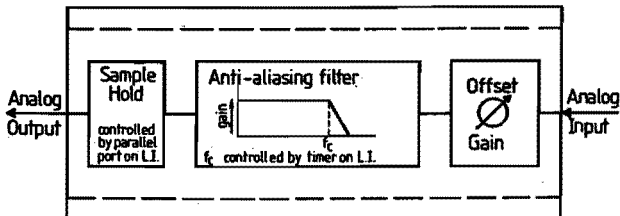


Fig. 3.5.2 Elements of each channel of the measurement control unit.

The analog input signal first can be adjusted in magnitude or offset. In general this is necessary to assure the signal to meet optimally the range of the ADC, as otherwise digitization errors are significant. This correction can be done manually using 2 potentiometers.

Next the analog signal is filtered by means of a 48 dB/octave low-pass Butterworth filter (National Semiconductor MF10CN Universal Dual Switched Capacitor Filter). The reason for using these filters is that in general the analog signal to be digitized with a sampling

frequency f_s Hz must satisfy Nyquist's criterion. This states that the highest frequency component in the analog signal must be less than $0.5*f_s$, as otherwise aliasing occurs resulting in erroneous measurements. If it cannot be guaranteed that the signal meets this criterion, its frequency contents must be limited. Two basic methods exist to filter the analog signal. The first method uses a high speed ADC in combination with a relatively simple analog filter. The sampled signal is subsequently filtered digitally and decimated to obtain the desired sampling frequency. This approach is favourable due to its flexibility, but as the digital filtering asks for a hardware implementation to obtain an acceptable throughput rate, the complexity of the DAS is considerably increased. For this reason it was decided to use a higher order low-pass analog filter with a programmable cut-off frequency. If desired, the digitized signals can be filtered further using a software implementation of a digital filter. The Butterworth filter mentioned was chosen because the magnitude of its transfer function is maximally flat in the pass-band, which is theoretically given by

$$|H(f)| = \frac{1}{\sqrt{1 + (f/f_c)^{2n}}} \quad (3.5.1)$$

The cut-off frequency f_c (-3 dB) of these filters is controlled by the frequency of a symmetric block wave obtained from one of the timers on the laboratory interface. As the timer-chip is programmable the cut-off frequency of the filters is under software control. For a cut-off frequency f_c of 100 Hz. Fig. 3.5.3 shows the transfer function of such a filter.

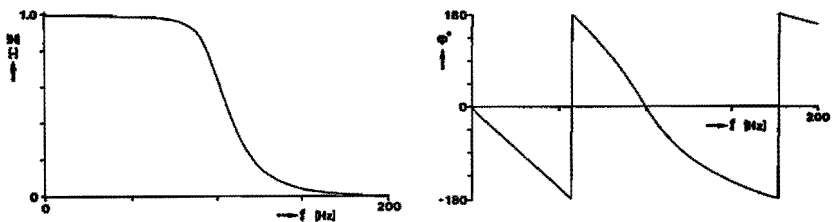


Fig. 3.5.3 The transfer function $H(f)$ of the Butterworth low-pass filters for a cut off frequency f_c of 100 Hz. $H(f)$ is given as the magnitude $|H|$ and phase ϕ ($H(f) = |H|\exp(j\phi)$).

An important characteristic of the filter is the phase shift. Ideally the phase shift is linear as a function of the frequency, because this results in a constant time-delay between input and output of the

filter (apart from a reduction in magnitude of the different frequency components in the signal). As the phase shift of the Butterworth filter is almost linear in the pass-band, the small deviations of linearity will not cause serious signal distortion. The filtered analog signal is next led to a sample-and-hold circuit (S/H). The S/H is controlled by one of the I/O lines of the PPI on the laboratory interface and is meant to allow of simultaneous measurement of all signals. The S/H are simultaneously activated, thus freezing all signals passed. The frozen signals can subsequently be multiplexed and converted to a digital representation. This approach allows of simultaneous measurement of all signals although a single ADC is used. A disadvantage is that the maximum sampling frequency achievable depends on the number of signals to be digitized. As the maximum conversion rate of the ADC is 30 KHz, in case of 1 signal theoretically the maximum sampling frequency is 30 KHz, whereas for 16 signals the maximum sampling frequency will be $30 \text{ KHz}/16 = 1875 \text{ Hz}$. These values are well beyond the upper frequency limit of 100 Hz for analysis of the knee joint.

3.5.4 The software package

The hardware of the DAS discussed in the previous paragraphs must be controlled by software. To obtain sufficient flexibility a software package has been developed that basically consists of two parts. The first part allows for interactively entering measurement specifications, while the second part takes care of the actual measurements. The measurement specifications consist of the channels selected to be measured, the desired sampling frequency, the desired cut-off frequency of the analog filters, the number of samples to be taken and some additional information used in further processing. Besides an option is included to define an analog signal to be generated during measurements. For this purpose one of the DAC's on the laboratory interface is used. This analog signal can be amplified and then be used to control the dynamic load on the knee joint specimen e.g.. This first part of the software package is written in Fortran (Micro-Soft Fortran-77 V3.20). The second part of the software package uses the specifications entered in the first part. The raw data from the ADC is stored either in memory or in a set of disk files and then can be used for further processing (graphical representation, transfer function analysis e.g.). The second part of the software package is written in assembly language (Micro-Soft Macro Assembler 4.00) to optimize the speed of the digitization process. The maximum sampling rate when measuring 16 channels is 900 Hz, which is satisfactory with respect to the adapted 100 Hz upper frequency limit for analysis of the dynamic behaviour of the knee joint.

3.6 Summary

In this chapter an overview has been given of an experimental strategy, proposed to analyse the dynamic behaviour of the human knee joint in post-mortem experiments. To deal with the expected non-linear, time-dependent behaviour of the joint a local linearization technique (LLT) was assumed to provide a useful tool for both experiments as well as parametrization of the experimental results. Modal analysis herein plays an essential role. The LLT consists of two steps. First a stable static equilibrium position of the joint will be created by means of static forces exerted on selected muscle tendons. Secondly small dynamic loads will be applied to the tibia. Parameters describing the kinematic behaviour of the tibia and the transmitted loads can then be measured and related to the applied load by means of transfer functions. These transfer functions can be formulated as a function of a set of modal parameters. Variation of the static equilibrium position and the static load on the muscle tendons and deliberate damaging of selected joint elements are to be included in experiments to investigate their influence on the dynamic behaviour of the joint. For this purpose various measurement methods and a multichannel data-acquisition system have been discussed which can be used to quantify the behaviour of the joint and which enable to extract the modal parameters from measured responses of the joint by means of some form of numerical post-processing. Chapter 4 focuses on experiments done to see whether the strategy proposed is valid. The transfer functions discussed in this chapter will be used extensively. To give insight in the meaning of a particular transfer function attention will be paid in chapter 4 to how changes in stiffness and damping characteristics of a single degree of freedom mechanical system influence the transfer functions for such a system.

Chapter 4 Experiments I: Analysis in the frequency domain

To clarify to what extent the experimental strategy discussed in chapter 3 applies, experiments have been performed on 10 knee joint specimens. This chapter gives an overview of the obtained results. To judge the validity of the results, it is necessary to have insight into factors such as measurement accuracy and the dynamic behaviour of the experimental set-up. As these factors must be considered in combination with the dynamic behaviour of the joint specimen, this chapter is composed as follows. Section 4.1 gives an overview of the nature of the experiments. In section 4.2 a brief overview is given of the meaning of the transfer functions described in this chapter. Besides it is illustrated how these transfer functions for a single degree-of-freedom mechanical system are to be interpreted. In section 4.3 typical results are given, primarily to give an insight into the order of magnitude of relevant parameters and to discuss the phenomena found. Hence this section can be considered to provide a framework for discussions in the remainder of this chapter. In section 4.4 these results are used to consider inaccuracies and disturbing factors, introduced in the experimental procedure, and the influence of the experimental set-up upon the results obtained. An elaboration of section 4.3 can be found in sections 4.5 and 4.6, where a more detailed discussion is given on how the results are influenced by the static load on the muscle tendons and the dynamic load applied to the tibia, respectively. Finally in section 4.7 an assessment is given of the validity of the experimental strategy proposed in chapter 3.

4.1 Description of the experiments

In chapter 3 several aspects of the experimental design described in this chapter have been discussed. This section gives an overview of the execution of the experiments.

Ten knee joint specimens were used which are denoted with KNEE1 through KNEE10. Some of these specimens have been used in what can be considered as preliminary experiments. These experiments were a try-out for the measuring techniques discussed before. Therefore the results of these experiments are not taken into consideration in this chapter, leaving five specimens (KNEE6 through KNEE10) to be discussed in the remainder of this chapter. The experiments on KNEE1 through KNEE5 also resulted in a standardized experimental procedure which will be discussed in this section, focusing on the following aspects:

- * preparation of the joint specimen;
- * installation of the joint specimen in the experimental set-up and installation of the various transducers;

- * creation of a static equilibrium position;
- * application of the dynamic load;

Preparation of the joint specimen

The experiments start with the preparation of the joint specimen the day before the actual measurements are done. This preparation takes about 4 hours. The description given below is valid for all specimens used in the experiments described in chapters 4 and 5 and results from a standard preparation procedure. All knee joint specimens were excised from macroscopically intact human cadavera, freshly frozen at -80°C . Each specimen has an overall length of 0.4 m in extension, with an equal length of the tibia and the femur of 0.2 m. The day prior to the experiments the specimen is thawed in approximately 4 hours in water of 20°C . The preparation starts with a removal of the skin and subcutis. Subsequently the heads of the muscles are removed, such that the relevant muscle tendons are mobilised but left intact (the tendons of the musculus rectus femoris, musculus biceps femoris, musculus gracilis, musculus sartorius and musculus semitendinosus). During preparation care is taken to keep the joint capsule and extra-capsular ligaments intact. To be able to exert the static load on the muscle tendons a minimum length of approximately 0.1 m of the tendons is required. This does not cause problems for the tendons of the musculus rectus femoris and the musculus biceps femoris. However, the minimum length for the muscle tendons on the medial side of the joint can not be obtained for each specimen due to biological variability. Therefore for each specimen individually a selection has to be made whether to use the musculus sartorius, the musculus gracilis or the musculus semitendinosus. This choice is also determined by the cross-sectional area of the tendons mentioned. To avoid rupture of the tendon when the static load is applied, the tendon with the largest cross-sectional area is selected by visual inspection. Of course such a criterion is rather arbitrary, as it is not assured that a larger cross-sectional area corresponds to a larger load carrying capacity. However, it has turned out to be a reasonable choice as no rupture of the tendons has occurred during the experiments carried out. It is recognized that the use of a particular muscle tendon on the medial side of the joint may influence the results. An analysis to which extent such a choice influences the behaviour is beyond the scope of this investigation, and was therefore not carried out. It is felt however that, due to the location of the attachment areas of the muscle tendons on the medial side of the joint, selection of a particular muscle tendon does not necessarily lead to marked differences in the behaviour of different joint specimens. After preparation of the muscle tendons, the ends of the tibia and femur are cleared from muscular tissue and periost over a length of approximately 0.07 m to obtain a smooth and clean surface. This is necessary as this part of the bones is used for fixation in a cylinder (section 3.2.2). Hereby care is taken that the

longitudinal axis of each of the cylinders coincides as well as possible with the longitudinal axis of the corresponding bone. This is done as these axes are taken as one of the coordinate axes of the vector bases connected to the tibia and the femur and therefore must have resemblance for the different joint specimens to be able to compare the results obtained. After the preparation, the specimen is stored overnight at 5 °C in Ringer's solution and used in experiments the day after.

Installation of the knee joint specimen in the experimental set-up

The actual experiments start with clamping the knee joint in the experimental set-up described in section 3.2.2. This is a fairly simple procedure: by means of three bolts the cylinder F is tightly secured in the clamping flange E. While mounting the specimen it is assured that

- * the longitudinal axis of the cylinder F coincides with the z-axis of the piezo-electric force platform (G) which is located between the clamping flange and the steel block C. The z-axis is perpendicular to gravity. The longitudinal axis of the femur therefore, in a good approximation, has the same direction as the z-axis of the force platform;
- * the x-axis of the force platform lies in the, approximated, medio-lateral plane of the femur.

The y-axis of the force platform lies, due to the selection of the direction of the x- and z-axis, in the sagittal plane of the femur. With these choices the definition for the inertial vector base \vec{e} is complete as the centre of the force platform is the origin O_F of this vector base. It is noticed that the description given above depends on a visual determination of the sagittal plane of the femur and therefore is rather subjective. It is felt however that this procedure yields an orientation of the femur with respect to the force platform which can well be compared for different joint specimens. When the joint specimen has been clamped, the next step is to mount the accelerometers on the cylinder P attached to the tibia. To assure that the accelerometers have the position and orientation assumed in chapter 3 and appendix C, the cylinder P has a number of fixed locations where the accelerometers can be mounted. To assure that the axes of the cylinder correspond to those assumed in appendix A, care must be taken when the tibia is cast in this cylinder. The origin O_T of the vector base \vec{e} connected to the tibia coincides with the centre of the tri-axial accelerometer mounted in the brass housing R (see section 3.4.2).

The static equilibrium position

With the femur clamped and all accelerometers mounted, the experiments may be started. First a static equilibrium must be created. To do this, the three bracing wires are attached to the muscle tendons by means of the tendon clamps H. Subsequently the force acting on the bracing wires is increased to obtain the desired configuration of the joint specimen. For all experiments described in this chapter a joint configuration was chosen in which exo-endo rotation and ad-abduction can be neglected. Therefore the orientation of the tibia with respect to the femur can be described with the flexion angle only which was set at values of 20° , 30° and 60° for the results described in this chapter. This joint configuration can be obtained by proper selection of the magnitude of the forces on the muscle tendons. This procedure has to be carried out iteratively, as due to the time-dependent behaviour of the joint an initially applied load decreases (usually within 15 minutes) to a certain constant value, which can be 50% lower (this applies for all bracing wires). Simultaneously the joint configuration alters due to this change of the load acting on the bracing wires. Therefore in general the load must be increased after its constant value is reached, until the desired joint configuration is obtained.

Application of the dynamic load

If the desired static equilibrium position of the joint is obtained, the dynamic force can be applied to the tibia. For this purpose an electromechanical shaker (Ling Dynamics type 403) is attached to the brass housing R. As discussed in section 3.3.2 the shaker must exert a force along one of the coordinate axes of the vector base $\vec{\xi}$. To be able to exert this force without introducing undesired torques or bending moments the connection given in Fig. 4.1.1 is used. A uni-axial piezo-electric force transducer (a) (Kistler type 9301A) is mounted on the brass housing (R) such that its longitudinal axis coincides with the desired axis of the vector base $\vec{\xi}$ for a particular measurement. To obtain a connection to the head of the shaker (e), a series connection of a magnet (d), a flexible hose (c) and a piece of wire (b) is used. This connection is axially stiff (to avoid buckling under the axial load exerted by the shaker), but has little resistance against transverse loads. The magnet (d) is included to assure that the contact between the shaker and the joint specimen can easily be broken. This is of importance when the static load on the muscle tendons must be changed. Leaving the shaker in contact with the joint specimen would result in an uncontrolled static load on the joint as the shaker itself is a flexible element. The magnet (d) also protects the joint against undesired excessive transverse loads or torques as the magnet provides a connection which fails under these (high) loads. The shaker is suspended in the hook of a remote control travelling crane. This system has 6 degrees of freedom and therefore the global direction in which the dynamic force is applied can be chosen

freely. The suspension of the shaker has a resonance frequency of approximately 2 Hz, which is well below the lower frequency limit of 5 Hz, dictated by the use of piezo-electric transducers.

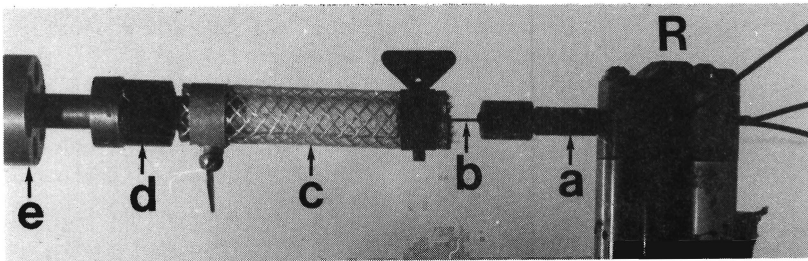
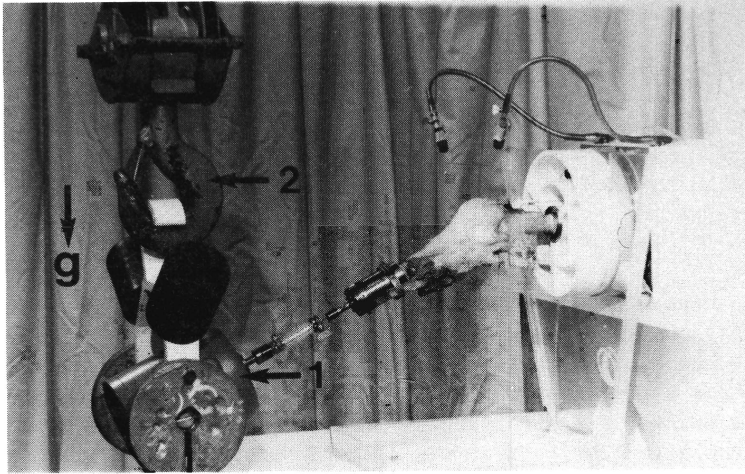


Fig. 4.1.1 The upper picture shows the electro-mechanical shaker (1), suspended in the hook (2) of a travelling crane, connected to the tibia by means of a flexible connection. This connection is shown in detail in the lower picture (see text)

The load applied to the tibia is derived from a random signal. To generate this random signal the data-acquisition system discussed in section 3.5 is used. The software package described there allows for definition of a band-width limited random signal which is generated during measurements by means of the DAC on the laboratory interface. This signal (-5 to +5 Volt) is amplified (Ling Dynamics PA300 amplifier) and used to control the shaker. The random excitation applied to the tibia has the typical shape given in Fig. 4.1.2.

A similar pattern is found for the responses of the joint (accelerations and transmitted loads). Bearing in mind the possible non-linearity of the joint, the magnitude of the dynamic load applied to the

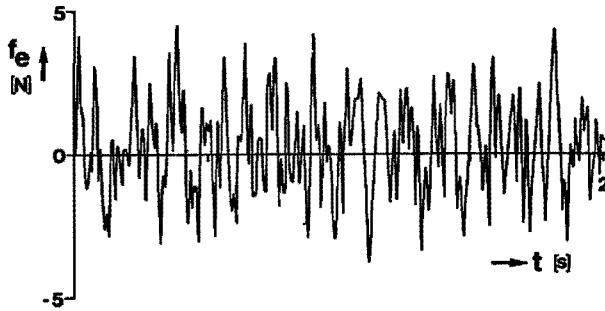


Fig. 4.1.2 Typical pattern of the force f_e applied to the tibia

tibia was taken as small as possible, but such that the signal to noise ratio was not endangered. In the experiments on KNEE1 through KNEE5 it was experienced that the coherence function (see section 3.3.2) is a useful tool for this purpose. Values of a coherence function below 0.8 (approximately) in the frequency range of interest are a strong indication that the dynamic load applied is too small (assumed that all charge amplifiers of the piezo-electric transducers used are adjusted to obtain a maximal analog signal to be measured). The variance σ_f^2 of the random excitation force therefore usually could not be set to values lower than approximately 1 N^2 . In the experiments the displacements of the loaded end of the tibia have a variance of maximally 10^{-6} m^2 . These displacements are hardly observed by eye and are not likely to result in geometrical non-linearities (which is essential in the local linearization technique).

4.2 Recapitulation and interpretation of the transfer functions

The experiments described in this chapter are represented by means of elements of the transfer function matrices $H_{\psi}(f)$ and $H_{F1,o}(f)$ derived in chapter 3.

The transfer function matrix $H_{\psi}(f)$ relates the displacements of the tibia to the applied force. An element $H_{\psi,ij}(f)$ is derived from the accelerations of accelerometer i ($i=1\dots 6$) and the force applied in direction j ($j=1\dots 3$).

As a reference a simplified representation of the joint is added to the figures in section 4.3, which has either of the shapes given in Fig. 4.2.1. The picture on the left in Fig. 4.2.1 indicates that the transfer function $H_{\psi,22}(f)$ considered relates the displacement of the end of the tibia in the β -direction ($i=2$) to the load applied in the same direction ($j=2$). Similarly the picture on the right indicates that the transfer function $H_{\psi,11}(f)$ considered relates the displacement of the end of the tibia in α -direction ($i=1$) to the load applied in the same direction ($j=1$).

The transfer function matrix $H_{F1,o}(f)$ relates the loads transmitted to the femur to the force applied to the tibia. An element $H_{F1,0ij}(f)$

relates the force applied in direction j ($j=1,2$ or 3) to the transmitted forces ($i=1,2$ or 3) or the transmitted moments ($i=4,5$ or 6). When such a transfer function is considered in section 4.3, a simplified representation of the joint to the corresponding figure is added as given in Fig. 4.2.2.

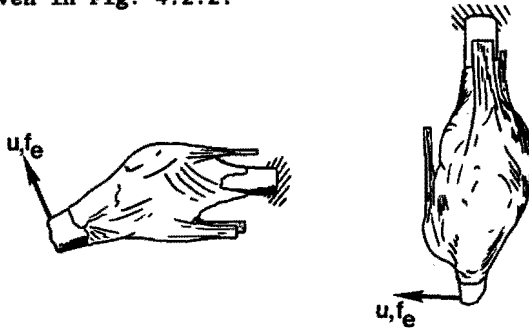


Fig. 4.2.1 Simplified representation of the joint and directions of the displacement and force applied for a particular transfer function $H_{\psi, ij}(f)$

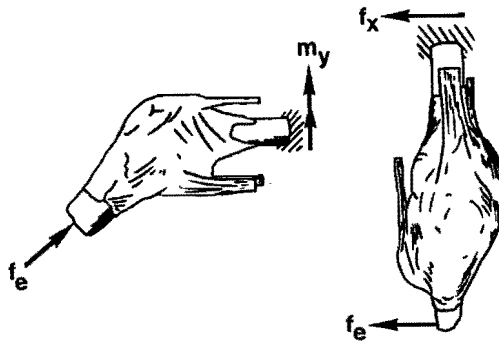


Fig. 4.2.2 Simplified representation of the joint and directions of the transmitted load and force applied for a particular transfer function $H_{F1, oij}(f)$

The picture on the left in Fig. 4.2.2 indicates that the transfer function $H_{F1, o11}(f)$ considered relates the force transmitted to the femur in x -direction ($i=1$) to the force applied in α -direction ($j=1$). Similarly the picture on the right in Fig. 4.2.2 indicates that the transfer function $H_{F1, o53}(f)$ considered relates the moment about the y -axis working on the femur ($i=5$) to the force applied in γ -direction ($j=3$).

To indicate how these transfer functions can be interpreted qualitatively, a single degree of freedom mechanical system given in Fig. 4.2.3 is considered.

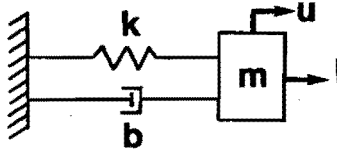


Fig. 4.2.3 A single degree of freedom mechanical system

For this system the transfer function matrix $H_\psi(f)$ has only one element $H_\psi(f)$ given by

$$H_\psi(f) = \frac{u(f)}{I(f)} = \frac{1}{-m(4\pi^2 f^2) + 2\pi jfb + k} \quad (4.2.1)$$

The transfer function matrix $H_{F1,0}(f)$ also contains only one element $H_{F1}(f)$ given by

$$H_{F1}(f) = \frac{(k + 2\pi jfb) u(f)}{I(f)} = \frac{k + 2\pi jfb}{-m(4\pi^2 f^2) + 2\pi jfb + k} \quad (4.2.2)$$

as the force f_F transmitted to ground is identical to

$$f_F = k u + b \dot{u} \quad (4.2.3)$$

Using the undamped resonance angular velocity $\omega_0 = \sqrt{(k/m)} = 2\pi f_0$ and the dimensionless damping $\xi = b/(2\sqrt{(km)})$ relations (4.2.2) and (4.2.3) yield

$$H_\psi(f) = \frac{1}{k} \frac{1}{1 - (f/f_0)^2 + 2\xi jf/f_0} \quad (4.2.4)$$

$$H_{F1}(f) = \frac{1 + 2\xi jf/f_0}{1 - (f/f_0)^2 + 2\xi jf/f_0} \quad (4.2.5)$$

Figs. 4.2.4 through 4.2.7 show the shape of these transfer functions for various values of b and k to indicate the influence of the damping and stiffness characteristics (the complex quantity $H(f)$ is given in terms of its magnitude $|H|$ and phase angle ϕ , which are related by $H(f) = |H|\exp(j\phi(f))$).

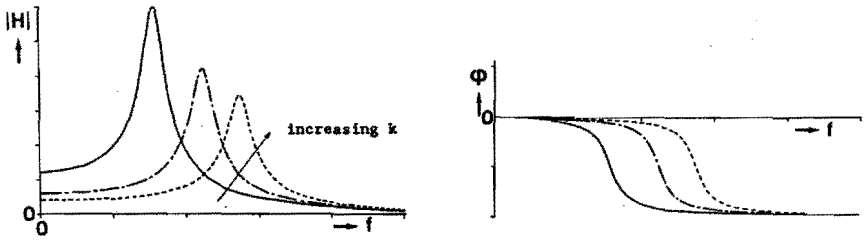


Fig. 4.2.4 Influence of the stiffness k on the transfer function $H_p(f)$

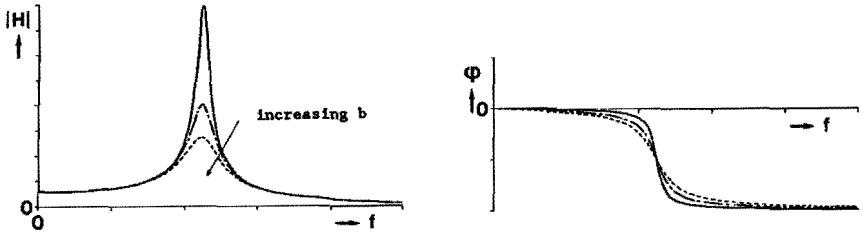


Fig. 4.2.5 Influence of the damping b on the transfer function $H_p(f)$

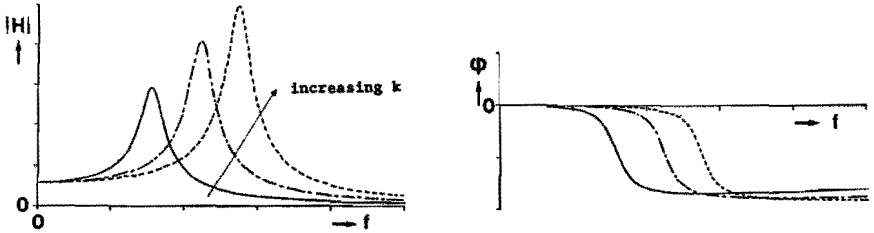


Fig. 4.2.6 Influence of the stiffness k on the transfer function $H_{FL}(f)$

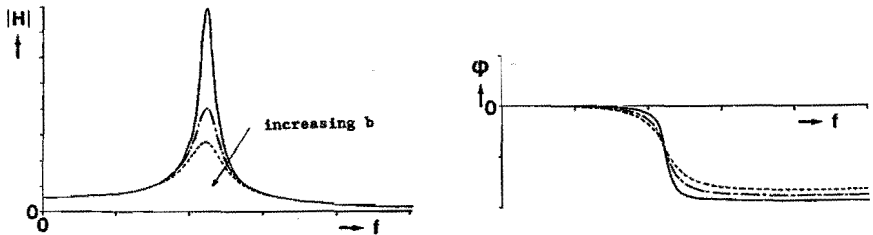


Fig. 4.2.7 Influence of the damping b on the transfer function $H_{FL}(f)$

4.3 Typical results for random excitation

The results for the experiments with random excitation on KNEE6 through KNEE9 will be discussed in this section, to provide a framework for the remainder of this chapter. To describe a particular experiment a number of parameters are relevant. These are gathered in a record of the following form:

KNEE@-H[row, col, dirf, σ_f^2 , ϕ , F_b , F_r , F_a]

The various symbols in such a record (which is used for annotation of figures) represent the following parameters:

@	represents the number of the knee joint specimen;
H	indicates which transfer function is considered ($H_\psi(f)$ or $H_{F1,0}(f)$);
row and col	determine the row and column number of the transfer function matrix a particular transfer function corresponds to;
dirf	is the direction along which the dynamic force was applied (dirf= α, β or γ)
σ_f^2	is the estimate for the variance of the dynamic load applied to the tibia, as determined from the signal measured with the uni-axial force transducer [N^2];
ϕ	is the flexion angle of the joint (degrees) as the prime characteristic for the static equilibrium position;
F_b, F_r, F_a	are the magnitude of the forces exerted on the muscle tendons [N].

First some of the elements of the transfer function matrix $H_\psi(f)$ are considered. For a particular experiment on KNEE9 (left knee, male, 36 years) Figs. 4.3.1 through 4.3.3 give three corresponding diagonal elements of the transfer function matrix $H_\psi(f)$. From these figures the following phenomena are observed which are common for all measurements. The frequency interval of interest is from 5 to 50 Hz. In this frequency range two distinct resonance frequencies are observed, which correspond to two vibration modes of the tibia. In the sequel these modes will be denoted with mode I and mode II, respectively. For mode I displacements of the tibia in β - and γ -direction are dominant, whereas for mode II the displacements of the tibia are mainly in α - and γ -direction.

Due to the non-linearity of the joint the value of the resonance frequencies depends on the static load on the muscle tendons etc. However, as a global measure modes I and II can be characterized by resonance frequencies of approximately 20 and 28 Hz, respectively.

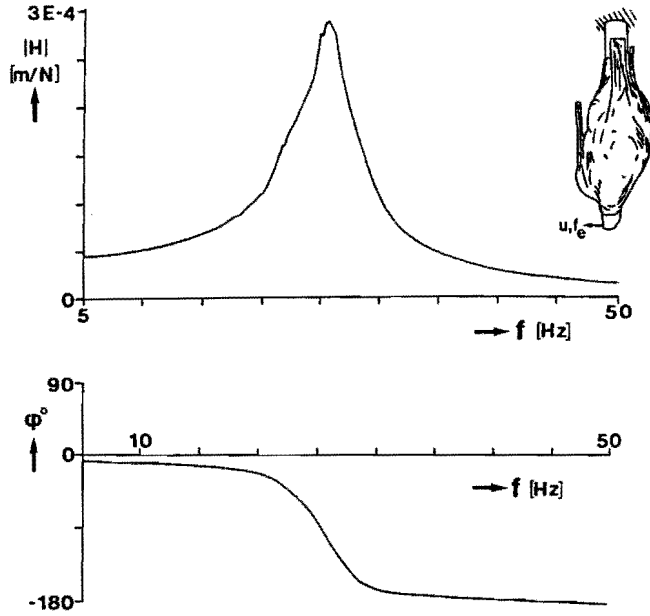


Fig. 4.3.1 KNEE9- H_ψ [1,1, α , $\sigma_F^2=15$, $\phi=30$, $F_D=118$, $F_T=240$, $F_a=97$]

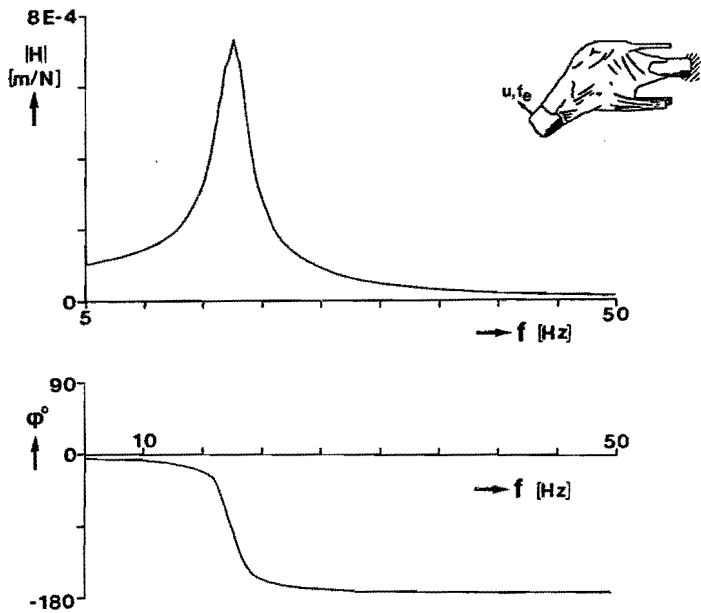


Fig. 4.3.2 KNEE9- H_ψ [2,2, β , $\sigma_F^2=15$, $\phi=30$, $F_D=118$, $F_T=240$, $F_a=97$]

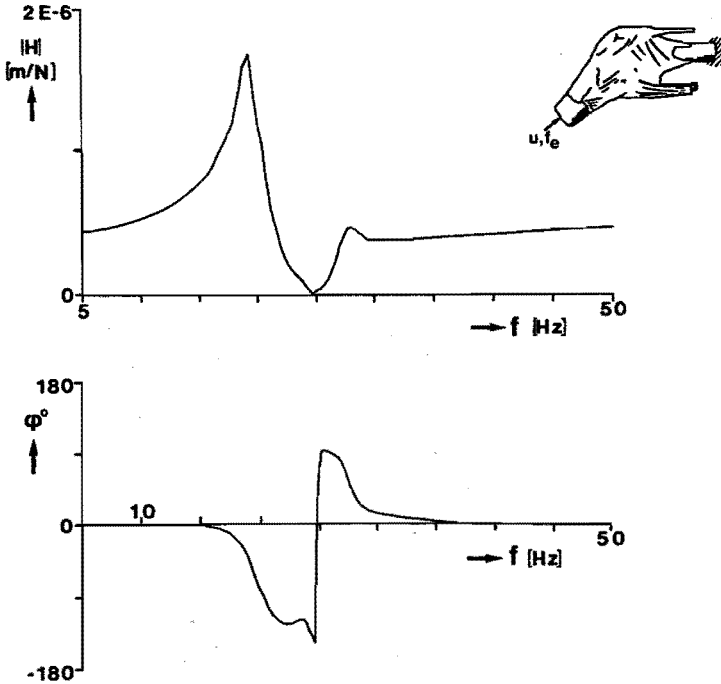


Fig. 4.3.3 KNEE9- H_{β} [3,3, γ , $\sigma_F^2=15$, $\phi=30$, $F_D=118$, $F_r=240$, $F_g=97$]

For the frequency interval from 0 to 5 Hz no information can be obtained. To assure that in this frequency range no resonance phenomena are falsely omitted, experiments were done with sinusoidal excitation in stead of random excitation. No additional resonance frequencies could be observed however. Similarly no additional resonance frequencies could be found in the frequency range from 50 to 100 Hz. From Figs. 4.3.1 through 4.3.3 it is seen that the elements of $H_{\beta}(f)$ have a marked difference in magnitude, depending on the particular frequency component considered. This indicates that the resistance of the knee joint against forces applied in the mutually orthogonal directions differs noticeably. For forces applied in the β -direction (flexion-extension) this resistance is least, whereas for forces applied in the γ -direction (axial loading) the highest resistance is found. From the results obtained it is seen that for mode I the kinematical behaviour of the tibia is dominated by displacements of the loaded end of the tibia in the β -direction. For mode II on the other hand, displacements of the loaded end of the tibia in the α -direction dominate.

The frequency dependent behaviour of the joint is also found in the elements of the transfer function matrix $H_{F1,o}(f)$, as illustrated in Figs. 4.3.4 through 4.3.6.

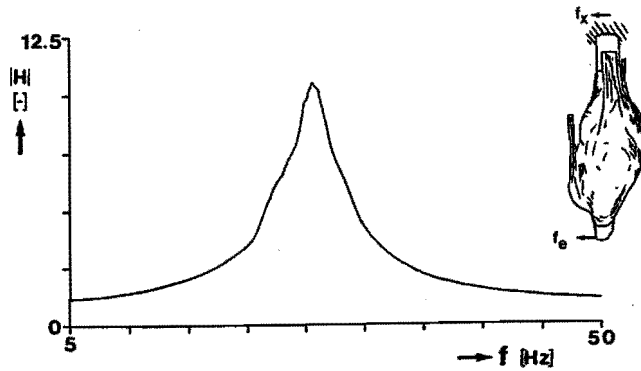


Fig. 4.3.4 KNEE9- $H_{F1,0}$ [1.1, α , $\sigma_F^2=15$, $\phi=30$, $F_b=118$, $F_r=240$, $F_a=97$]

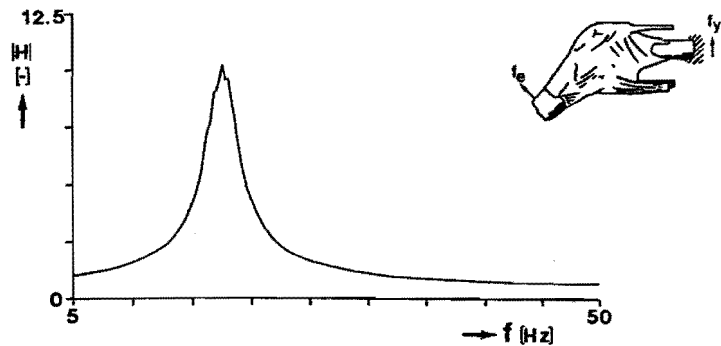


Fig. 4.3.5 KNEE9- $H_{F1,0}$ [2.2, β , $\sigma_F^2=15$, $\phi=30$, $F_b=118$, $F_r=240$, $F_a=97$]

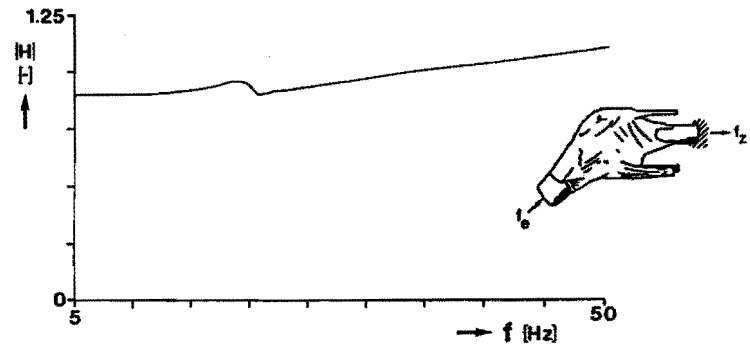


Fig. 4.3.6 KNEE9- $H_{F1,0}$ [3.3, γ , $\sigma_F^2=15$, $\phi=30$, $F_b=118$, $F_r=240$, $F_a=97$]

It is seen that the force transmission is influenced by the resonances of the tibia (as was expected, see section 4.2).

To indicate the influence of the static equilibrium position, Figs. 4.3.7 through 4.3.9 are considered, which give the transfer functions $H_{\phi,11}(f)$, $H_{\phi,22}(f)$ and $H_{\phi,33}(f)$, respectively, for various flexion angles of KNEE8 (left knee, female, 47 years).

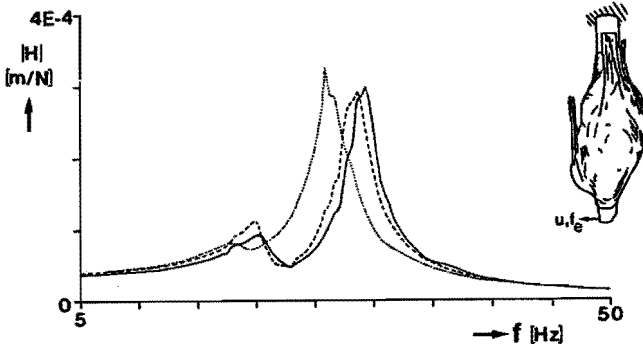


Fig. 4.3.7 Influence of the flexion angle of the joint upon

the transfer function $H_{\psi, 11}(f)$

— KNEE8- H_{ψ} [1,1, α , $\sigma_f^2=20$, $\phi=20$, $F_b=131$, $F_r=200$, $F_a=133$]

- - - KNEE8- H_{ψ} [1,1, α , $\sigma_f^2=20$, $\phi=30$, $F_b=131$, $F_r=200$, $F_a=133$]

..... KNEE8- H_{ψ} [1,1, α , $\sigma_f^2=20$, $\phi=60$, $F_b=131$, $F_r=200$, $F_a=133$]

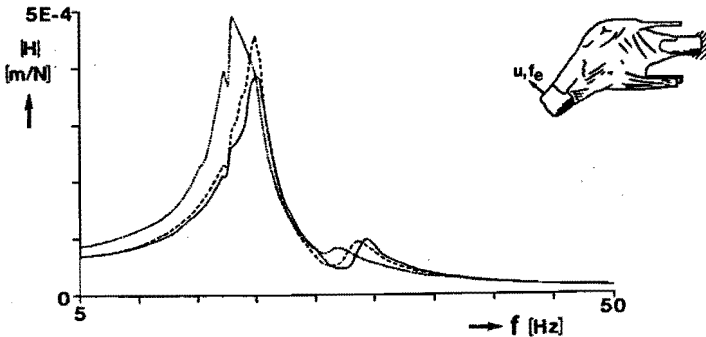


Fig. 4.3.8 Influence of the flexion angle of the joint upon

the transfer function $H_{\psi, 22}(f)$

— KNEE8- H_{ψ} [2,2, β , $\sigma_f^2=20$, $\phi=20$, $F_b=131$, $F_r=200$, $F_a=133$]

- - - KNEE8- H_{ψ} [2,2, β , $\sigma_f^2=20$, $\phi=30$, $F_b=131$, $F_r=200$, $F_a=133$]

..... KNEE8- H_{ψ} [2,2, β , $\sigma_f^2=20$, $\phi=60$, $F_b=131$, $F_r=200$, $F_a=133$]

It is observed that changes in the static equilibrium position result in measurable changes in the transfer functions. For mode I, increase of the flexion angle leads to a decrease in the resonance frequency. This indicates a reduction of resistance of the joint against forces applied in β -direction (see Fig. 4.2.3). For mode II a similar pattern is found, indicating that also resistance of the joint against forces applied in α -direction decreases with increasing flexion

angle. Simultaneously the axial stiffness of the joint decreases as can be seen from Fig. 4.3.9.

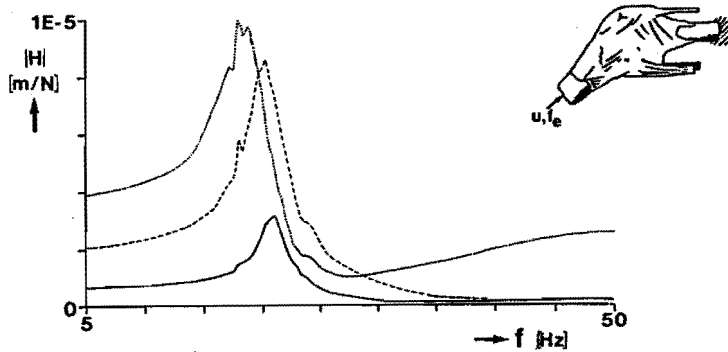


Fig. 4.3.9 Influence of the flexion angle of the joint upon the transfer function $H_{\psi,33}(f)$

- KNEE8- $H_{\psi}[3,3,\gamma,\sigma_f^2=20,\phi=20,F_b=131,F_r=200,F_a=133]$
 - - - KNEE8- $H_{\psi}[3,3,\gamma,\sigma_f^2=20,\phi=30,F_b=131,F_r=200,F_a=133]$
 ····· KNEE8- $H_{\psi}[3,3,\gamma,\sigma_f^2=20,\phi=60,F_b=131,F_r=200,F_a=133]$

Another important parameter influencing the results is the static load exerted on the muscle tendons. Fig. 4.3.10 gives the transfer function $H_{\psi,22}(f)$ for three levels of the static load applied to KNEE6 (right knee, male, 36 years).

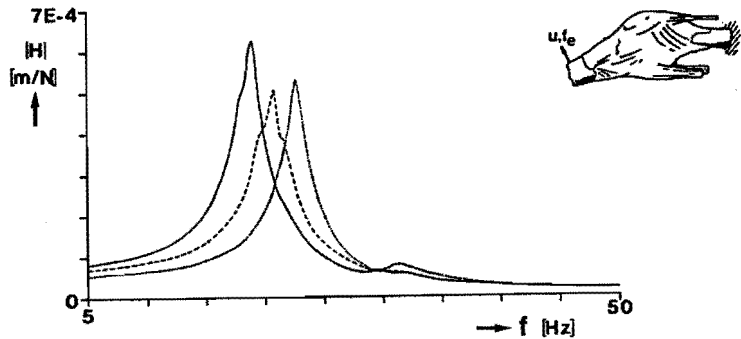


Fig. 4.3.10 Influence of the static load on the muscle tendons upon the transfer function $H_{\psi,22}(f)$

- KNEE6- $H_{\psi}[2,2,\beta,\sigma_f^2=2,\phi=20,F_b=40,F_r=90,F_a=60]$
 - - - KNEE6- $H_{\psi}[2,2,\beta,\sigma_f^2=2,\phi=20,F_b=84,F_r=210,F_a=90]$
 ····· KNEE6- $H_{\psi}[2,2,\beta,\sigma_f^2=2,\phi=20,F_b=224,F_r=396,F_a=244]$

Obviously an increase of the forces on the muscle tendons results in an increase of the resistance of the joint against forces applied in β -direction, resulting in an increase of the resonance frequency for mode I. A similar pattern was found for mode II.

To see if deliberate damaging of the joint specimen yields a measurable change in the behaviour of the joint, a preliminary experiment was done on KNEE6 in which the anterior horn of the lateral meniscus was cut radially. This yields the result for the transfer function $H_{\psi,33}(f)$ given in Fig. 4.3.11, indicating a decrease of the axial stiffness of the joint.

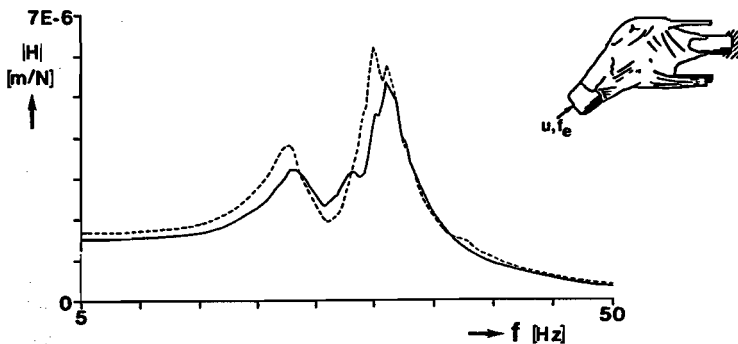


Fig. 4.3.11 Influence of cutting the anterior horn of the lateral meniscus upon the transfer function $H_{\psi,33}(f)$

— intact KNEE6- $H_{\psi}[3,3,\gamma,\sigma_F^2=7,\phi=20,F_b=90,F_r=210,F_a=90]$
 - - - damaged KNEE6- $H_{\psi}[3,3,\gamma,\sigma_F^2=7,\phi=20,F_b=90,F_r=210,F_a=90]$

An essential assumption made in chapter 3 is that the joint behaves as a linear system for the magnitude of the applied dynamic load. To verify this, the magnitude of the dynamic load applied to the tibia was varied (indicated by the measurement parameter σ_F^2). Figs 4.3.12 and 4.3.13 give results for such experiments, indicating that this assumption does not hold. This phenomenon will be discussed in detail in section 4.6.

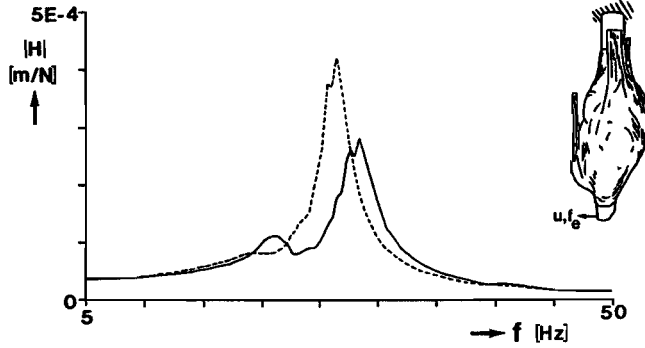


Fig. 4.3.12 Influence of the magnitude of the dynamic load applied to the tibia upon the transfer function $H_{\psi,11}(f)$

— KNEE8- $H_{\psi}[1,1,\alpha,\sigma_{\underline{f}}^2=4, \phi=20, F_b=178, F_r=361, F_a=177]$
 - - - KNEE8- $H_{\psi}[1,1,\alpha,\sigma_{\underline{f}}^2=20, \phi=20, F_b=178, F_r=361, F_a=177]$

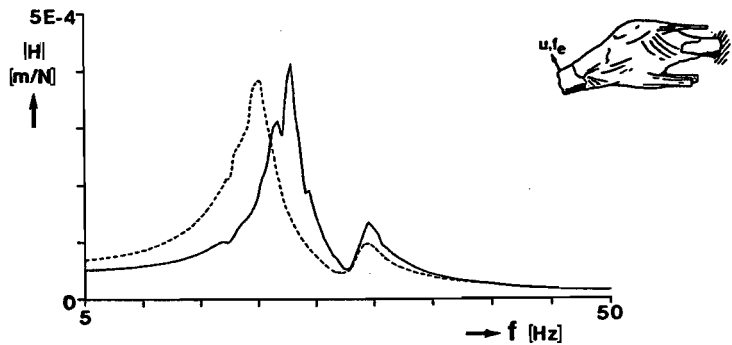


Fig. 4.3.13 Influence of the magnitude of the dynamic load applied to the tibia upon the transfer function $H_{\psi,22}(f)$

— KNEE8- $H_{\psi}[2,2,\beta,\sigma_{\underline{f}}^2=7, \phi=20, F_b=131, F_r=200, F_a=133]$
 - - - KNEE8- $H_{\psi}[2,2,\beta,\sigma_{\underline{f}}^2=20, \phi=20, F_b=131, F_r=200, F_a=133]$

A final point of interest is the influence of the stiffness of the bracing wires upon the results obtained. In chapter 3 it was assumed that their longitudinal stiffness of 110 N/mm is sufficiently low (in comparison with the stiffness properties of the joint). Figs. 4.3.14 and 4.3.15 give results for experiments on KNEE8 in which the diameter of the bracing wires was changed to 0.75 mm (instead of 1 mm).

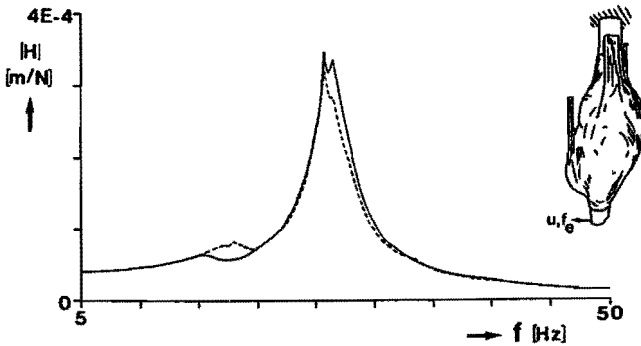


Fig. 4.3.14 Influence of the diameter of the bracing wires upon the transfer function $H_{\psi, 11}(f)$

ϕ 0.75 mm ——— KNEE8- $H_{\psi}[1, 1, \alpha, \sigma_F^2=20, \phi=60, F_b=131, F_r=200, F_a=133]$

ϕ 1.00 mm - - - KNEE8- $H_{\psi}[1, 1, \alpha, \sigma_F^2=20, \phi=60, F_b=131, F_r=200, F_a=133]$

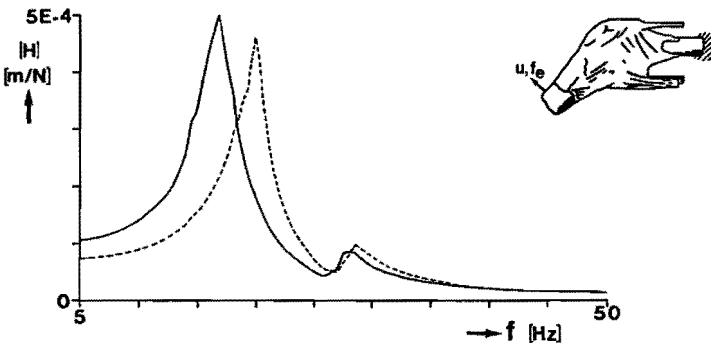


Fig. 4.3.15 Influence of the diameter of the bracing wires upon the transfer function $H_{\psi, 22}(f)$

ϕ 0.75 mm ——— KNEE8- $H_{\psi}[2, 2, \beta, \sigma_F^2=6, \phi=30, F_b=120, F_r=210, F_a=133]$

ϕ 1.00 mm - - - KNEE8- $H_{\psi}[2, 2, \beta, \sigma_F^2=6, \phi=30, F_b=120, F_r=210, F_a=133]$

From Fig. 4.3.14 follows that vibration mode II is hardly affected by the stiffness of the bracing wires. Fig. 4.3.15 indicates that for vibration mode I the stiffness of the bracing wires is of importance. In section 4.4 this aspect will be discussed in detail.

4.4 Inaccuracies and disturbing factors

With the results given in section 4.3, in this section attention is paid to the influence of inaccuracies and disturbing factors in the experimental procedure upon the results obtained. The inaccuracies and disturbing factors considered are

* inaccuracies due to autolysis of the knee joint specimen;

- * inaccuracies in and disturbance of the results obtained by a non-ideal dynamic behaviour of the experimental set-up;
- * inaccuracies due to the use of technical instruments to quantify the dynamic behaviour of the joint (measurement errors, errors due to the chosen form of digital post-processing).

4.4.1 Effects of autolysis

Dealing with a biological structure taken out of its natural surrounding, autolysis is a problem of interest. In the preliminary experiments on KNEE1 through KNEE5 it was observed that after 2 days of experiments at room temperature (20 °C), autolysis became perceptible (autolysis results in development of malodorous hydrogen-sulphide). As it is not assured at which point of progress autolysis produces notable effects on the mechanical behaviour of the joint, the use of knee joint specimens was limited to 2 days. Autolysis may be influenced by the static and the dynamic load applied. During the experiments the static load on the muscle tendons is maintained for several hours. This may cause fluids to be squeezed out of the articular cartilage, e.g., and therefore may stimulate autolysis. Similarly the dynamic load applied may damage the joint, as random excitation applied for several minutes is not likely to be a physiological load. By repetition of some experiments a first check was carried out to see if the dynamic properties of the joint change within the time interval of the experiments on one day. This yielded no significant changes in the transfer functions however: these changes were well in the confidence intervals give in section 4.3.3. As the influence of the applied loads on the autolysis of soft tissues is unknown, some precaution was taken. The experiments done on one day, were done within 5 or 6 hours to limit the time the static load acts on the joint. The maximally possible static load (1500 N per bracing wire) was not applied in the experiments, for safety reasons again. Also the time the joint was subjected to random excitation was minimized. This aspect will be discussed further in section 4.4.3, as this has influence on the accuracy of the calculated power spectra. A second check to assure that the joint specimen did not suffer from the applied loads was carried out after the experiments by visual examination of the cartilage layers. For all specimens used no damage could be found.

4.4.2 Influence of the experimental set-up

Considering the influence of the experimental set-up upon the results obtained, two (potentially) disturbing factors are focused on. First attention will be paid to the rigidity of the foundation of the experimental set-up and secondly the influence of the bracing wires will be dealt with.

Rigidity of the foundation

To discuss the rigidity of the foundation of the experimental set-up, Fig. 4.4.1 is considered, which is a simplified representation of the experimental set-up given in Fig. 3.2.2.

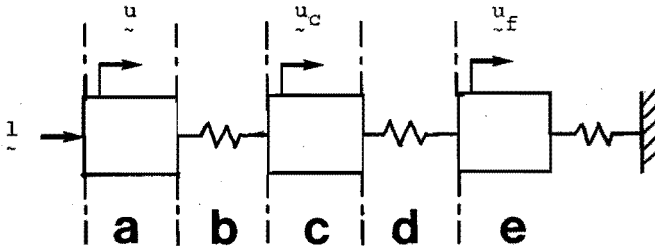


Fig. 4.4.1 A simplified representation of the knee joint specimen in the experimental set-up. a-tibia, b-knee joint, c-femur and clamping device, d-load cells of the force platform, e-foundation

The assembly of concrete block A, steel plate B, steel block C and the bottom plate V_2 of the force platform can be considered as a non-rigid foundation, which has its own dynamic behaviour. Also the load cells of the force platform are deformable elements (deformations of the quartz elements in the load cells result in analog signals related to the applied loads). The femur, the clamping flange E and the top plate V_1 of the force platform are considered to constitute a rigid element c. For the experiments the knee joint, seen as a flexible connection b between the tibia and the femur, and the tibia are the essential parts in Fig. 4.4.1. The dynamic load l applied to the tibia will result in displacements u of the tibia, u_c of the rigid element c and u_f of the foundation. Using a rigorous mathematical treatment it is possible to derive an expression for the various displacements due to the load l , taking into account the dynamic properties of the flexible elements. For the sake of brevity such a complex mathematical description is omitted here. Instead a more physical argumentation will be used to consider the influence of the various elements in the experimental set-up.

As the displacements of the tibia are derived from accelerometers, which measure absolute accelerations, it is obvious that the displacements u_c must be essentially smaller than the displacements u (otherwise the centre of the force platform can not be taken as a fixed origin). Therefore the combination of the force platform and the foundation must have a dynamic stiffness (or impedance, which is the inverse of the transfer function matrix relating displacements to loads applied) that is far larger (in magnitude) than that of the knee joint. This condition is not sufficient, however. As the load cells of the force platform respond to relative displacements between

the top plate V_1 and the bottom plate V_2 , the displacements of the foundation must be essentially smaller than those of the top plate V_1 . If this condition is violated, loads are measured with the force platform that are only due to vibrations of the foundation. Therefore a second condition is that the dynamic stiffness of the foundation is far larger than that of the loadcells of the force platform (as an indication: the static stiffness of the loadcells typically has a value of 10^9 N/m).

To assure that the second condition is met, measurements were carried out in which a force was applied directly to the clamping flange E in various directions. From these measurements followed that in the frequency range of 0 to 100 Hz, the force platform works properly (which means that a stiffness of the foundation of typically 10^{11} N/m is sufficiently high). From the results given in section 4.3 follows that for the knee joint specimen typical stiffness values of 10^4 to 10^6 N/m are obtained. These values are sufficiently low in comparison with the stiffness of the load cells of the force platform to assure that also the first condition is met. Therefore the foundation of the experimental set-up can be considered rigid for the experiments on the knee joint specimen.

Influence of the bracing wires

The second point of interest regarding the influence of the experimental set-up upon the obtained results, is the influence of the bracing wires. From Fig. 4.3.14 follows that mode II is unaffected by the finite stiffness of the bracing wires. This is to be expected as for displacements in the α -direction, the transversal stiffness of the bracing wires is important. This stiffness is very small however and therefore will not result in artificial joint stiffness.

Fig. 4.3.15 indicates that this does not hold for mode I. The results given in Fig. 4.3.15 can be used in a simple model to indicate to which extent the stiffness of the bracing wires contributes to the apparent stiffness of the joint. If it is assumed that the transfer function $H_{\psi,22}(f)$ corresponds to that of a linear system it can be written

$$H_{\psi,22}(f) = (-m_{22} 4\pi^2 f^2 + b_{22} 2\pi j f + k_{22})^{-1} \quad (4.4.1)$$

where k_{22} , b_{22} and m_{22} represent mass, damping and stiffness characteristics, respectively, determining the displacements of the joint in β -direction for loads applied in the β -direction. It is assumed that only vibration mode I is relevant, as vibration mode II does not significantly contribute to the transfer functions given in Fig. 4.3.15. As the only difference between the two measurements given in Fig. 4.3.15 is the stiffness of the bracing wires, the mass m_{22} and damping b_{22} will be identical for both situations. Also the static load on the muscle tendons, the static equilibrium position and the magnitude of the dynamic load applied to the tibia are identical.

Therefore the difference between the results for the experiments can be considered to be due to the different stiffness of the bracing wires only, such that only the stiffness k_{22} is influenced. The stiffness k_{22} can be seen as the sum of two stiffness values, $k_{22,j}$ and $k_{22,w}$. $k_{22,j}$ represents the contribution of the joint (which should have been determined), whereas $k_{22,w}$ is determined by the longitudinal stiffness of the bracing wires. For both situations $k_{22,j}$ will be equal. $k_{22,w}$ is proportional to d_w^2 , with d_w as the diameter of the bracing wires. Now the following relations hold

$$k_{22}^{1.0} = k_{22,j} + k_{22,w}^{1.0} \quad (4.4.2)$$

$$k_{22}^{0.75} = k_{22,j} + k_{22,w}^{0.75} = k_{22,j} + 0.75^2 k_{22,w}^{1.0} \quad (4.4.3)$$

(with $k_{22}^{1.0}$ as the stiffness k_{22} for a diameter of 1.0 mm of the bracing wires etc.).

Using the curve-fit procedure proposed by Mergeay (1980), from the transfer functions given in Fig. 4.3.15 the following parameter values were obtained

$$m_{22} = 0.9 \text{ kg}; \quad b_{22} = 17.5 \text{ Ns/m}; \quad (4.4.4)$$

$$k_{22}^{1.0} = 14500 \text{ N/m}; \quad k_{22}^{0.75} = 10470 \text{ N/m}$$

Substitution of these values in relations (4.4.3) and (4.4.4) leads to

$$k_{22,j} = 5300 \text{ N/m} \quad (4.4.5)$$

$$k_{22,w}^{1.0} = 9200 \text{ N/m}$$

Hence it follows that for this experiment the stiffness of the bracing wires yields a contribution to the apparent stiffness k_{22} of the joint which is about a factor 1.8 larger than the stiffness of the joint itself. Similar results are obtained for experiments in which the flexion angle was varied. It may therefore be concluded that the bracing wires must be included when considering the dynamic behaviour of the joint. The stiffness of the bracing wires does not dominate the behaviour of the joint. This was also observed in section 4.3 as the magnitude of the load on the muscle tendons and the magnitude of the dynamic load applied to the tibia have their influence on vibration mode I. In case the stiffness of the bracing wires would be dominant, this would not have been found because the bracing wires behave as a linear system, independent of the applied static and dynamic load.

To eliminate the influence of the bracing wires their stiffness must be decreased considerably. This can not be taken into consideration as this either results in excessive long wires or very thin wires which can not withstand the loads to be applied. It is recognized that in this case their influence must be taken into consideration in

a numerical model (to be developed). This is not felt to cause problems as the bracing wires are relatively simple mechanical structures. For the experiments to be discussed in chapter 5 the diameter of the bracing wires was changed to 0.75 mm to reduce their influence.

4.4.3 Measurement- and postprocessing errors

To obtain the transfer functions describing the behaviour of the joint, a number of quantities are measured and subsequently used for digital postprocessing. In this section attention will be paid to the influence of errors introduced in these two steps.

A first type of measurement errors includes errors in the parameters describing the static equilibrium position, the load acting on the muscle tendons, the location where and the direction in which the dynamic force is exerted on the tibia and the location and the measuring direction of the accelerometers. As the dynamic load acts in a fixed point on the brass housing (R) connected to the tibia and as the geometrical parameters for the accelerometers are fixed, errors in the alignment of the longitudinal axis of the shaker with respect to the coordinate axes of the vector base connected to the tibia are most significant. However, disconnection of the shaker and proper repetition of a particular experiment yields no significant changes in the transfer functions (as was checked in the experiments on KNEE1 through KNEE5 and therefore omitted in the experiments on KNEE6 through KNEE10). A more drastic check to study the influence of these measurement errors is repetition of a particular experiment, done on the first day of the experiments, on the second day of the experiments. This involves a complete removal of the joint specimen from the experimental set-up, and requires re-installation of all transducers, the static equilibrium position and the load on the bracing wires. Such a check was carried out yielding fairly reproducible results. A more systematic verification of this procedure will be discussed in chapter 5.

The second type of measurement errors is due to the digitization of the analog signals. Proper amplification of the analog signals is essential to assure that they cover the range of the ADC in the data acquisition system. This was checked for each particular experiment. The influence of (random) errors in the digitized signals is readily retrieved from the coherence function introduced in section 3.3.2.

At this point the influence of postprocessing errors must be considered. On forehand it is mentioned that all calculations were done on the personal computer included in the data-acquisition system with real*4 arithmetic. Errors due to a finite word length in arithmetical operations can be neglected compared to other error sources to be discussed in this section. This was verified by using real*8 arith-

metic in stead of real*4, which yielded no differences in the calculated power spectra and corresponding transfer- and coherence functions. Therefore real*4 arithmetic was applied as this reduces post-processing time and in core storage. The prime potential error sources in the computational process to obtain the power spectra are signal leakage and random errors in the digitized signals. Signal leakage results from the use of non-periodic signals to calculate the power spectra by means of a Discrete Fourier Transformation. It results in a smearing of frequency components but can largely be reduced by the use of a periodic (Hanning) window function and a sufficiently small frequency resolution Δf (see appendix D). To reduce the influence of random measurement errors, the power spectra are determined in an averaging process (appendix D). Bendat and Piersol (1980) derived a formula to calculate the 95% confidence interval for a transfer function $H_e(f)$ estimated from these spectra with the transfer function $H(f)$

$$|H(f)| (1 - 2\epsilon[|H(f)|]) \leq |H_e(f)| \leq |H(f)| (1 + 2\epsilon[|H(f)|])$$

$$\phi(f) + 2\epsilon[|H(f)|] \leq \phi_e(f) \leq \phi(f) + 2\epsilon[|H(f)|] \quad (4.4.6)$$

Here $|H_e(f)|$ and $\phi_e(f)$ are the magnitude and phase of the exact (or unbiased) transfer function $H_e(f)$, respectively, and $\epsilon[|H(f)|]$ is the normalized error for $|H(f)|$ given by

$$\epsilon[|H(f)|] = \frac{\sqrt{[1 - \gamma^2(f)]}}{|\gamma(f)| \sqrt{2} \sqrt{N_a}} \quad (4.4.7)$$

Relation (4.4.7) shows that the coherence function $\gamma^2(f)$ must be almost unity to obtain an acceptable estimate for the transfer function $H_e(f)$, as only a limited number of averages is used (N_a was set to 40, based on a measurement time of 137 s and use of a 512-point FFT). Fig. 4.4.2 gives a characteristic picture for the coherence functions obtained.

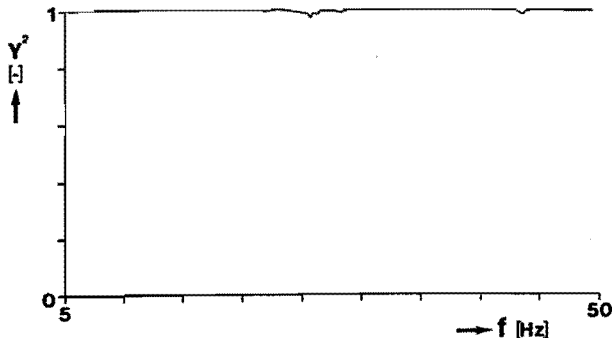


Fig. 4.4.2 A typical coherence function $\gamma^2(f)$

As the coherence function attains values of at least 0.95 in the frequency range of interest, random errors are not likely to play an important role ($\epsilon[|H(f)|] \leq 0.04$).

4.5 The static behaviour of the joint: influence of the static load

To be able to discuss the experimental results, in this section some aspects of the static behaviour of the joint are discussed. In particular, the influence of the static load on the muscle tendons on the static equilibrium position and the reproducibility of the results will be considered.

An important step in the LLT is the creation of a stable static equilibrium position by means of static forces on three muscle tendons. In the experiments on KNEE1 through KNEE9 it was observed that any desired joint configuration could be obtained and maintained for several hours by proper selection of the magnitude of the forces on the bracing wires. Simultaneously it was observed that small changes in the direction of the bracing wires do not influence the joint configuration (within the limits of measurement accuracy). These small changes can be brought about by movement of the stud-and-nut combinations (N) in the slots of the grate (M), resulting in changes in the direction of the bracing wires of maximally 5° .

An important aspect of the static behaviour of the joint is that a clearly non-linear relation governs the interaction between the static forces on the muscle tendons and the static equilibrium position. This statement results from the following observations. For a given combination of forces on the bracing wires various joint configurations can be obtained. On the other hand a certain joint configuration can be installed with various combinations of the forces on the bracing wires (within the limits of measurement accuracy of course). It was also noticed that, to obtain a certain joint configuration, the way in which the forces on the bracing wires are subsequently increased plays an important role. For example, if the flexion angle of the joint must be decreased (lifting of the tibia), an increase of the force on the musculus rectus femoris does not always yield the desired result. Frequently situations were encountered in which a kind of locking occurs, such that an increase of the force on the musculus rectus femoris does not result in measurable changes of the joint configuration. To obtain the desired flexion angle, the only solution is to decrease the force on the musculus biceps femoris and the muscle on the medial side, followed by an increase of the force on the musculus rectus femoris and next an increase of the forces on the other two tendons (again).

This phenomenon clearly indicates the non-linear behaviour of the joint. It also complicates the measurements, especially when the joint configuration must be altered majorly. The locking phenomenon, requiring repeated adaptation of the forces on the bracing wires, in combination with the time-dependent behaviour of the joint, resulting

in a force reduction and a change of the static equilibrium position after a certain load has initially been applied, may result in excessive time needed to generate a certain joint configuration with corresponding desired forces on the muscle tendons. The behaviour of the joint described above has repercussions on the number of experiments that can be carried out on a particular joint specimen, because in ultimate cases it may take 1 hour to obtain the desired joint configuration.

4.6 The dynamic behaviour of the joint: influence of the dynamic load

As was shown by Figs. 4.3.12 and 4.3.13, the magnitude of the dynamic load has a marked influence on the transfer functions obtained. Additional experiments done on KNEE9 for various magnitudes of the dynamic load illustrate this phenomenon as is shown in Figs. 4.6.1 through 4.6.3.

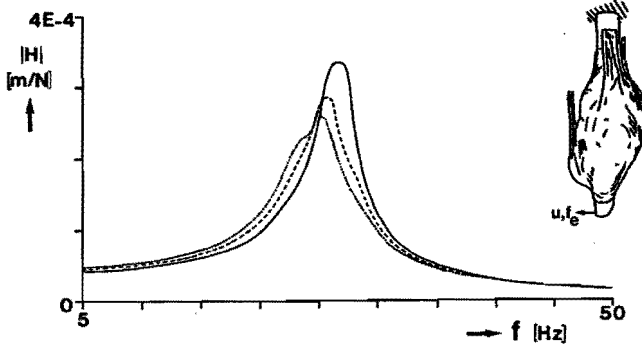


Fig. 4.6.1 Influence of the dynamic load applied to the tibia upon the transfer function $H_{\psi, 11}(f)$

— KNEE9- $H_{\psi}[1, 1, \alpha, \sigma_F^2=7.5, \phi=30, F_b=118, F_r=240, F_a=97]$

- - - KNEE9- $H_{\psi}[1, 1, \alpha, \sigma_F^2=15, \phi=30, F_b=118, F_r=240, F_a=97]$

----- KNEE9- $H_{\psi}[1, 1, \alpha, \sigma_F^2=25, \phi=30, F_b=118, F_r=240, F_a=97]$

These experiments were also done for several flexion angles and static load levels and in all cases the same typical results were obtained. Increase of the magnitude of the dynamic load leads to a decrease of the stiffness of the joint (as can be seen from Fig. 4.2.4 and 4.2.5) and to an increase of the damping, when the elements of $H_{\psi}(f)$ are considered. Fig. 4.6.3 shows that this is confirmed by the elements of the transfer function matrix $H_{F1, 0}(f)$ (see Fig. 4.2.6 and 4.2.7). As is seen from section 4.3 these changes in the stiffness of the joint are of the same order as changes due to changes in the static load on the muscle tendons, changes of the static equilibrium position and damaging of the joint. This observation indicates a

failure of the Local Linearization Technique proposed in chapter 3, as the modal parameters determined from the transfer functions depend on the magnitude of the dynamic load applied to the tibia. This is in conflict with the assumed linearity of the joint for the magnitude of the dynamic loads applied. One of the possible reasons for failure indicated in chapter 3 may play a role, as the magnitude of the dynamic load applied can not be decreased substantially, without invoking a decrease of the signal to noise ratio (due to the finite sensitivity of the piezo-electric transducers).

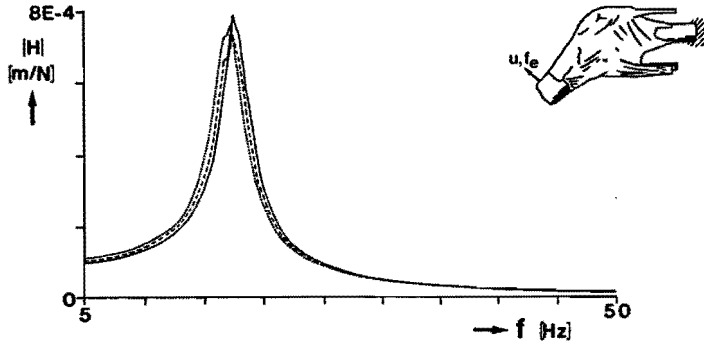


Fig. 4.6.2 Influence of the dynamic load applied to the tibia upon the transfer function $H_{\psi, 22}(f)$

— KNEE9- $H_{\psi, 22}[2, 2, \beta, \underline{\sigma_F^2=7.5}, \phi=30, F_b=118, F_r=240, F_a=97]$
 - - - KNEE9- $H_{\psi, 22}[2, 2, \beta, \underline{\sigma_F^2=15}, \phi=30, F_b=118, F_r=240, F_a=97]$
 - - - - KNEE9- $H_{\psi, 22}[2, 2, \beta, \underline{\sigma_F^2=25}, \phi=30, F_b=118, F_r=240, F_a=97]$

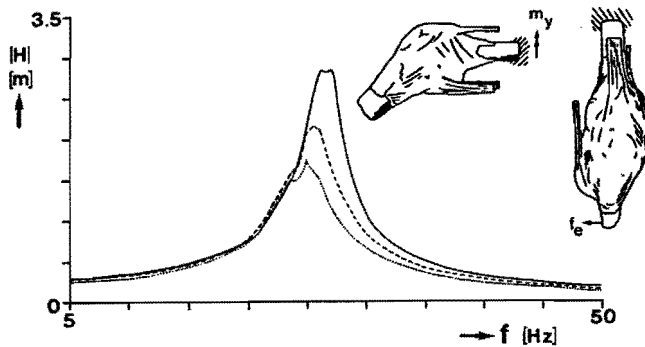


Fig. 4.6.3 Influence of the dynamic load applied to the tibia upon the transfer function $H_{F1, 051}(f)$

— KNEE9- $H_{F1, 051}[5, 1, \alpha, \underline{\sigma_F^2=7.5}, \phi=30, F_b=118, F_r=240, F_a=97]$
 - - - KNEE9- $H_{F1, 051}[5, 1, \alpha, \underline{\sigma_F^2=15}, \phi=30, F_b=118, F_r=240, F_a=97]$
 - - - - KNEE9- $H_{F1, 051}[5, 1, \alpha, \underline{\sigma_F^2=25}, \phi=30, F_b=118, F_r=240, F_a=97]$

Consequently, the magnitude of the forces applied to the tibia may be too large to allow for linearization of the dynamic behaviour of the joint. A further reduction of the dynamic loads applied may be considered (with a corresponding selection of more sensitive transducers). It is felt however that such a reduction results in loads applied to the tibia which are well out of any physiological range, such that the practical use of the results obtained becomes questionable. To illustrate this the results from the experiments of Voloshin and Wosk (1983) are considered as given in Fig. 2.3.2. From these measurements it follows that for level walking, upon heel strike the accelerations on the tibia have a typical value of 20 m/s^2 , which is in agreement with the acceleration levels given by Günther (1968). To compare these values with the accelerations of the tibia in the experiments discussed in section 4.2, the 95% confidence intervals for the accelerations during three particular experiments are given in Table 4.6.1.

$$\text{KNEE9-H}_\psi[1.1.\alpha, \sigma_F^2=15, \phi=30, F_b=118, F_r=240, F_a=97] : -16..+16 \text{ m/s}^2$$

$$\text{KNEE9-H}_\psi[2.2.\beta, \sigma_F^2=15, \phi=30, F_b=118, F_r=240, F_a=97] : -15..+15 \text{ m/s}^2$$

$$\text{KNEE9-H}_\psi[3.3.\gamma, \sigma_F^2=15, \phi=30, F_b=118, F_r=240, F_a=97] : -0.8..+0.8 \text{ m/s}^2$$

Table 4.6.1 95% confidence intervals for the accelerations corresponding to the transfer functions indicated by the records given above

The transfer functions corresponding to these experiments are given in Fig. 4.3.1 through 4.3.3. It is seen that for these experiments the accelerations are in the range of those found by Voloshin and Wosk (1983). A further reduction of the loads applied to the tibia, would result in accelerations that are far below those encountered during level walking, reducing the practical use of the results obtained. Of course this argumentation contains uncertainties due to the limited knowledge about the physiological accelerations. Another factor that may influence the validity of the argumentation given above is the shape of the accelerations in the experiments (see section 4.1) which does not match those measured by Voloshin and Wosk (1983). To verify whether the shape of the excitation signal influences the occurrence of non-linear phenomena, another type of excitation was applied which results in a more physiological pattern of the accelerations.

Sinusoidal excitation was selected for this purpose. Experiments were done on KNEE10 (right knee, male, 55 years), in which the magnitude and the frequency of the sinusoidal load were varied. The only difference between these experiments and those with random excitation is the shape of the dynamic load applied to the tibia. It turned out that the accelerations of the tibia are sinusoidal also with no additional frequency components (as may occur for non-linear behaviour due to friction, e.g.). Therefore the amplitude of the measured

accelerations and the amplitude of the load applied to the tibia can be related directly. Denoting the amplitude of the acceleration \bar{s}_i ($i=1\dots 6$) with $|\bar{s}_i|$ and the amplitude of the sinusoidal force f_e with $|f_e|$ it holds

$$|H_{\psi,ij}(f_{\sin})| = \frac{|\bar{s}_i|}{|f_e|} \frac{1}{4\pi^2 f_{\sin}^2} \quad (4.6.1)$$

if the force is applied along coordinate axis j ($j=1,2,3$) of the vector base connected to the tibia. f_{\sin} is the frequency of the sinusoidal force. Fig. 4.6.4 gives the results for such experiments, in which f_{\sin} was set to 10, 20, 30 and 40 Hz and $|f_e|$ was varied.

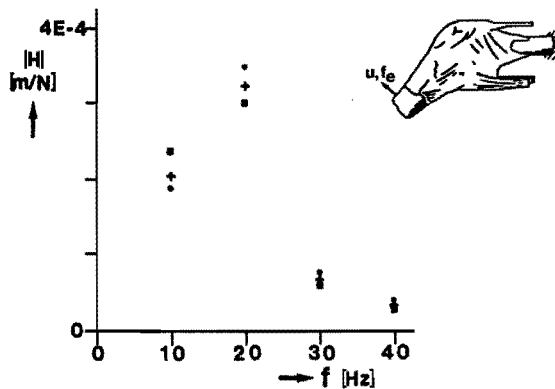


Fig. 4.6.4 The transfer function $H_{\psi,22}(f)$ obtained for experiments with sinusoidal loading.
 ● $|f_e| = 1.8$ N; + $|f_e| = 2.4$ N; ■ $|f_e| = 3.0$ N

$ f_e $ ([N])	1.8	2.4	3.0
f_{\sin}			
10	1.35	1.94	2.84
20	9.95	12.13	14.21
30	4.80	5.97	6.40
40	3.41	3.79	4.17

Table 4.6.2 Amplitude of the accelerations for the experiments given in Fig. 4.6.4

The results obtained agree both quantitatively and qualitatively with those obtained for random excitation. To illustrate this Fig. 4.6.2 is considered. For random excitation it was found that an increase of the magnitude of the applied load leads to a decrease of the stiffness of the joint. For frequencies smaller than the resonance frequency an increase of the magnitude of the transfer function is found

when the magnitude of the dynamic load is increased. For frequencies higher than the resonance frequency the opposite behaviour is found. Both these characteristics are also obtained for sinusoidal loading. It may therefore be concluded that the non-linearities are not bound to a particular excitation signal.

For the experiments with sinusoidal loading given in Fig. 4.6.4 the amplitude of the accelerations [m/s^2] attains the values given in Table 4.6.2. These values can well be compared with those found by Voloshin and Wosk (1983). It is seen that in this range of the magnitude of the accelerations on the tibia, the non-linearity of the dynamic behaviour of the joint is an important phenomenon. A reduction of the magnitude of the dynamic load applied to the tibia to see if the LLT applies for these smaller loads, is therefore not taken into consideration. The value of the results given in section 4.2 and a possible method to deal with the non-linearities found will be discussed in section 4.7.

4.7 Evaluation of the results obtained for random and sinusoidal excitation

In this chapter a number of aspects of the dynamic behaviour of the knee joint have been discussed. Using the LLT proposed in chapter 3 the dynamic behaviour of the joint can be quantified, although it turns out that linearization of the behaviour of the joint is not allowed for the range of the loads applied to the tibia. The transfer functions for various load levels show a marked shift, indicating a decrease of the stiffness of the joint with increasing load level. The value of the results is that they essentially give a good insight in the behaviour of the joint and typical parameter values for stiffness and damping can be obtained.

An important observation is that the results for various knee joint specimens may well be compared. Also the results for random and sinusoidal loading agree fairly well. It must be kept in mind however that the obtained results depend on the magnitude of the applied dynamic load.

Due to the use of spectral analysis (which is an averaging process as discussed in appendix D) and random excitation, the transfer functions must be seen as to give an "average" behaviour of the joint for the loads applied. The non-linearities of the behaviour of the joint are translated to a kind of effective stiffness and damping. As the coherence function for all measurements was almost unity, the transfer functions seem to give an acceptable measure for the behaviour of the joint, despite the non-linearities involved. This may partly be due to the use of random excitation which is considered as a rather gentle excitation (compared to impuls- or step-like excitation). A description of the behaviour of the joint using the transfer functions obtained may therefore be considered. As was done in the work

of van Heck (1984), in this case the stiffness and damping characteristics of the joint can be calculated for various levels of the dynamic load applied. Such an approach may yield valuable information on the degree of non-linearity. It is noticed however that in this case no direct insight is given, as the non-linearities may partly be smoothed due to the use of spectral analysis and random excitation. This disadvantage may partly be eliminated by application of a time-domain analysis technique. Using measured time domain signals, the best fitting linear system can be determined to obtain stiffness and damping values for various levels of the dynamic load applied. Evidently such an approach may result in discrepancies between the measured and best fitting signals, which can only be resolved by use of a non-linear dynamic model of the knee joint. Such a model is not provided, however, and must be focused on in future research. Therefore the use of a best fitting linear model is considered as an unavoidable alternative. On the other hand such a model may provide valuable information for development of a non-linear dynamic model of the knee joint. Chapter 5 focuses on such a best fitting linear model obtained from a time-domain analysis technique.

4.8 Summary

An overview of the results for experiments on 5 knee joint specimens has been given in this chapter. It turns out that the behaviour of the joint and the influence of various measurement parameters (static load on the muscle tendons, static equilibrium position and damaging of the joint) can be quantified. Two factors have a significant influence: the stiffness of the bracing wires and the magnitude of the dynamic load applied to the tibia. As the influence of the magnitude of the dynamic load is significant it has to be concluded that in essence the knee joint has to be regarded as a non-linear system, making application of a Local Linearization Technique questionable. However, including the magnitude of the dynamic load as an additional measurement parameter, an indication can be obtained about the behaviour of the joint and the degree of non-linearity. It is noticed however that these non-linearities may partly be smoothed due to the use of random excitation and spectral analysis. Therefore a time-domain analysis technique may provide a more suitable tool to analyse the behaviour of the joint, as will be discussed in chapter 5.

Chapter 5 Experiments II: Analysis in the time-domain

From the experimental results for random and sinusoidal excitation given in chapter 4 it was concluded that a time-domain analysis may yield a more appropriate method to deal with the non-linearities encountered. This chapter gives an overview of the experiments carried out for such an analysis. Section 5.1 deals with the selection of the excitation technique and of a method to realize the chosen excitation. A description of the experiments carried out is given in section 5.2. In section 5.3 attention is paid to a method to obtain the parameters describing the best-fitting linear system from the measured responses of the joint subjected to this excitation. The results for these experiments are given in section 5.4, and discussed in summary in section 5.5.

5.1 Selection of an excitation technique

With regard to the results discussed in chapter 4 for random excitation, it is felt that a description of the knee joint in terms of a linear system is acceptable, if the system parameters are considered to depend on the magnitude of the applied dynamic load. To investigate this dependence a simple excitation technique may be applied such that the relevant system parameters may be extracted from measured time-domain signals. The decision to apply step excitation for this purpose is motivated as follows:

- * due to the non-linearity of the behaviour of the joint, the results obtained from such an analysis are likely to depend on the shape of the excitation signal and on the initial conditions (displacements and velocities at the start of the experiment). These can (fairly) well be controlled for step excitation.
- * step excitation yields an excitation signal in which all relevant frequency components are excited, such that the expected resonance phenomena become observable (in contrast to sinusoidal excitation in which only one particular frequency component is excited).
- * extraction of the relevant system parameters for the best-fitting linear system can be done efficiently (see section 5.3).
- * step excitation results in accelerations of the tibia which have a more or less physiological pattern (see section 5.4).

To analyse the behaviour of the joint under step excitation, experiments can be carried out similar to those described in chapters 3 and 4 (merely the type of the excitation signal is changed). Therefore a number of topics discussed in these chapters will also be applied in the present chapter.

Suppose a force f_e is applied along one of the coordinate axes of the vector base connected to the tibia, which has the pattern given in Fig. 5.1.1

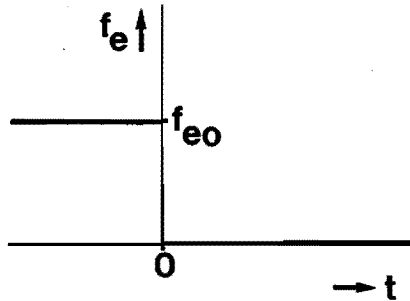


Fig. 5.1.1 Pattern of the force exerted on the tibia for step excitation

An initially applied constant force f_{e0} is released at $t=0$. This particular form of step excitation can be applied by means of the installation shown in Fig. 5.1.2.

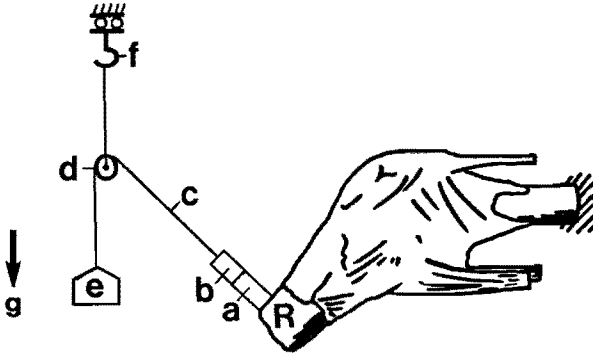


Fig. 5.1.2 Schematical representation of the installation to apply the step excitation (see text)

A force transducer (a) is connected to the brass housing R. This force transducer is connected to a small-sized electromagnet (b), which on its turn is connected to a loading weight (e) by means of a flexible rope (c) (length approximately 0.5 m). This rope is led over a pulley (d) which is flexibly suspended in the hook (f) of the

remote control travelling crane already mentioned in section 4.1. With this installation the step excitation shown in Fig. 5.1.1 can be realized as follows:

- * the electromagnet (b) is activated and a loading weight is attached to the rope (c). The pulley (d) is included to assure that friction does not significantly influence the force acting on the joint, as might occur when the rope (c) is led directly over the hook (f);
- * next the orientation of the rope (c) is adjusted, by movements of the travelling crane, to meet the desired orientation which is inspected visually. This method provides sufficient accuracy, because, as will be shown in section 5.4, repeated experiments (requiring a re-installation of a loading configuration) yield fairly identical results;
- * after the knee joint and the loading installation have attained a static equilibrium position (usually within 30 seconds), the static force f_{eo} acting on the joint can be measured with the force transducer. This force can be varied by proper selection of the mass of the loading weight (e);
- * next the electromagnet (b) is de-activated. The force f_{eo} will rapidly decrease as the electromagnet (b) is pulled away by the falling weight (e), resulting in a step excitation in which the force f_{eo} is released in approximately 2 ms. This finite time needed to apply the step excitation cannot be avoided as a pure step excitation is physically impossible. A time interval of 2 ms to release the force f_{eo} is sufficiently small, however, to be neglected for the experiments carried out. This can be proven by analyzing the response of a linear system, with the system parameters given in section 5.4, to a ramp-like excitation with a rise-time of approximately 2 ms.

This particular excitation technique was selected because

- * the electromagnetic shaker used for the random and sinusoidal excitation can not exert a static force during a longer period of time;
- * for step excitation the dynamic behaviour of a possibly used mechanical loading device (a hydraulical shaker e.g.) may result in undesired disturbances. In case the force f_e should suddenly be increased or decreased, the step-response of such a loading device is a critical characteristic, as undesired force fluctuations can be introduced due to vibrations of the loading device connected to the joint. With the excitation technique described above such fluctuations are negligible,

due to the rapid decoupling of the entire loading installation.

5.2 Description of the experiments

Experiments were carried out on 3 knee joint specimens, KNEE11, KNEE12 and KNEE13 (where KNEE11 was used in preliminary experiments). The experiments discussed here were done with three prime objectives:

- * determination of the behaviour of the joint for various values of the force f_{e0} ;
- * determination of the effect of deliberate damaging of selected joint elements;
- * to get an indication about the reproducibility of the results.

As a consequence the static equilibrium position and the forces on the muscle tendons were not varied in these experiments. This reduction of the number of experiments had to be applied for the following reasons:

- * in comparison with the experiments with random excitation, the experiments with step excitation are more time consuming. This is due to
 - an increased time needed for proper adjustment of all charge amplifiers. For random excitation this can easily be done as a continuous response can be generated, whereas for step excitation this is not possible;
 - the need for repetition of each experiment to get an impression about the reproducibility of the experimental results, which requires proper installation of the loading mechanism discussed in section 5.1;
- * after change of the static equilibrium position and/or the load on the muscle tendons reconstruction of a previously used configuration must be done accurately if the effect of damaging of joint elements must be determined for various equilibrium positions and/or loads on the muscle tendons.

The static equilibrium position selected for this purpose is characterized by a flexion angle of 20° . This configuration was chosen because for level walking this flexion angle determines the configuration of the lower leg at heel strike, where a "step-like" excitation is most likely to occur.

A point of interest for the experiments is that the diameter of the bracing wires was reduced from 1 to 0.75 mm. As discussed in section 4.4. such a reduction, introduced to reduce the contribution of the stiffness of the bracing wires, leads to a decrease of the resonance frequency for vibration mode I.

Operations on the knee joint specimen

The experiments were done on knee joint specimens prepared as discussed in section 4.1.

In the experiments a number of measurements were done for different values of the force f_{e0} to obtain an impression about the behaviour of the undamaged joint. Next these measurements were repeated after damaging the joint. For this purpose it was decided to try and determine for KNEE12 the influence of cutting the medial meniscus and the anterior cruciate ligament, whereas for KNEE13 additionally the lateral meniscus was cut. These operations were done in situ without removing the joint specimen from the experimental set-up.

To be able to reach the anatomical structures mentioned above, an incision has to be made along the patellar ligament. When the knee joint specimen is mounted in the experimental set-up, areas of the capsular fibres can be determined by palpation along the patellar ligament which can be considered unloaded (in comparison with the patellar ligament itself). It therefore seems reasonable to assume that in these areas incisions can be made without disturbing the force transmission through the knee joint. The length of these incisions is approximately 40 mm. After these incisions are made, a window was dissected carefully in the joint capsule on either side of the patellar ligament (see Fig. 5.2.1).

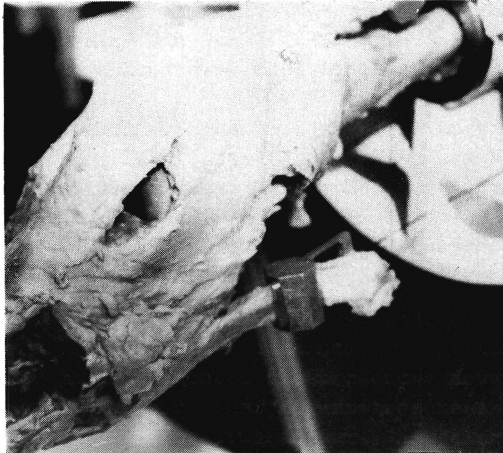
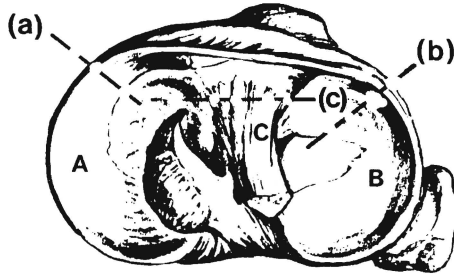


Fig. 5.2.1 View on the femur through the window on the lateral side of a knee joint specimen

These windows have a width of approximately 30 mm. Through these openings the infrapatellar pad of fat can be removed to obtain an empty volume between the patellar ligament and the tibia and the femur which is necessary to get a view on the anterior cruciate ligament. Next the anterior horn of the medial meniscus is cut first, by means of a radial incision (a) as is indicated schematically in Fig. 5.2.2.



A = medial meniscus, B = lateral meniscus,
C = anterior cruciate ligament

Fig. 5.2.2 Top view on the tibia with incisions made to cut the anterior horn of the menisci and the anterior cruciate ligament indicated by dashed lines

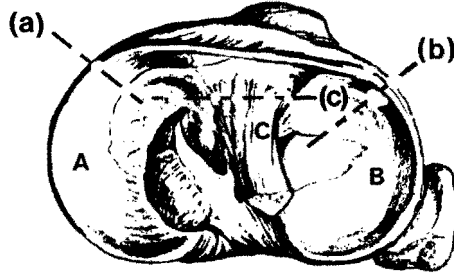
After this operation, the anterior cruciate ligament is cut (Fig. 5.2.2 (c)) which is a more difficult operation due to the limited view on this ligament in the joint configuration handled (20° flexion). Finally (for KNEE13) the lateral meniscus can be cut in a way similar to the medial meniscus (Fig. 5.2.2 (b)). To assure that the damage intended to be brought about is actually realized, the specimens were inspected visually after the experiments confirming the effectiveness of the operations described above.

For the operations carried out no change in the static load on the muscle tendons or the static equilibrium position could be measured. Measurements carried out before and after creation of the windows and removal of the infrapatellar pad of fat neither showed significant changes in the recorded behaviour of the joint.

5.3 Determination of the best-fitting linear system for step excitation

The response of the joint to the step excitation described in section 5.1, will be described in terms of the best-fitting linear system. For this purpose the 6×6 transfer function matrix $\underline{H}_p(f)$ introduced in chapter 3 will be used, relating the displacements of the tibia to the applied dynamic load.

These windows have a width of approximately 30 mm. Through these openings the infrapatellar pad of fat can be removed to obtain an empty volume between the patellar ligament and the tibia and the femur which is necessary to get a view on the anterior cruciate ligament. Next the anterior horn of the medial meniscus is cut first, by means of a radial incision (a) as is indicated schematically in Fig. 5.2.2.



A = medial meniscus, B = lateral meniscus,
C = anterior cruciate ligament

Fig. 5.2.2 Top view on the tibia with incisions made to cut the anterior horn of the menisci and the anterior cruciate ligament indicated by dashed lines

After this operation, the anterior cruciate ligament is cut (Fig. 5.2.2 (c)) which is a more difficult operation due to the limited view on this ligament in the joint configuration handled (20° flexion). Finally (for KNEE13) the lateral meniscus can be cut in a way similar to the medial meniscus (Fig. 5.2.2 (b)). To assure that the damage intended to be brought about is actually realized, the specimens were inspected visually after the experiments confirming the effectiveness of the operations described above.

For the operations carried out no change in the static load on the muscle tendons or the static equilibrium position could be measured. Measurements carried out before and after creation of the windows and removal of the infrapatellar pad of fat neither showed significant changes in the recorded behaviour of the joint.

5.3 Determination of the best-fitting linear system for step excitation

The response of the joint to the step excitation described in section 5.1, will be described in terms of the best-fitting linear system. For this purpose the 6×6 transfer function matrix $H_p(f)$ introduced in chapter 3 will be used, relating the displacements of the tibia to the applied dynamic load.

5.3.1 Theoretical concept for a curve-fit procedure

In chapter 3 it was derived (relations (3.3.43) and 3.3.60)

$$\ddot{\underline{x}}(f) = -4\pi^2 f^2 \underline{H}_\psi(f) \left| \begin{array}{c} \underline{n}_{e0} \\ \underline{0} \end{array} \right| f_e(f) \quad (5.3.1)$$

for a force f_e applied along a line \underline{n}_{e0} which coincides with one of the coordinate axes of the vector base connected to the tibia. The transfer function matrix $\underline{H}_\psi(f)$ can be written as

$$\underline{H}_\psi(f) = \sum_{k=1}^{N_m} \frac{\underline{A}_{\psi k}}{2\pi j f - s_k} + \frac{\underline{A}_{\psi k}}{2\pi j f - \bar{s}_k} \quad (5.3.2)$$

where $\underline{A}_{\psi k}$ and s_k are the residue matrix and pole, respectively, for each of the N_m vibration modes in the frequency range of interest. If the step excitation is applied along coordinate axis j ($j=1,2,3$) it holds

$$f_e(f) = \left(\frac{1}{2} \delta(f) - \frac{1}{2\pi j f} \right) f_{e0} \quad (5.3.3)$$

$$\ddot{\underline{x}} = - \sum_{k=1}^{N_m} s_k \exp(s_k t) \underline{a}_k^j + \bar{s}_k \exp(\bar{s}_k t) \underline{a}_k^j \quad (5.3.4)$$

$$\dot{\underline{x}} = - \sum_{k=1}^{N_m} \exp(s_k t) \underline{a}_k^j + \exp(\bar{s}_k t) \underline{a}_k^j \quad (5.3.5)$$

$$\underline{x} = - \sum_{k=1}^{N_m} \frac{1}{s_k} \exp(s_k t) \underline{a}_k^j + \frac{1}{\bar{s}_k} \exp(\bar{s}_k t) \underline{a}_k^j \quad (5.3.6)$$

Here $\delta(f)$ is Dirac's delta function for $f=0$. The 6×1 complex valued matrices \underline{a}_k^j are given by

$$\underline{a}_k^j = f_{e0} \underline{A}_{\psi k} \left| \begin{array}{c} \underline{n}_{e0} \\ \underline{0} \end{array} \right| := f_{e0} \underline{a}_k^j \quad (5.3.7)$$

As \underline{n}_{e0} coincides with coordinate axis j , \underline{a}_k^j is identical to column j of the residue matrix $\underline{A}_{\psi k}$. In appendix E it is indicated how the poles s_k and the column matrices \underline{a}_k^j can be obtained from the measured accelerations for such an experiment by means of a least-squares curve-fit procedure which uses relation (5.3.4) as a starting point. This curve-fit procedure is similar to the curve fit procedure developed by Mergeay (1980) to determine the modal parameters from measured impulse responses. This particular curve-fit procedure was selected because essentially it consists of a double linear regression to obtain the poles and residues. This is an advantage over time-consuming, general purpose non-linear curve-fit procedures which also require an initial guess for the unknown parameters. The former

curve-fit procedure mentioned above requires only little computational effort and does not require an initial estimate for the unknown parameters.

To assure that the velocity $\dot{\underline{z}}$ at $t=0$ vanishes, the following constraint equation must be included (see appendix B)

$$\sum_{k=1}^{N_m} \underline{A}_k \phi_k + \underline{\bar{A}}_k \phi_k = \underline{0} \quad (5.3.8)$$

yielding with relation (5.3.7) the requirement

$$\sum_{k=1}^{N_m} \underline{a}_k^j + \underline{\bar{a}}_k^j = \underline{0} \quad (5.3.9)$$

The complex column matrices \underline{a}_k^j determine the vibration pattern of the tibia. It is obvious that these complex quantities cannot be related directly to physical displacements. Due to damping the vibration pattern depends on the specific load exerted. If damping is neglected, the columns \underline{a}_k^j and the poles s_k are purely imaginary and the vibration pattern can easily be represented. In this case the imaginary part of the columns \underline{a}_k^j is proportional to the physical displacements measured in case mode k is excited. Representation of the vibration pattern for a particular vibration mode k is therefore simplified. Such an approach may also be followed for lightly damped systems to get an impression about the characteristics of a vibration mode. This will be elucidated in section 5.4.

5.3.2 Application of the curve-fit procedure

To illustrate how the curve-fit procedure was used for the measured signals, a typical experiment is considered, which yielded the accelerations \bar{s}_1 and \bar{s}_2 as shown in Fig. 5.3.1.

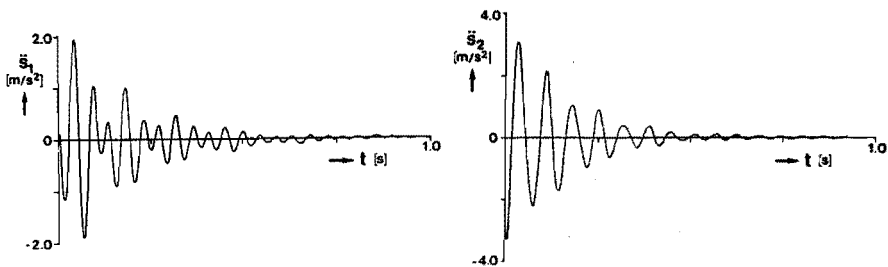


Fig. 5.3.1 Accelerations \bar{s}_1 and \bar{s}_2 measured for step excitation with a force applied in β -direction

These signals were obtained using a sampling frequency of 900 Hz. It is seen that no step is found for the accelerations at $t=0$ which

should occur for a linear system (see Fig. 5.3.3 also). Whether this is due to non-linearities cannot be gathered from the signals, as here the step-response of the analog filters in the data-acquisition system (cut-off frequency 100 Hz) plays a role, resulting in transients in the measured accelerations. Also the finite time in which the force f_{e0} is released may play a role, although this is not likely to be important. It is obvious that these transients must be dealt with in the curve-fit procedure, which is based on an ideal step response. From numerical simulations of theoretical step responses for a linear system (with the characteristic shape given in Fig. 5.3.1) it was found that a good approximation for the poles and residues can be obtained if in the curve-fit procedure only the data for $t \geq 0.05$ s are used. In these simulations the analog filters were incorporated using a digital implementation of the Butterworth filters in the data-acquisition system (Ahmed and Natarajan 1983). Therefore also the experimental results obtained were treated similarly.

The signals \ddot{s}_1 and \ddot{s}_2 contain two dominant frequency components. This is illustrated by means of the autopower spectrum of these signals, given in Fig. 5.3.2.

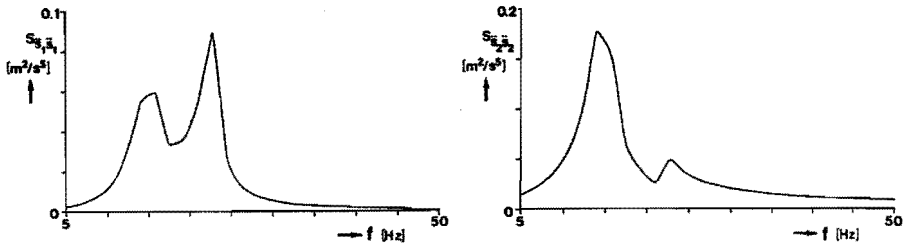


Fig. 5.3.2 Autopower spectrum of the signals \ddot{s}_1 and \ddot{s}_2 given in Fig. 5.3.1

From these figures it is seen that, like for random excitation, two resonance frequencies seem to be present. Therefore the curve-fit procedure was used to estimate the system parameters for 2 vibration

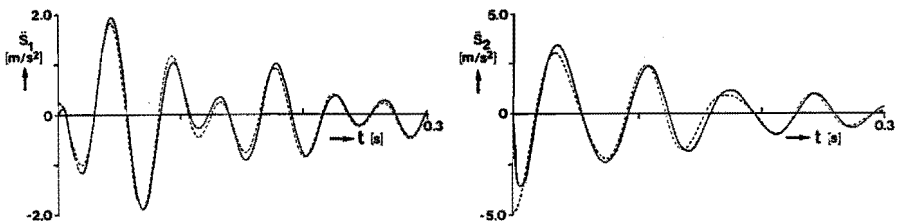


Fig. 5.3.3 Measured (—) and fitted (----) signals \ddot{s}_1 and \ddot{s}_2

modes ($N_m = 2$; mode I and mode II as introduced in chapter 4). A standard time interval of 0.5 s for the curve-fit procedure is used (therefore the system parameters are estimated from the data in the time interval 0.05-0.55 s), resulting in the original and fitted signals \bar{s}_1 and \bar{s}_2 as given in Fig. 5.3.3. It is seen that a reasonable agreement is obtained, which is representative for all measurements carried out.

5.4 Pre- and post-operative results for step excitation

In this section the results for the experiments on KNEE12 and KNEE13 are summarized. In section 5.4.1 attention is paid to the influence of the parameters magnitude of the force f_{e0} and damaging of joint elements on the resonance frequencies and damping values. Section 5.4.2 deals with the vibration modes of the tibia, whereas the reproducibility of the results is focused on in section 5.4.3.

The experiments discussed were carried out on KNEE12 (left knee, female, 38 years) and KNEE13 (right knee, female, 38 years). These knees are a bilateral pair. For both specimens a flexion angle of 20° was used, whereas also the forces on the muscle tendons were chosen identically ($F_a = 120$ N, $F_r = 150$ N, $F_b = 110$ N). All experiments for a particular specimen (except those done to test the reproducibility of the results) were carried out within 6 hours on one day.

5.4.1 Resonance frequencies and damping

As discussed in section 5.3.2, the measured accelerations were used to determine the system parameters (poles and residues) for 2 vibration modes (mode I and mode II). On forehand it is noted that the undamped resonance frequencies f_{OI} and f_{OII} , for mode I and mode II respectively, have typical values of 12 and 23 Hz, which may well be compared with those found for random excitation in chapter 4 (taken into account the reduction of the diameter of the bracing wires to 0.75 mm). Furthermore the vibration modes agree fairly well with the corresponding modes described in chapter 4. Mode I mainly involves displacements of the loaded end of the tibia in β -direction (flexion-extension) whereas for mode II displacements of the end of the tibia in α -direction dominate.

Fig. 5.4.1 gives the undamped angular velocity $\omega_{OI}^\beta = 2\pi f_{OI}^\beta$ for KNEE12 for experiments in which the force f_{e0} was applied in β -direction. As can be seen ω_{OI}^β decreases with increasing force values, being a clear indication for the non-linear behaviour of the joint. After cutting the medial meniscus the resonance frequency increases. If the resonance frequency is related to the stiffness of the joint this would indicate an increase of the stiffness (for this vibration mode) after cutting the medial meniscus. After subsequently cutting the anterior cruciate ligament ω_{OI}^β decreases, being an indication for a decrease

of the stiffness of the joint. After cutting the anterior cruciate ligament the stiffness of the joint is still larger than for the

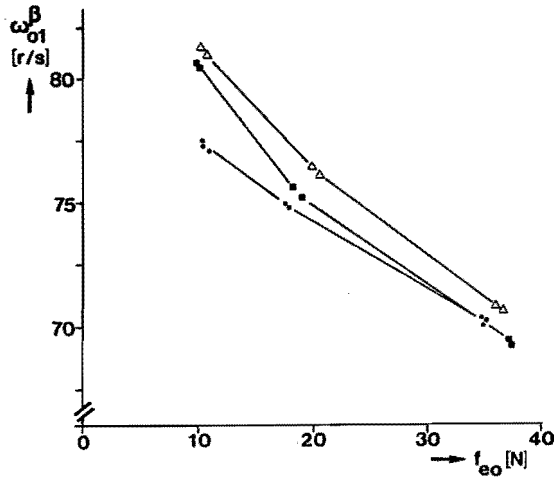


Fig. 5.4.1 The undamped angular velocity ω_o for vibration mode I for a force f_{eo} applied in β -direction

- KNEE12, intact
- △ KNEE12, medial meniscus cut
- KNEE12, anterior cruciate ligament cut

intact joint however. Fig. 5.4.1 also shows that the effect of damaging of joint elements is not identical for the various magnitudes of the force f_{eo} applied. Cutting the medial meniscus yields the most pronounced changes for a force of approximately 10 N, whereas subsequently cutting the anterior cruciate ligament mainly influences the results for a force f_{eo} of 20 N.

As can be seen from Fig. 5.4.1 repetition of a particular experiment yields almost identical results. Variations in ω_{OI}^β for a repeated experiment are far smaller than those due to a change in the applied force f_{eo} or due to damaging of the joint. This indicates that the experimental procedure used to apply the step excitation can be carried out with sufficient reproducibility.

Similar experiments were carried out for KNEE13 yielding the results for ω_{OI}^β given in Fig. 5.4.2. For the undamaged joint a similar behaviour is found as for KNEE12, except that the values for ω_{OI}^β are at a higher level. Successive cutting of the medial meniscus, the anterior cruciate ligament and the lateral meniscus yields a marked reduction of ω_{OI}^β indicating a clear decrease of the stiffness of the joint resulting from each of these operations. This behaviour might have been expected on fore-hand, if it is assumed that the joint elements mentioned contribute to the stiffness of the joint and loss of their function does not

influence the behaviour of the remainder of the joint elements. Obviously for KNEE12 this assumption does not hold.

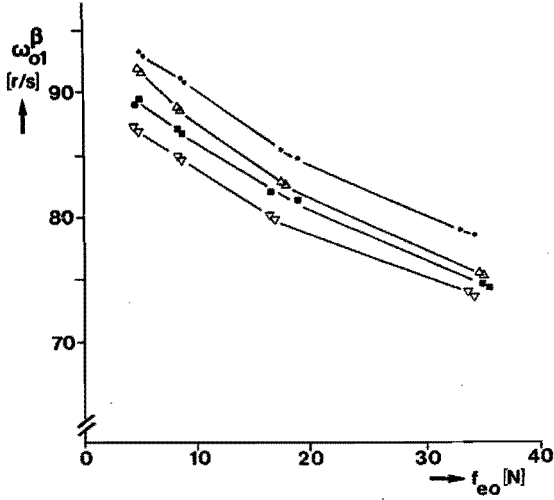


Fig. 5.4.2 The undamped angular velocity ω_o for vibration mode I for a force f_{e0} applied in β -direction

- KNEE13, intact
- △ KNEE13, medial meniscus cut
- KNEE13, anterior cruciate ligament cut
- ▽ KNEE13, lateral meniscus cut

The values for the dimensionless damping ξ_I^β corresponding to the values for ω_{O1}^β given above are presented in Fig. 5.4.3 and 5.4.4, for KNEE12 and KNEE13 respectively.

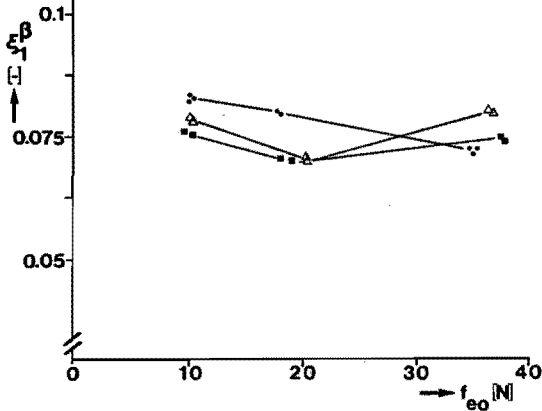


Fig. 5.4.3 The dimensionless damping ξ for vibration mode I for a force applied in β -direction

- KNEE12, intact
- △ KNEE12, medial meniscus cut
- KNEE12, anterior cruciate ligament cut

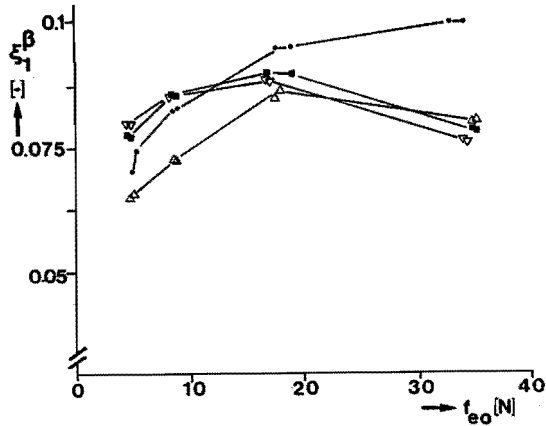


Fig. 5.4.4 The dimensionless damping ξ for vibration mode I for a force applied in β -direction

- KNEE13, intact
- △ KNEE13, medial meniscus cut
- KNEE13, anterior cruciate ligament cut
- ▽ KNEE13, lateral meniscus cut

For KNEE12, ξ_I^β for the intact joint decreases with increasing value of f_{e0} although these changes are only modest compared to those found for KNEE13. Cutting the medial meniscus results in a decrease of the damping ξ_I^β (except for the highest applied force f_{e0}). Subsequently cutting the anterior cruciate ligament does not significantly influence the damping values, except for the highest applied force f_{e0} .

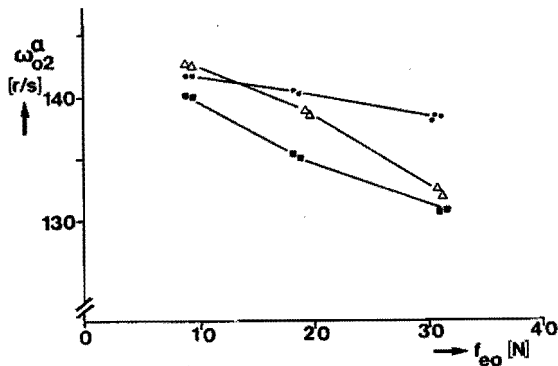


Fig. 5.4.5 The undamped angular velocity ω_0 for vibration mode II for a force f_{e0} applied in α -direction

- KNEE12, intact
- △ KNEE12, medial meniscus cut
- KNEE12, anterior cruciate ligament cut

For KNEE13 a rather different pattern is found. For the intact joint the damping ξ_I^β increases with increasing force f_{e0} . On cutting the medial meniscus a clear decrease of the damping is found. Subsequently cutting the anterior cruciate ligament results in an increase of the damping except for the highest applied force f_{e0} . Subsequently cutting the lateral meniscus does not significantly influence the damping value ξ_I^β .

For KNEE12 experiments were done in which the force f_{e0} was applied in α -direction. For the undamped resonance angular velocity ω_{OII}^α this yielded the results given in Fig. 5.4.5.

For the intact joint ω_{OII}^α decreases with increasing force f_{e0} . Cutting the medial meniscus yields a decrease of ω_{OII}^α , except for the smallest force f_{e0} applied, while cutting the anterior cruciate ligament yields a further decrease. These results indicate a decrease of the stiffness of the joint for this vibration mode. Fig. 5.4.6 gives the corresponding values for the damping ξ_{II}^α , indicating an increase of the damping with both increasing force f_{e0} and subsequent damage brought about. Obviously cutting the anterior cruciate ligament has a more significant influence for this vibration mode (unfortunately these experiments could not be carried out for KNEE13 due to the limited time available after a number of experiments were done to be able to get an impression about the reproducibility of the results.)

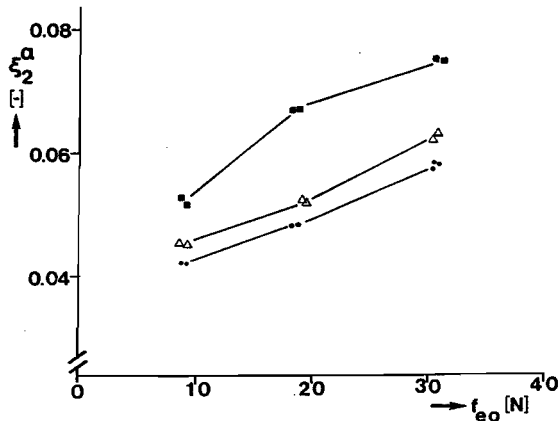


Fig. 5.4.6 The dimensionless damping ξ for vibration mode II for a force applied in α -direction

- KNEE12, intact
- \triangle KNEE12, medial meniscus cut
- \blacksquare KNEE12, anterior cruciate ligament cut

The results given above confirm the essentially non-linear behaviour of the joint, with stiffness and damping properties that depend upon the magnitude of the load applied, as found for random and sinusoidal excitation. Besides it is shown that damage brought about to some selected joint elements yields changes in the stiffness and damping

properties that can well be determined. Interpretation of the results obtained is complicated however, which emphasizes the need for a numerical model to study the behaviour of the joint.

5.4.2 Vibration modes

As discussed in section 5.3 the imaginary part of the column matrices \underline{g}_k^j (which are the columns of the residue matrices $\underline{A}_{\psi k}$) may be used to visualize the vibration modes of the tibia. In the sequel these imaginary parts are denoted with \underline{u}_k^j . They represent the modal displacements of the particular point and in the direction an accelerometer is mounted.

To describe the movements of the tibia these displacements can be used to determine the modal finite helical or instantaneous rotation axis (Spoor and Veldpaus 1980, Woltring et al. 1985). In this case the movements of the tibia with respect to the static equilibrium position (or with respect to the femur) are represented by a rotation π_h about and a translation t_h along a line with unit direction vector \vec{n}_h as illustrated in Fig. 5.4.7.

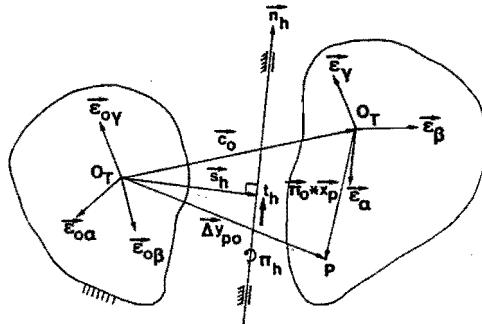


Fig. 5.4.7 Description of the kinematics of the tibia by means of helical parameters

As depicted in chapter 3 the displacement Δy_{po} of an arbitrary point on the tibia with respect to the static equilibrium position is given by

$$\Delta y_{po} = \underline{c}_0 + \underline{\pi}_0 * \underline{x}_p \tag{5.4.1}$$

where \underline{x}_p is the column matrix describing the position of point P with respect to the vector base $\vec{\underline{e}}_0^T = [\vec{e}_{0a} \ \vec{e}_{0b} \ \vec{e}_{0a}]$. \underline{c}_0 and $\underline{\pi}_0$ describe the translations and rotations, respectively, with respect to the static equilibrium position and orientation and can be obtained from (relation (3.3.41)).

$$\begin{vmatrix} \underline{c}_0 \\ \underline{\pi}_0 \end{vmatrix} = \underline{\Psi}^{-1} \underline{g} \tag{5.4.2}$$

with \underline{g} as the 6*1 column matrix containing the displacements obtained from the 6 accelerometers on the tibia and $\underline{\Psi}^{-1}$ as the 6*6 matrix given by relation (3.3.58). Now relation (5.4.1) can also be written in terms of the helical axis parameters

$$\Delta y_{po} = t_h \underline{n}_h + \pi_h \underline{n}_h * (\underline{x}_p - \underline{z}_h) \quad (5.4.3)$$

$$\underline{n}_h^T \underline{n}_h = 1 \quad ; \quad \underline{n}_h^T \underline{z}_h = 0 \quad (5.4.4)$$

$$\underline{z}_o = \pi_h \underline{n}_h \quad (5.4.5)$$

$$t_h = \underline{n}_h^T \underline{z}_o \quad (5.4.6)$$

$$\underline{z}_h = (\underline{n}_h * \underline{z}_o) / \pi_h \quad (5.4.7)$$

(in this time-domain description only t_h and π_h are a function of time, \underline{n}_h and \underline{z}_h are constants).

Now relation (5.4.3) can simply be transformed to the modal domain to yield the modal helical axis parameters t_{hk}^j , \underline{n}_{hk}^j , π_{hk}^j and \underline{z}_{hk}^j for vibration mode k and a force applied in direction j ($j=1,2$ or 3). These are related to the corresponding modal translations and rotations \underline{z}_{ok}^j and π_{ok}^j by (relation (5.4.2)).

$$\begin{bmatrix} \underline{z}_{ok}^j \\ \pi_{ok}^j \end{bmatrix} = \underline{\Psi}^{-1} \underline{u}_k^j \quad (5.4.8)$$

and can be determined from the modal equivalent of relations (5.4.3) through (5.4.7).

To indicate how the modal helical parameters can be obtained it is written

$$(\underline{z}_{ok}^j)^T = [c_{ok1}^j \quad c_{ok2}^j \quad c_{ok3}^j] \quad (5.4.9)$$

$$(\pi_{ok}^j)^T = [\pi_{ok1}^j \quad \pi_{ok2}^j \quad \pi_{ok3}^j] \quad (5.4.10)$$

$$(\underline{u}_k^j)^T = [u_{k1}^j \quad u_{k2}^j \quad \dots \quad u_{k6}^j] \quad (5.4.11)$$

From relations (5.4.8) and (3.3.58) it then easily can be derived that

$$c_{ok1}^j = u_{k1}^j \quad ; \quad c_{ok2}^j = u_{k2}^j \quad ; \quad c_{ok3}^j = u_{k3}^j \quad (5.4.12)$$

$$\pi_{ok1}^j = (u_{k2}^j - u_{k6}^j) / z_5 \quad ; \quad \pi_{ok2}^j = (u_{k4}^j - u_{k1}^j) / z_5$$

$$\pi_{ok3}^j = (u_{k4}^j - u_{k1}^j) / y_5 \quad (5.4.13)$$

Relation (5.4.13) can now easily be used to determine the modal rotation π_{ok1}^j , π_{ok2}^j and π_{ok3}^j by means of the Reuleaux method. This is illustrated for the parameter π_{ok1}^j in Fig. 5.4.8.

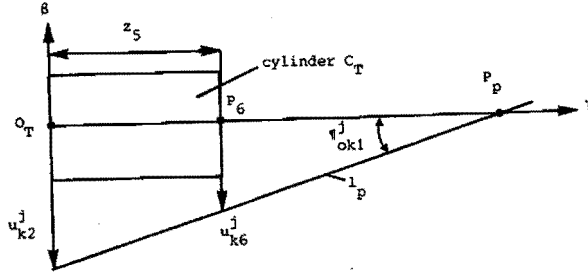


Fig. 5.4.8 Determination of the modal rotation parameter π_{okl}^j by means of the Reuleaux method from calculated modal displacements u_{k2}^j and u_{k6}^j (see text)

The modal displacements u_{k2}^j and u_{k6}^j are drawn as vectors in the β - γ plane, their endpoints being connected by a straight line l_p (note that u_{k2}^j and u_{k6}^j are obtained from accelerometers with measurement direction in the β - γ plane, such that u_{k2}^j results from the triaxial accelerometer mounted at O_T and u_{k6}^j from the uni-axial accelerometer mounted at point P_6 with coordinates $\mathbf{x}_{P_6}^T = [0 \ z_5 \ y_5]$). The modal rotation parameter π_{okl}^j is now obtained from the angle between the line l_p and the γ -axis. A similar procedure can be applied to determine the parameters π_{ok2}^j and π_{ok3}^j . Once these parameters have been determined, the parameters π_{hk}^j , t_{hk}^j , h_{hk}^j and z_{hk}^j can easily be found from the modal equivalent of relations (5.4.4) through (5.4.7).

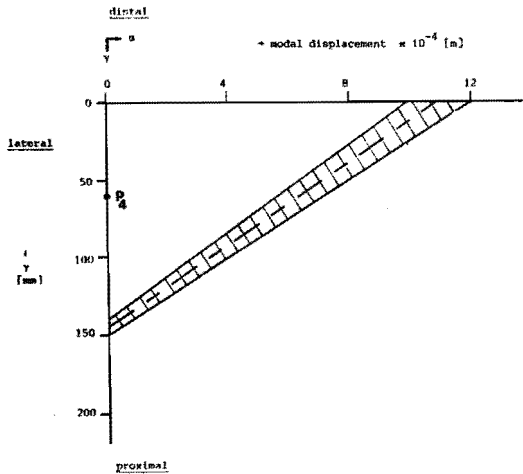


Fig. 5.4.9 Reconstructions for the modal rotation parameter π_{012}^β for KNEE12. The dashed area is the envelope of all reconstructions (see text)

On forehand it is expected that the modal helical parameters are influenced by the magnitude of the load applied and damaging of joint elements. For this purpose the Reuleaux plots (as given in Fig. 5.4.8) were composed for KNEE12 and KNEE13, combining all measurements carried out in one picture. This yields the pattern as given in Fig. 5.4.9 for KNEE12 to obtain the parameter π_{012}^{β} . The dashed area is the envelope of all reconstructions which vary without any observable pattern.

Whether this is due to errors (measurement errors, curve-fit errors) can not be specified. Therefore the average intersection (indicated by the dash-line) was taken to compute the averaged modal helical axis parameters. This was carried out for KNEE12 for a force applied in α - and β - direction and for KNEE13 for a load applied in β -direction, yielding the results in Table 5.4.1.

Table 5.4.1 Modal helical parameters for KNEE12 and KNEE13

KNEE12 vibration mode I, force applied in β -direction

$$\pi_{h1}^{\beta} = -0.037 \text{ [rad]} \quad ; \quad t_{h1}^{\beta} = -2.10^{-4} \text{ [m]}$$

$$(\underline{n}_{h1}^{\beta})^T = [0.97 \quad 0.2 \quad 0.12] \quad ; \quad (\underline{s}_{h1}^{\beta})^T = [-0.02 \quad -0.01 \quad 0.17] \text{ [m]}$$

KNEE12 vibration mode II, force applied in α -direction

$$\pi_{h2}^{\alpha} = 0.014 \text{ [rad]} \quad ; \quad t_{h2}^{\alpha} = -3.10^{-4} \text{ [m]}$$

$$(\underline{n}_{h2}^{\alpha})^T = [-0.09 \quad 0.79 \quad 0.6] \quad ; \quad (\underline{s}_{h2}^{\alpha})^T = [+0.01 \quad -0.10 \quad 0.14] \text{ [m]}$$

KNEE13 vibration mode I, force applied in β -direction

$$\pi_{h1}^{\beta} = -0.026 \text{ [rad]} \quad ; \quad t_{h1}^{\beta} = -1.10^{-3} \text{ [m]}$$

$$(\underline{n}_{h1}^{\beta})^T = [0.92 \quad -0.34 \quad -0.19] \quad ; \quad (\underline{s}_{h1}^{\beta})^T = [0.034 \quad 0 \quad 0.18] \text{ [m]}$$

For an interpretation of these results it is essential to recall that KNEE12 and KNEE13 are a bilateral left and right knee joint, respectively. The modal helical axis parameters are represented in Fig. 5.4.10 as their projections on the α - β and α - γ plane.

A first conclusion is that qualitatively the modal helical axis for mode I obtained for KNEE12 and KNEE13 is mirrored with respect to the β - γ plane, which might be expected for a bilateral pair.

Possibly mode I is determined by the contact between the tibia and the femur in the lateral compartment, whereas mode II (determined for KNEE12) seems to be determined by the contact between the tibia and the femur in the medial compartment. From the data given for KNEE12 and KNEE13 in Table 5.4.1 it follows also that mode I mainly involves rotations about the α - and β -axis (flexion-extension and exo-endo rotation) where for mode II exo-endo rotation and ad-abduction are

dominant. These findings clearly demonstrate the three dimensional nature of the dynamic behaviour of the joint.

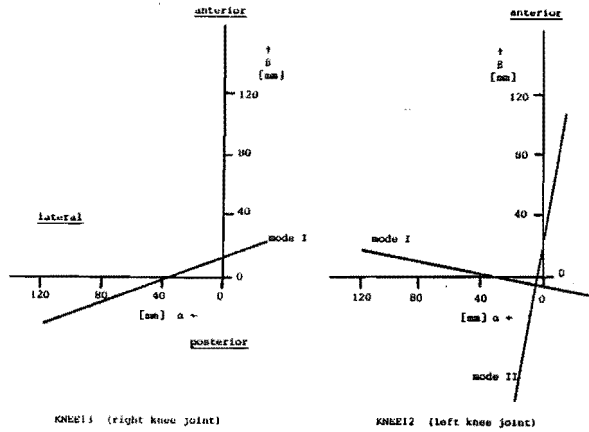


Fig. 5.4.10a Projections of the modal helical axes for KNEE12 and KNEE13 on the α - β plane, according to the data given in Table 5.4.1.

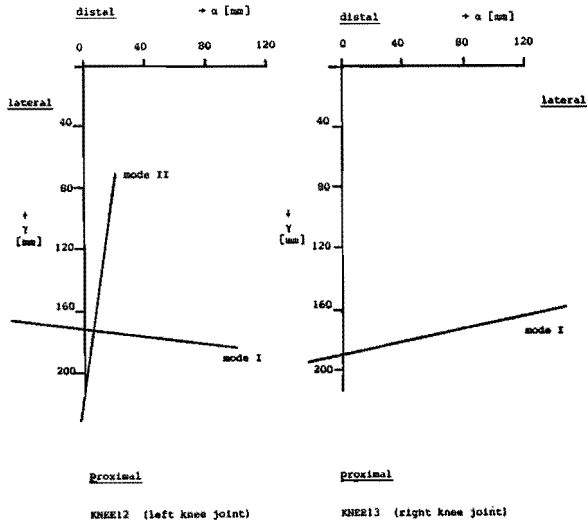


Fig. 5.4.10b Projections of the modal helical axes for KNEE12 and KNEE13 on the α - γ plane, according to the data given in Table 5.4.1. The tibial plateau is located at $\gamma = 190$ mm (approximately)

5.4.3 Reproducibility of the results

As mentioned in chapter 4, for the experiments with random excitation removal of the knee joint specimen from the experimental set-up, storage overnight and re-installation of the specimen the day after did not yield significant changes in the results obtained. This was not analysed in detail, however. For the experiments with step excitation on KNEE13 this was focused on in more detail. Before presenting the results for such repeated experiments on day 1 and day 2 it is noticed that this procedure may be influenced by

- * differences in the static equilibrium position of the specimen (which were kept as small as possible by proper measurement of the position of a number of fixed points on the tibia relative to the foundation of the experimental set-up);
- * differences in the load exerted on the muscle tendons (which were kept within 5 N);
- * differences in the behaviour of the joint due to progress of autolysis.

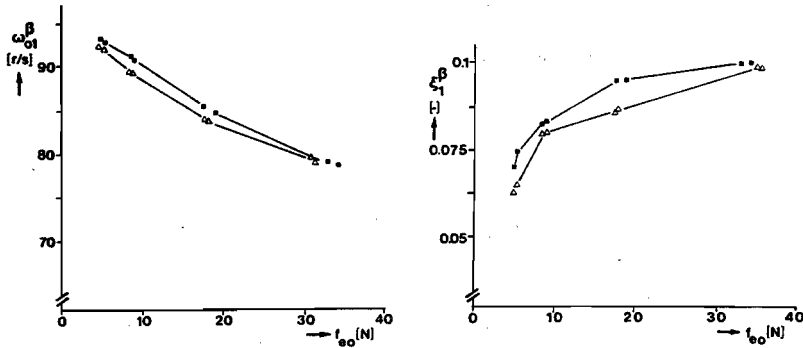


Fig. 5.4.11 The undamped angular velocity ω_{OI}^{β} and the dimensionless damping ξ_I^{β} for vibration mode I for a force applied in β -direction

△ KNEE13 day 1

■ KNEE13 day 2

Therefore it is felt that the results for the parameters ω_{OI}^{β} and ξ_I^{β} shown in Fig. 5.4.11 show a good reproducibility, although both the resonance angular velocity and the damping attain a somewhat higher value on day 2.

5.5 Discussion of the results

In section 5.4 the results from a time-domain analysis for two knee joint specimens have been presented in terms of the modal parameters describing the best-fitting linear system. From the data given the following conclusions can be drawn:

- * the dependence of the stiffness and damping characteristics of the joint on the magnitude of the applied force must be taken into account as this influence cannot be neglected compared to the influence of damaging of the joint.
- * for the intact joint, the resonance frequencies and damping values decrease and increase, respectively, with increasing force f_{e0} . This is in agreement with the results obtained for random excitation (see section 4.6) where an increase of the variance σ_f^2 of the excitation signal yielded the same characteristics.
- * the spatial orientation of the vibration modes for the undamped joint shows a scatter which can not be explained at this juncture.
- * the influence of damaging of joint elements upon the stiffness and damping characteristics can well be determined. Although the changes found are well bounded, they are significant as they are far larger than the variances in the results obtained for repeated experiments. This also indicates that step excitation is a useful tool to analyse the behaviour of the joint.

The results obtained for KNEE12 and KNEE13 show a rather distinct behaviour for vibration mode I after cutting the medial meniscus and the anterior cruciate ligament. Further research is necessary to establish whether these phenomena are typical or whether this is the result of uncontrolled changes in the parameters describing the static equilibrium position of the joint. Especially this applies for the static equilibrium position of the joint which could only be measured with limited accuracy. A numerical model of the knee joint is indispensable for such an analysis as this provides a tool for systematic analysis of the influence of various measurement parameters.

5.6 Summary

In this chapter a description has been given of the results obtained for step excitation of the knee joint using a time-domain analysis technique. As was expected from the results in chapter 4, the magnitude of the dynamic load applied has a marked influence upon the

stiffness and damping values for both vibration modes. Deliberate damaging of selected joint elements also yields a well observable change in the dynamic behaviour of the joint although these changes are difficult to interpret. Here the use of a non-linear dynamic numerical model of the knee joint seems inevitable. An important observation is however, that the experimental method discussed here enables to quantify the behaviour of the joint and therefore may provide a valuable tool for validation of such a model.

Chapter 6 Conclusions and recommendations

In this chapter a recapitulation is given of the conclusions that can be drawn from chapters 2 through 5 (section 6.1), as well as a number of recommendations for further research (section 6.2).

6.1 Conclusions

The present thesis deals with aspects of the dynamic behaviour of the human knee joint. Emphasis was laid on an experimental strategy to try and find the important characteristics and parameters for the behaviour of the joint under dynamic loading in post-mortem experiments. This approach was adapted to obtain guidelines for development of a numerical model describing the dynamic behaviour of the joint.

Although both the (quasi-)static and dynamic behaviour of the joint have been focused on in a number of experimental and theoretical studies, a literature review revealed that a lack of knowledge exists on 3 important subjects:

- * an understanding of the dynamic behaviour of the joint is not provided, neither from experiments nor from theoretical studies. This not only refers to the behaviour of the joint as a whole, but also to the influence of the individual joint elements and the interactions between them;
- * the constitutive behaviour of the soft tissues (ligamentous structures, menisci, articular cartilage) is only known to a limited extent. Especially for 2 or 3-D loading configurations both the experimental tools and numerical models must be developed or are to be validated;
- * (estimates for) the in vivo loads acting on the joint as a whole or on the individual joint elements are only poorly known.

Due to the complexity of the non-linear, time-dependent behaviour of the joint, experiments can only provide part of the knowledge required. Use of a numerical model is unescapable as neither from in vivo nor from post-mortem experiments the function of the knee joint for the force transmission in the musculoskeletal system can be fully understood. This is due to:

- * the limited number of parameters that can be determined from in vivo experiments;

- * the limited number of experiments that can be done in post-mortem experiments on an individual joint specimen due to progress of autolysis;
- * the irreversibility of experiments in which some part of the joint is damaged to assess its influence, whereas the sequence in which such operations are carried out may be of importance because of the non-linearity of the mechanical behaviour of the joint;
- * it difficult to assess what are to be considered as typical characteristics of the behaviour of the joint due to biological variability;
- * robust changes in the material properties of the joint elements can not be introduced, although this might be a useful tool to examine the effect of the joint elements upon the dynamic characteristics of the joint.

The use of a numerical model eliminates these handicaps to a large extent. Moreover such a model may provide guidelines for experiments to validate the model or to come to refinements in both the theoretical concept as well as the experimental techniques required.

A mathematical model of the human knee joint should be formulated starting from basic knowledge of the behaviour of the joint. For this purpose in chapter 3 an experimental strategy was presented intended to result in guidelines (obtained from experiments) for development of such a model. In view of the expected non-linearity of the behaviour of the joint, an approach was proposed to eliminate geometrical non-linearities by considering only small deflections with respect to a static equilibrium position. This linearization procedure (LLT) was also expected to reduce physical non-linearities. The LLT results in a description of the joint by means of a linear system with system parameters (poles and residues) dependent on the static equilibrium position of the joint, the magnitude of the loads exerted on selected muscle tendons to create this equilibrium position and the degree to which damage is brought about to individual joint elements. To obtain these system parameters transfer function analysis was selected as an efficient tool to relate the measured responses (accelerations and transmitted loads) to the dynamic load applied to the tibia.

In chapter 4 the results for the approach proposed in chapter 3 were given as obtained from experiments with random excitation. Four important conclusions could be drawn from these experiments:

- * creation of a stable, static equilibrium position of the joint by means of forces on the musculus biceps femoris, the musculus rectus femoris and a muscle on the medial side of the joint is possible, although the non-linear time-dependent

behaviour of the joint causes experimental difficulties. A non-bijective relationship was found to exist between the loads exerted on the muscle tendons and the spatial position and orientation of the tibia relative to the femur. Additionally, relaxation phenomena cause a problem for the experiments;

- * the dynamic behaviour of the joint has a relevant frequency range of 0 to 50 Hz, in which two vibration modes seem to be present. The finite stiffness of the bracing wires used to apply forces on the muscle tendons must be taken into account.
- * a description of the dynamic behaviour of the joint by means of transfer functions enables to quantify the influence of the static equilibrium position, the magnitude of the loads on the muscle tendons and damaging of joint elements;
- * the linearization procedure described in chapter 3 fails due to the essential non-linear behaviour of the joint, as the stiffness and damping characteristics obtained depend on the magnitude of the applied dynamic load, although the coherence function for the transfer functions does not indicate this (and therefore should be treated with care). A reduction of the magnitude of the applied loads was not taken into consideration because of an undesired decrease of the signal to noise ratio and the observation that the accelerations of the tibia in the experiments would then attain values well out of any physiological range. This finding is important for development of a numerical model as any linear model of the joint is to be rejected.

The non-linearity of the behaviour of the joint can be taken into account by introducing a dependence of the system parameters for the best-fitting linear system on the magnitude of the applied load. This strategy has been worked out in chapter 5 where step-excitation in combination with a time-domain analysis technique was applied. In these experiments only one static equilibrium position and corresponding forces on the muscle tendons were considered. The results of these experiments confirm the results described in chapter 4 as to the non-linearity of the joint. The effect of damaging the menisci and the anterior cruciate ligament could well be determined. Interpretation of the results is difficult, especially as the two specimen analysed show a different behaviour. This may be due to some uncontrolled changes in the static equilibrium position which could only be measured with limited accuracy. On the other hand it must be recalled that the response of the joint is described by means of the best-fitting linear system, which does not necessarily lead to a

physically interpretable description of the non-linear system considered. A numerical model of the joint is indispensable at this juncture.

Reviewing the results obtained for the experiments described in chapters 4 and 5, it is observed that the non-linear behaviour of the joint results in a decrease of the apparent stiffness and an increase of the apparent damping if the magnitude of the applied load is increased (which is a phenomenon found for random, sinusoidal as well as step excitation). As the 3-D static load-displacement characteristics of the joint given in literature seem to lend themselves (without problems) to local linearization, it is conceivable that the non-linearities found are due to essentially non-linear damping, such that an increase of the vibration amplitudes (or velocities) results in an increase of the damping (higher order velocity dependent damping may be thought of). Such a non-linearity may partly explain the results obtained for KNEE13 (chapter 5). Damaging the menisci or the anterior cruciate ligament is expected (and found) to yield a decrease of the stiffness. This reduction of the stiffness of the joint will, for the same magnitude of the load applied, result in larger vibration amplitudes as compared to the undamaged joint. If the damping depends on the vibration amplitudes as described above, damaging of a joint element will result in an increase of the damping. On the other hand damaging of a joint element may lead to a decrease of the damping due to the loss of its functionality for the joint as a whole. The degree to which each of these factors plays a role can not be clarified at this stage, but the results for KNEE13 indicate that by cutting the medial meniscus a substantial loss of damping is introduced which is not counterbalanced by an increase of the damping due to increased vibration amplitudes. After cutting the anterior cruciate ligament a reversed behaviour is found, whereas the effect of cutting the lateral meniscus is far less pronounced. Whether the phenomena discussed above are of importance can be analysed in a numerical model of the joint. In any case it may be concluded that the behaviour of the knee joint is not only determined by contributions of the different joint elements, but also by the interactions between them. Non-linear phenomena result in findings that are not in agreement with expectations based on the idea that the knee joint is a connection with elements whose function directly determines the behaviour of the joint as a whole. It is also essential that, if the non-linearities found are due to non-linear damping, (quasi)-static joint analysis is likely to provide only limited knowledge about the behaviour of the joint. Time-dependent phenomena must then be included as they are of eminent importance for the force transmission through the joint.

The experimental methods applied in this thesis allow for determination of the behaviour of the joint as a whole and of the influence of various parameters. Therefore it is believed that these methods may be used successfully for validation of a numerical model. Another, more short-term, application of this research is found in comparative studies in which the effects of partial or total knee replacement are

examined in post-mortem experiments. From these experiments guidelines for optimization of existing or development of new prostheses or prosthetic elements can be derived such that they, from a mechanical point of view, maximally resemble their biological counterparts. The methods described in this thesis may provide a contribution to this research.

Some modifications and extensions may increase the value of these methods:

- * a more sophisticated measurement method to obtain the parameters describing the kinematics of the tibia may result in a more accurate control of the static equilibrium position. Recent developments in the field of digital image processing allow for rapid determination of the 3-D kinematics of the tibia for both static and dynamic loading configurations;
- * the stiffness and damping values given in chapters 4 and 5 may provide guidelines for development of a device to apply the static load to the joint, such that its dynamic behaviour does not need to be taken into account in a numerical model (as is the case for the bracing wires);
- * use of a control system for adjustment of the forces on the bracing wires may be a good solution for the problems involved with manual adaptation of these forces.

6.2 Recommendations

As mentioned in section 6.1 it is felt that further research should focus on a non-linear numerical model of the human knee joint to get grip on the results from the experiments and to provide guidelines for further experiments. The results presented in this thesis and in literature indicate that in such a model all important joint elements should be incorporated (ligamentous structures, menisci, articular cartilage, bony parts and muscle tendons). It is questionable whether such a highly complex model should be focused on from the start as it will contain a number of parameters that are only poorly known. A step-wise development of such a model seems more appropriate. Such a step-wise development might start from the consideration that the knee joint may be regarded as a complex connection, in essence made up of two interacting subconnections, namely the ligamentous structures and the contact (direct or indirect via the menisci) between the articular cartilage layers. Each of these connections can be studied in detail before gathering their describing models in a complete knee joint model. Focusing on the ligamentous structures requires knowledge of their constitutive behaviour for 2 and 3-D loading configurations, in which highly anisotropic and time-

dependent material properties are essential. Non-linear Finite Element modelling (Roddeman 1988) and experimental techniques to measure stress and strain fields in these structures are inevitable here as well as for similar structures in other joints of the human body (Peters 1987). The contact phenomenon in the knee joint can also be focused on in detail. Again Finite Element modelling seems appropriate to deal with the non-linear, time-dependent material properties and complex geometries involved. Use of mixture theories (Mak 1986 and Oomens 1985) to describe the behaviour of the soft articular cartilage layers seems essential. To verify a theoretical model for such a complex connection use of a physical model (dummy) of the joint may be of great importance to be able to carry out experiments without the disturbing influence of autolysis. Besides such a physical model may be instrumented to obtain characteristics that are difficult to measure in post-mortem experiments (pressure distributions in the contact areas e.g.). Such a physical model also allows for variation of material properties to study their effect upon the force transmission.

If it is assumed that such a complete numerical model of the human knee joint can be formulated, the in vivo loads acting on the joint must also be known. Here another serious problem is encountered as methods to obtain these loads are to be developed (which is a factor common for a number of studies on subsystems or connections of the musculoskeletal system).

In the development of a theoretical model of the knee joint, experimental work as described in this thesis still is of importance. Validation of such a model requires a number of experiments not yet carried out (paying attention to the influence of exo-endo rotation, the flexion angle of the joint and the magnitude of the static load applied e.g.). An analysis of the influence of these measurement parameters may result in a well documented set of characteristics of what might be called an "average knee joint" (preferably as an internationally exchangeable data-base), in which non-typical experimental results have been eliminated. These characteristics can be used for validation of a numerical model and for development of a physical model of the knee.

Appendix A:

Coordinate systems and relative motions of the knee joint

In literature motions of the tibia relative to the femur (translations and rotations) are commonly specified with terms referring to a fixed coordinate system attached to the femur and which is defined by directions in anatomical planes as shown in Fig. A.1.

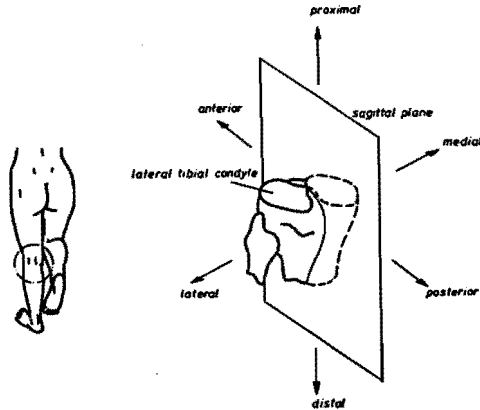


Fig. A.1 The tibia of a left knee joint with anatomical directions

Motions of the tibia relative to the femur are generally denoted with terms as flexion-extension, exo-endorotation, ad-abduction or varus-valgus, anterior-posterior displacements etc. Use of these terms provides an easy means for communication but may also result in confusion as the same expressions are used if motions of the femur relative to the tibia are meant, although it is not explicitly stated which bone should be taken as a reference. Throughout this thesis the motions in the joint are meant to be motions of the tibia relative to the femur. To give a more precise description for joint motions use must be made of two coordinate systems rigidly attached to the tibia and the femur at a particular point. Here a problem is faced as these origins can not be located uniquely due to the absence of landmarks common for all knee joints. Use of the principal (orthogonal) inertial axes and the center of gravity of a bone may be considered, but due to biological variability these parameters do not provide a unique reference. Use of Euler-parameters for the description of joint movements does neither remove this handicap, although screw-axes can be a useful tool to visualize relative rotations in the joint (Woltring et al. 1985). It is felt however that some coordinate axes can be defined that resemble for different joint specimens. To describe these axes Fig. A.2 is considered.

Imaginary cylinders C_T and C_F are placed around the distal part of the tibia and the proximal part of the femur respectively, such that the longitudinal axis of each cylinder coincides with the longitudinal axis of the particular bone.

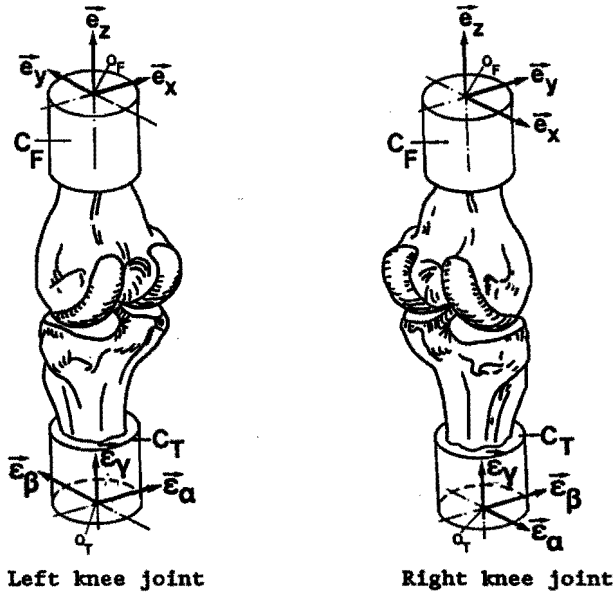


Fig. A.2 Definition of vector bases connected to the femur and the tibia

Now two coordinate systems can be introduced. An orthogonal coordinate system (x,y,z) with base vectors \vec{e}_x , \vec{e}_y and \vec{e}_z is rigidly attached to the femur with its origin O_F in the centre of the bottom plane of the cylinder C_F . This coordinate system can be regarded as an inertial reference frame. An orthogonal coordinate system (α,β,γ) with base vectors \vec{e}_α , \vec{e}_β and \vec{e}_γ is rigidly attached to the tibia with its origin O_T in the centre of the bottom plane of the cylinder C_T . The z - and γ -axis coincide with the longitudinal axis of the cylinders whereas the x - and α -axis are chosen to be located in the medio-lateral plane of the femur and the tibia, respectively. To provide a reference configuration it is assumed that in extension the vectorbases $\vec{g}^T = [\vec{e}_x \ \vec{e}_y \ \vec{e}_z]$ and $\vec{\xi}^T = [\vec{e}_\alpha \ \vec{e}_\beta \ \vec{e}_\gamma]$ are identical. Translations of the tibia relative to the femur can now be described by means of the translation vector \vec{a} , pointing from O_F to O_T , or its matrix representation $\underline{a}^T = [a_x \ a_y \ a_z]$ with respect to vector base \vec{g} ($\vec{a} = \underline{a}^T \vec{g}$). Rotations of the tibia relative to the femur can be described by means of the rotation tensor R , relating the orientation of the vector bases $\vec{\xi}$ and \vec{g} , or its matrix representation \underline{R} with respect to vectorbase \vec{g} ($R = \vec{\xi}^T \vec{g} = \vec{g}^T \underline{R} \vec{g}$). As the rotation tensor R is orthogonal ($R^C \cdot R = R \cdot R^C = I$) it can be written as a function of

three independent kinematical parameters, rotation angles e.g.. The spatial orientation of vector base \vec{e} can now be thought of as the result of successive rotations about fixed or floating axes (Andrews 1984, Wittenburg 1977) which results in a description by means of Euler, Cardan or Bryant angles e.g.. Here the description by means of the 3 successive rotations ϕ , θ and ω as shown in Fig. A.3 will be used. Similarly the frequently applied medical terminology for rotations can be interpreted. However, this interpretation does not cover the entire contents of these terms. In fact it is more appropriate to describe these motions as being a combination of translations and rotations, resulting from a specific external load, having one major component due to the mechanical behaviour of the loaded joint.

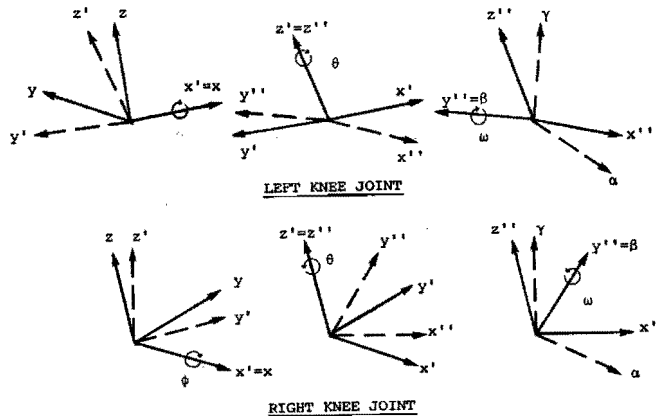


Fig. A.3 Definition of rotation parameters

Flexion-extension e.g. can be seen as the motion of the tibia due to a pure (follower) moment about the α -axis, resulting in a major rotation about the x-axis, smaller rotations about the y- and z-axis and additionally some small translational movements. As one major motion component can be distinguished, this medical terminology can be used to describe joint motions, but obviously lacks precision. In Table A.1 an overview is given of medical terminology for joint movements and their major components expressed in terms of the translations a_x , a_y and a_z and the rotations ϕ , θ and ω for a left knee joint.

Table A.1 Terminology for joint movements expressed in kinematical parameters for a right knee joint

<u>translations</u>	<u>rotations</u>
$a_x > 0$: lateral translation ¹	$\phi < 0$: extension
$a_x < 0$: medial translation	$\phi > 0$: flexion
$a_y > 0$: anterior translation	$\theta < 0$: exorotation
$a_y < 0$: posterior translation	$\theta > 0$: endorotation
$a_z > 0$: proximal translation	$\omega > 0$: adduction
$a_z < 0$: distal translation	$\omega < 0$: abduction

1 - also indicated by displacement

Appendix B:

Derivation of the transfer function matrix for a linear mechanical system with non-symmetric system matrices

In this appendix a description is given of the most essential steps, involved with the derivation of the transfer function matrix $\underline{H}(f)$ for a second-order linear mechanical system with constant, non-symmetric system matrices. For a detailed discussion of this subject see Natke (1983).

As a starting point consider the second-order set of N coupled linear differential equations relating a $N \times 1$ displacement matrix \underline{u} and the $N \times 1$ load matrix \underline{l}

$$\underline{M} \ddot{\underline{u}} + \underline{B} \dot{\underline{u}} + \underline{K} \underline{u} = \underline{l} \quad (\text{B.1})$$

It is assumed that \underline{M} , \underline{B} and \underline{K} are constant, non-symmetric, $N \times N$ real matrices representing mass, damping and stiffness characteristics, respectively. \underline{M} and \underline{K} are assumed to be positive definite. To solve relation (B.1) for \underline{u} in case \underline{l} is given, use can be made of forward and backward Laplace transform (or Fourier transform if desired). Without loss of generality it can be assumed that \underline{u} and $\dot{\underline{u}}$ vanish for $t=0$, which yields

$$(s^2 \underline{M} + s \underline{B} + \underline{K}) \underline{u}(s) = \underline{l}(s) \quad (\text{B.2})$$

where $\underline{x}(s)$ is the Laplace transform of \underline{x}

$$\underline{x}(s) = \int_0^{\infty} \underline{x}(t) \exp(-st) dt \quad (\text{B.3})$$

with s as the Laplace variable.

The transfer function matrix $\underline{H}(f)$ is now defined by

$$\underline{u}(f) = \underline{H}(f) \underline{l}(f) \quad (\text{B.4})$$

with $s = 2\pi j f$ to switch from the Laplace to the Fourier (frequency) domain. According to relation (B.2) $\underline{H}(f)$ formally can be written as

$$\underline{H}(f) = (-4\pi^2 f^2 \underline{M} + 2\pi j f \underline{B} + \underline{K})^{-1} \quad (\text{B.5})$$

Although relation (B.5) can be used to determine $\underline{H}(f)$, a transformation can be applied which yields a more tractable description of $\underline{H}(f)$ in the so-called modal domain.

For a start relation (B.1) is rewritten as a set of $2N$ first-order differential equations

$$\begin{vmatrix} \underline{B} & \underline{M} \\ \underline{M} & \underline{Q} \end{vmatrix} \begin{vmatrix} \dot{\underline{u}} \\ \underline{u} \end{vmatrix} + \begin{vmatrix} \underline{K} & \underline{O} \\ \underline{O} & -\underline{M} \end{vmatrix} \begin{vmatrix} \underline{u} \\ \dot{\underline{u}} \end{vmatrix} = \begin{vmatrix} \underline{1} \\ \underline{g} \end{vmatrix} \quad (\text{B.6})$$

where the trivial equation $\underline{M} \dot{\underline{u}} = \underline{M} \dot{\underline{u}}$ has been added. \underline{O} and \underline{g} represent a $N \times N$ and a $N \times 1$ null matrix, respectively. Introduction of the $2N \times 2N$ matrices

$$\underline{C} = \begin{vmatrix} \underline{B} & \underline{M} \\ \underline{M} & \underline{Q} \end{vmatrix} \quad \text{and} \quad \underline{D} = \begin{vmatrix} \underline{K} & \underline{O} \\ \underline{O} & -\underline{M} \end{vmatrix} \quad (\text{B.7})$$

and the $2N \times 1$ matrices

$$\underline{y} = \begin{vmatrix} \underline{u} \\ \dot{\underline{u}} \end{vmatrix} \quad \text{and} \quad \underline{g} = \begin{vmatrix} \underline{1} \\ \underline{g} \end{vmatrix} \quad (\text{B.8})$$

yields the so-called state description for the system

$$\underline{C} \dot{\underline{y}} + \underline{D} \underline{y} = \underline{g} \quad (\text{B.9})$$

Relation (B.9) can be transformed to the Laplace domain

$$(\underline{sC} + \underline{D})\underline{y}(s) = \underline{g}(s) \quad (\text{B.10})$$

To solve relation (B.10) for the column $\underline{y}(s)$ first the (right) eigenproblem

$$(\underline{sC} + \underline{D})\underline{y} = \underline{g} \quad (\text{B.11})$$

and the associated transposed (left) eigenproblem

$$(\underline{sC}^T + \underline{D}^T)\underline{y} = \underline{g} \quad (\text{B.12})$$

are considered. For a system with symmetric system matrices relations (B.11) and (B.12) are identical, yielding only one set of eigenvalues and eigenvectors. These eigenvectors can then be used to decouple relation (B.10) by means of a coordinate transformation. For a system with non-symmetric system matrices a similar decoupling of relation (B.10) will be applied which requires the use of the eigenvectors of the right and the left eigenproblem.

Solving relations (B.11) and (B.12) $2N$ eigenvalues s_k ($k=1 \dots 2N$) and corresponding eigenvectors \underline{v}_k and \underline{w}_k are obtained. For real matrices \underline{C} and \underline{D} the eigenvalues and eigenvectors are either real or occur in complex conjugate pairs. The eigenvectors can be partitioned according to

$$\underline{y}_k = \begin{vmatrix} \underline{x}_k \\ s_k \underline{x}_k \end{vmatrix} \text{ and } \underline{w}_k = \begin{vmatrix} \underline{t}_k \\ s_k \underline{t}_k \end{vmatrix} \quad (\text{B.13})$$

Here \underline{x}_k is a solution of the original second-order eigenproblem, emanating from (B.1)

$$(s^2 \underline{M} + s \underline{B} + \underline{K}) \underline{x} = \underline{0} \quad (\text{B.14})$$

and \underline{t}_k of the associated transposed eigenproblem

$$(s^2 \underline{M}^T + s \underline{B}^T + \underline{K}^T) \underline{t} = \underline{0} \quad (\text{B.15})$$

The eigenvalues s_k and eigenvectors \underline{x}_k and \underline{t}_k are generally referred to as the modal parameters of the linear system. For symmetric system matrices \underline{x}_k and \underline{t}_k are identical. It must be noted that the $4N$ eigenvectors must be scaled. Norm conditions often applied are

$$\underline{w}_k^T \underline{C} \underline{y}_k = 1 \quad (k=1 \dots 2N) \quad (\text{B.16})$$

and

$$\underline{w}_k^T \underline{\bar{w}}_k = \underline{y}_k^T \underline{\bar{y}}_k \quad (k=1 \dots 2N) \quad (\text{B.17})$$

which yield $4N$ norm equations.

All eigenvalues s_k and eigenvectors \underline{x}_k and \underline{t}_k are now stored in the matrices

$$\underline{S}^d = \begin{vmatrix} s_1 \\ s_2 \\ \vdots \\ s_{2N} \end{vmatrix} \quad (\text{B.18})$$

$$\underline{R} = [\underline{x}_1 \ \underline{x}_2 \ \dots \ \underline{x}_{2N}] \quad (\text{B.19})$$

$$\underline{T} = [\underline{t}_1 \ \underline{t}_2 \ \dots \ \underline{t}_{2N}] \quad (\text{B.20})$$

where \underline{S}^d is a $2N \times 2N$ matrix and \underline{R} and \underline{T} are $N \times 2N$ matrices. In a similar way the eigenvectors \underline{y}_k and \underline{w}_k are stored in $2N \times 2N$ matrices \underline{V} and \underline{W} respectively

$$\underline{V} = \begin{vmatrix} \underline{R} \\ \underline{R} \underline{S}^d \end{vmatrix} \text{ and } \underline{W} = \begin{vmatrix} \underline{T} \\ \underline{T} \underline{S}^d \end{vmatrix} \quad (\text{B.21})$$

With the use of relations (B.18) through (B.21) the eigenproblems (B.11), (B.12), (B.14) and (B.15) can now briefly be written as

$$\underline{C} \underline{V} \underline{S}^d + \underline{D} \underline{V} = \underline{0} \quad (\text{B.22})$$

$$\underline{C}^T \underline{W} \underline{S}^d + \underline{D}^T \underline{W} = \underline{0} \quad (\text{B.23})$$

$$\underline{M} \underline{R} \underline{S}^d \underline{S}^d + \underline{B} \underline{R} \underline{S}^d + \underline{K} \underline{R} = \underline{0} \quad (\text{B.24})$$

$$\underline{M}^T \underline{T} \underline{S}^d \underline{S}^d + \underline{B}^T \underline{T} \underline{S}^d + \underline{K}^T \underline{T} = \underline{0} \quad (\text{B.25})$$

Using relations (B.16) and (B.22) it can easily be shown that the matrices $\underline{W}^T \underline{C} \underline{V}$ and $\underline{W}^T \underline{D} \underline{V}$ are diagonal matrices. With relation (B.16) follows

$$\underline{W}^T \underline{C} \underline{V} = \underline{I} \quad (\text{B.26})$$

$$\underline{W}^T \underline{D} \underline{V} = -\underline{S}^d \quad (\text{B.27})$$

Relation (B.27) states that the eigenvalue problems can be decoupled using the eigenvectors introduced. To solve relation (B.10) for the column $\underline{y}(s)$ this decoupling property is usefull. Introduction of the so-called modal displacements \underline{z} with

$$\underline{y} = \underline{V} \underline{z} \quad (\text{B.28})$$

and pre-multiplication of relation (B.10) with the matrix \underline{W}^T yields

$$(s\underline{I} - \underline{S}^d)\underline{z}(s) = \underline{W}^T \underline{g}(s) \quad (\text{B.29})$$

where relations (B.26) and (B.27) have been used. The diagonal matrix $s\underline{I} - \underline{S}^d$ can easily be inverted and thus $\underline{y}(s)$ is obtained

$$\underline{y}(s) = \underline{V} (s\underline{I} - \underline{S}^d)^{-1} \underline{W}^T \underline{g}(s) \quad (\text{B.30})$$

From relation (B.8) it is seen that the columns $\underline{y}(s)$ and $\underline{g}(s)$ can be partitioned according to

$$\underline{y}(s) = \begin{vmatrix} \underline{u}(s) \\ s\underline{u}(s) \end{vmatrix} \quad \text{and} \quad \underline{g}(s) = \begin{vmatrix} \underline{l}(s) \\ \underline{q} \end{vmatrix} \quad (\text{B.31})$$

Substitution of the partitioned matrices \underline{V} and \underline{W} according to relation (B.21) and relation (B.31) in relation (B.30) yields the relation between $\underline{u}(s)$ and $\underline{l}(s)$

$$\underline{u}(s) = \underline{H}(s) \underline{l}(s) \quad (\text{B.32})$$

$$\underline{H}(s) = \underline{R} (s\underline{I} - \underline{S}^d)^{-1} \underline{T}^T \quad (\text{B.33})$$

From relation (B.33) the transfer function matrix $\underline{H}(f)$ expressed in the modal parameters is easily found by substitution of $s=2\pi jf$

$$\underline{H}(f) = \underline{R} (2\pi jf\underline{I} - \underline{S}^d)^{-1} \underline{T}^T \quad (\text{B.34})$$

$$= \sum_{k=1}^{2N} \frac{\underline{I}_k \underline{t}_k^T}{2\pi jf - s_k} \quad (\text{B.35})$$

The $2N$ non-symmetric matrices $\underline{\xi}_k \underline{\xi}_k^T$ are generally called the modal residual matrices or residues \underline{A}_k , whereas the eigenvalues s_k are often referred to as poles. For a real pole s_k the corresponding residue \underline{A}_k is real too, whereas complex conjugate poles result in complex conjugate residues.

The residues \underline{A}_k are not independent. To prove this the matrix \underline{D} is considered. Use of relation (B.27) gives

$$\underline{D}^{-1} = -\underline{V} (\underline{S}^d)^{-1} \underline{W}^T \quad (\text{B.36})$$

whereas from relation (B.7) \underline{D}^{-1} is found to be

$$\underline{D}^{-1} = \begin{vmatrix} \underline{K}^{-1} & \underline{0} \\ \underline{0} & -\underline{M}^{-1} \end{vmatrix} \quad (\text{B.37})$$

Elaboration of relation (B.36) with the partition of matrices \underline{V} and \underline{W} given in relation (B.21) results in the following equalities

$$\underline{K}^{-1} = -\underline{R} (\underline{S}^d)^{-1} \underline{T}^T \quad (\text{B.38})$$

$$\underline{M}^{-1} = \underline{R} \underline{S}^d \underline{T}^T \quad (\text{B.49})$$

$$\underline{0} = \underline{R} \underline{T}^T \quad (\text{B.40})$$

Relation (B.40) reveals the dependency of the residues \underline{A}_k

$$\underline{R} \underline{T}^T = \sum_{k=1}^{2N} \underline{\xi}_k \underline{\xi}_k^T = \sum_{k=1}^{2N} \underline{A}_k = \underline{0} \quad (\text{B.41})$$

The relations discussed so far can be used to determine the transfer function matrix $\underline{H}(f)$ in terms of the modal parameters. One particular case must be mentioned as this is frequently encountered when dealing with mechanical systems. Up to now real poles have been included but these will not occur for a lightly or undercritically damped system. In this case all poles and residues are complex quantities. This results in the following expression for $\underline{H}(f)$

$$\underline{H}(f) = \sum_{k=1}^N \frac{\underline{A}_k}{2\pi j f - s_k} + \frac{\underline{A}_k}{2\pi j f - \bar{s}_k} \quad (\text{B.42})$$

Stability of the system also assures that the poles have a negative real part. Consequently s_k can be written as

$$s_k = -\xi_k \omega_{0k} + j\omega_{0k} \sqrt{(1-\xi_k^2)} \quad (\text{B.43})$$

where ξ_k is the dimensionless damping ($0 < \xi_k < 1$) and ω_{0k} the undamped resonance angular velocity of mode k .

Appendix C:

Determination of $R_O^C \cdot \vec{\pi}$ and $R_O^C \cdot \vec{c}$ from measured uni-axial displacements of the tibia

Suppose M signals ($M \geq 6$) s_p ($p=1..M$) are measured using a uni-axial displacement transducer such that

$$s_p = \vec{n}_p \cdot R_O^C \cdot \vec{c} + (\vec{x}_p * \vec{n}_p) \cdot R_O^C \cdot \vec{\pi} + \epsilon_p \quad (C.1)$$

where ϵ_p is introduced to account for measurement errors. For the sake of simplicity $R_O^C \cdot \vec{c}$ and $R_O^C \cdot \vec{\pi}$ are replaced with the symbols \vec{t} and \vec{r} , respectively, whereas $\vec{x}_p * \vec{n}_p$ is denoted with \vec{p}_p

$$s_p = \vec{n}_p \cdot \vec{t} + \vec{p}_p \cdot \vec{r} + \epsilon_p \quad (C.2)$$

To arrive at an expression for estimates for \vec{t} and \vec{r} , a least squares method will be employed to minimize the functional

$$F(\vec{t}, \vec{r}) = \sum_{p=1}^M (s_p - \vec{n}_p \cdot \vec{t} - \vec{p}_p \cdot \vec{r})^2 \quad (C.3)$$

Requiring F to be stationary for infinitesimal small and mutually independent variations $\delta \vec{t}$ and $\delta \vec{r}$ of \vec{t} and \vec{r} , respectively, the following set of equations is obtained

$$\sum_{p=1}^M s_p \vec{n}_p = \sum_{p=1}^M \vec{n}_p \vec{n}_p \cdot \vec{t} + \sum_{p=1}^M \vec{n}_p \vec{p}_p \cdot \vec{r} \quad (C.4)$$

$$\sum_{p=1}^M s_p \vec{p}_p = \sum_{p=1}^M \vec{p}_p \vec{n}_p \cdot \vec{t} + \sum_{p=1}^M \vec{p}_p \vec{p}_p \cdot \vec{r} \quad (C.5)$$

It must be noted that no additional index is included to emphasize that the vectors \vec{t} and \vec{r} in relations (C.4) and (C.5) are estimates in a least squares sense. Introduction of the tensors

$$N = \sum_{p=1}^M \vec{n}_p \vec{n}_p ; P = \sum_{p=1}^M \vec{p}_p \vec{p}_p ; H = \sum_{p=1}^M \vec{n}_p \vec{p}_p \quad (C.6)$$

and the vectors

$$\vec{s} = \sum_{p=1}^M s_p \vec{n}_p \text{ and } \vec{q} = \sum_{p=1}^M s_p \vec{p}_p \quad (C.7)$$

yields a simplified notation of relations (C.4) and (C.5)

$$\begin{vmatrix} N & H \\ H^C & P \end{vmatrix} \cdot \begin{vmatrix} \vec{t} \\ \vec{r} \end{vmatrix} = \begin{vmatrix} \vec{s} \\ \vec{q} \end{vmatrix} \quad (C.8)$$

Relation (C.8) represents 6 simultaneous equations for the components of the unknown vectors \vec{t} and \vec{r} and can be solved if the left-hand tensor matrix is regular. Whether it is regular or not depends on the choice of the vectors \vec{n}_p and \vec{p}_p .

Application to the tibial component

To apply the method discussed above for the determination of the kinematics of the tibia, Fig. C.1. is considered

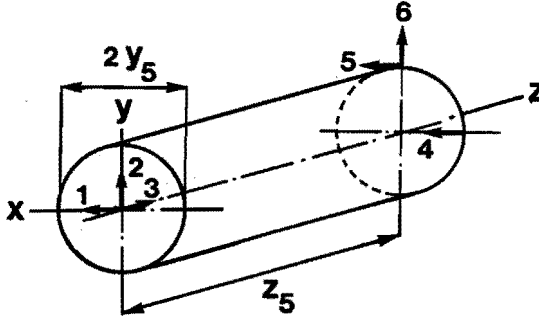


Fig. C.1 Displacements measured on the tibial component with 6 uni-axial displacement transducers mounted on a cylinder

It is assumed that 6 displacements are measured such that

$$\vec{x}_1 = \vec{0} ; \vec{n}_1 = \vec{e}_x ; \vec{p}_1 = \vec{0} \quad (C.9)$$

$$\vec{x}_2 = \vec{0} ; \vec{n}_2 = \vec{e}_y ; \vec{p}_2 = \vec{0}$$

$$\vec{x}_3 = \vec{0} ; \vec{n}_3 = \vec{e}_z ; \vec{p}_3 = \vec{0}$$

$$\vec{x}_4 = x_4 \vec{e}_x + z_5 \vec{e}_z ; \vec{n}_4 = \vec{e}_x ; \vec{p}_4 = z_5 \vec{e}_y$$

$$\vec{x}_5 = y_5 \vec{e}_y + z_5 \vec{e}_z ; \vec{n}_5 = \vec{e}_x ; \vec{p}_5 = z_5 \vec{e}_y - y_5 \vec{e}_z$$

$$\vec{x}_6 = y_5 \vec{e}_y + z_5 \vec{e}_z ; \vec{n}_6 = \vec{e}_y ; \vec{p}_6 = -z_5 \vec{e}_x$$

with y_5 and $z_5 \geq 0$.

A lengthy but straightforward derivation yields the following expressions for the estimates \vec{t} and \vec{r}

$$\vec{t} = s_1 \vec{e}_x + s_2 \vec{e}_y + s_3 \vec{e}_z \quad (C.10)$$

$$\vec{r} = \frac{(s_2 - s_6)}{z_5} \vec{e}_x + \frac{(s_4 - s_1)}{z_5} \vec{e}_y + \frac{(s_4 - s_5)}{y_5} \vec{e}_z \quad (C.11)$$

It is noticed that the coordinate x_4 cancels out and therefore can be chosen arbitrarily.

Relations (C.10) and (C.11) can be written more conveniently as

$$R_O^C \cdot \vec{c} = \vec{\alpha}^T \underline{\xi} ; \quad R_O^C \cdot \vec{\pi} = \vec{\beta}^T \underline{\xi} \quad (C.12)$$

with

$$\underline{\xi}^T = [s_1 \ s_2 \ s_3 \ s_4 \ s_5 \ s_6] \quad (C.13)$$

$$\vec{\alpha}^T = [\vec{e}_x \ \vec{e}_y \ \vec{e}_z \ \vec{0} \ \vec{0} \ \vec{0}] \quad (C.14)$$

$$\vec{\beta}^T = [-\frac{1}{z_5} \vec{e}_y \ \frac{1}{z_5} \vec{e}_x \ \vec{0} \ \frac{1}{z_5} \vec{e}_y + \frac{1}{y_5} \vec{e}_z \ -\frac{1}{y_5} \vec{e}_z \ -\frac{1}{z_5} \vec{e}_x] \quad (C.15)$$

Relations (C.12) can also be inverted

$$\underline{\xi} = \underline{\Psi} \cdot \begin{vmatrix} R_O^C \cdot \vec{c} \\ R_O^C \cdot \vec{\pi} \end{vmatrix} \quad (C.16)$$

with the vectormatrix $\underline{\Psi}$ given by

$$\underline{\Psi}^T = \begin{vmatrix} \vec{e}_x & \vec{e}_y & \vec{e}_z & \vec{e}_x & \vec{e}_x & \vec{e}_y \\ \vec{0} & \vec{0} & \vec{0} & z_5 \vec{e}_y & z_5 \vec{e}_y - y_5 \vec{e}_z & -z_5 \vec{e}_x \end{vmatrix} \quad (C.17)$$

Appendix D:

A brief overview of spectral analysis

To describe the essential steps involved with the determination of the transfer function $H(f)$ of a linear system, Fig. D.1 is considered.

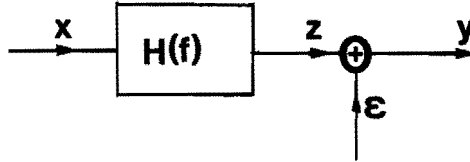


Fig. D.1 Input x and output y of a linear system with transfer function $H(f)$, subjected to noise ϵ

The signals y and x are simultaneously measured with a constant sampling frequency $f_s = 1/\Delta t_s$ Hz, where the measured response y is considered to be the sum of the response z of the system to an excitation x and a signal ϵ which represents an error signal and which is assumed to be statistically independent of the signal x .

Suppose M measurements are done such that each measurement results in a set or record x^m and y^m ($m=0 \dots M-1$) of N samples for the signals x and y , respectively. Consequently each measurement represents a measurement time of $T_r = N \Delta t_s$ s. A sample n ($n=0 \dots N-1$), taken at time $t=(n-1)\Delta t_s$, in measurement m of the signals x and y is denoted with x_n^m and y_n^m , respectively. For the sake of simplicity it is assumed that N is a power of 2 (512, 1024 or 2048 e.g.). By means of a Fast Fourier Transform (F.F.T.) algorithm, the Discrete Fourier Transform (D.F.T.) $x^m(f)$ and $y^m(f)$ of the records x^m and y^m , respectively, is calculated

$$x^m(f=k\Delta f) = \sum_{n=0}^{N-1} x_n^m \exp(-2\pi j * k * n / N) \Delta t_s \quad (k=0 \dots N-1) \quad (D.1)$$

$$y^m(f=k\Delta f) = \sum_{n=0}^{N-1} y_n^m \exp(-2\pi j * k * n / N) \Delta t_s \quad (k=0 \dots N-1) \quad (D.2)$$

with

$$\Delta f = 1/T_r \quad (D.3)$$

as the frequency resolution of the D.F.T. An essential property of the D.F.T. is that for real signals x and y only the first $N/2$ frequency points (spectral lines) are relevant which represent the

frequency interval from 0 to $f_s/2$ Hz (folding property of the D.F.T.). The M Fourier transforms are related by

$$y^m(f) = H(f) x^m(f) + \varepsilon^m(f) \quad (D.4)$$

For stationary signals x and y an estimate for $H(f)$ can be obtained from (Bendat and Piersol 1980)

$$H(f) = \frac{S_{yx}(f)}{S_{xx}(f)} \quad (D.5)$$

with

$$S_{yx}(f) = \frac{1}{M T_r} \sum_{m=0}^{M-1} y^m(f) \bar{x}^m(f) \quad (D.6)$$

$$S_{xx}(f) = \frac{1}{M T_r} \sum_{m=0}^{M-1} x^m(f) \bar{x}^m(f) \quad (D.7)$$

Here $S_{yx}(f)$ is an estimate for the crosspower spectrum of the signals y and x , whereas $S_{xx}(f)$ is an estimate for the autopower spectrum of the signal x . An estimate for the autopower spectrum of the signal ε is given by

$$S_{\varepsilon\varepsilon}(f) = S_{yy}(f) (1 - \gamma_{yx}^2(f)) \quad (D.8)$$

with

$$S_{yy}(f) = \frac{1}{M T_r} \sum_{m=0}^{M-1} y^m(f) \bar{y}^m(f) \quad (D.9)$$

$$\gamma_{yx}^2(f) = \frac{S_{yx}(f) S_{yx}(f)}{S_{yy}(f) S_{xx}(f)} \quad (D.10)$$

$S_{yy}(f)$ and $\gamma_{yx}^2(f)$ are estimates for the autopower spectrum of the signal y and the coherence function, respectively. The coherence function is a real number between 0 and 1 and is a measure for the influence of errors. For an ideal measurement the coherence function is 1 in the frequency range of interest, whereas the coherence function attains values of approximately 0 for signals y and x which are virtually uncorrelated.

When using the computational scheme given above, two important error sources must be considered:

* aliasing

If the signals x and y are sampled without satisfying Nyquist's criterion (see section 3.5) the frequency components with a frequency $> f_s/2$ Hz are falsely measured. They will appear in the frequency interval from 0 to $f_s/2$ Hz when

the D.F.T. is applied. This error source can be eliminated by proper filtering of the signals before they are digitized (see section 3.5).

* signal-leakage

As the D.F.T. is an approximation for the Fourier transformation, an error is introduced if the signals are non-periodic within the time interval T_r . This results in a smearing of frequency components over the discrete frequencies (spectral lines) handled in the D.F.T. To reduce this error use can be made of a periodic window function w . The sampled signals are multiplied with this function to obtain periodic signals. For random signals e.g., the Hanning window is often used

$$w(t) = 0.5*(1 - \cos(2\pi t/T_r)) \quad (D.11)$$

With this window the records x^m and y^m are modified to records \tilde{x}^m and \tilde{y}^m given by

$$\tilde{x}_n^m = x_n^m w(t=(n-1)\Delta t_s) \quad (n=0\dots N-1) \quad (D.12)$$

$$\tilde{y}_n^m = y_n^m w(t=(n-1)\Delta t_s) \quad (n=0\dots N-1) \quad (D.13)$$

The records \tilde{x}^m and \tilde{y}^m are subsequently used in stead of the original records x^m and y^m . In general such a correction suffices to reduce signal-leakage for random signals, although for lightly damped systems with a clear resonance frequency additionally Δf must be chosen sufficiently small to yield the correct result (Dortmans and de Kraker 1987). This can be obtained by selection of a sufficiently high number of samples N (at the cost of increasing time to calculate the D.F.T.'s) or by application of zoom-spectral analysis (Bendat and Piersol 1980).

Appendix E

A modal parameter estimation technique using time domain data for step excitation

In this appendix an outline is given of a numerical method for extraction of the modal parameters from measured accelerations of a linear system subjected to step excitation (see section 5.1). The modal parameters to be determined are the poles and modal displacements corresponding to the vibration modes in the frequency range of interest. The method considered has been deduced from the method proposed by Mergeay (1980), to calculate modal parameters from measured impulse responses. An extension brought in here is the inclusion of a constraint equation to assure that the impulse response at $t=0$ vanishes.

Suppose N components \ddot{s}_i ($i=1\dots N$) of the $N \times 1$ matrix $\ddot{\mathbf{s}}$ have been measured, which represent the accelerations of an N degree of freedom undercritically damped linear system subjected to step excitation. It is assumed that in the frequency range of interest N_m vibration modes have to be determined. If the signals are sampled with a constant sampling frequency $f_s = 1/\Delta t_s$ Hz, a sample m ($m=0\dots M-1$) taken at time $t=t_m = m\Delta t_s$ is given by (relation 5.3.4)

$$\begin{aligned} \ddot{\mathbf{s}}(t=t_m) = \ddot{\mathbf{s}}_m = & - \sum_{k=1}^{N_m} s_k \exp(s_k m \Delta t_s) \mathbf{a}_k + \\ & - \sum_{k=1}^{N_m} \bar{s}_k \exp(\bar{s}_k m \Delta t_s) \bar{\mathbf{a}}_k + \boldsymbol{\varepsilon}_m \end{aligned} \quad (\text{E.1})$$

after scaling with the applied force f_{e0} . Here s_k is the pole corresponding to vibration mode k ($k=1\dots N_m$). \mathbf{a}_k ($k=1\dots N_m$) is the column matrix containing the modal displacements for mode k for a particular experiment. $\boldsymbol{\varepsilon}_m = \boldsymbol{\varepsilon}(t=t_m)$ is included to account for measurement errors. Relation (E.1) can be written more conveniently as

$$\ddot{\mathbf{s}}_m = - \sum_{k=1}^{2N_m} s_k (P_k)^m \mathbf{a}_k + \boldsymbol{\varepsilon}_m \quad (\text{E.2})$$

with

$$P_k = P_{k+N_m} = \exp(s_k \Delta t_s) \quad (k=1\dots N_m) \quad (\text{E.3})$$

$$\mathbf{a}_k = \bar{\mathbf{a}}_{k+N_m} \quad (k=1\dots N_m)$$

The factors P_k can be seen as the roots of the polynomial of order $2N_m$

$$\prod_{k=1}^{2N_m} (P - P_k) = 0 \quad (\text{E.4})$$

or

$$\sum_{k=0}^{2N_m} \alpha_k P^k = 0 \quad ; \alpha_{2N_m} = 1 \quad (\text{E.5})$$

where the coefficients α_k are real numbers. Obviously the factors P_k can be determined from relation (E.5) if the coefficients α_k are known. With known P_k the poles s_k can be determined according to

$$s_k = \ln(P_k) / \Delta t_s \quad (k=1 \dots N_m) \quad (\text{E.6})$$

To obtain an expression for the $2N_m$ unknown coefficients α_k relation (E.2) is used

$$\sum_{m=0}^{2N_m} \ddot{\xi}_m \alpha_m = - \sum_{k=1}^{2N_m} s_k \ddot{g}_k \sum_{m=0}^{2N_m} \alpha_m (P_k)^m + \sum_{m=0}^{2N_m} \dot{\xi}_m \alpha_m \quad (\text{E.7})$$

With the use of relation (E.5) it is seen that the first term on the right hand side of relation (E.7) vanishes, which yields

$$\sum_{m=0}^{2N_m} \ddot{\xi}_m \alpha_m = \sum_{m=0}^{2N_m} \dot{\xi}_m \alpha_m \quad := \dot{\xi}_{2N_m} \quad (\text{E.8})$$

As $\alpha_{2N_m} = 1$ it holds

$$\ddot{\xi}_{2N_m} = - \sum_{m=0}^{2N_m-1} \ddot{\xi}_m \alpha_m + \dot{\xi}_{2N_m} \quad (\text{E.9})$$

Relation (E.9) states that for an ideal measurement $2N_m$ successive samples are sufficient to determine $\ddot{\xi}_{2N_m}$. Similarly it can be deduced that a shift of m_0 samples in relation (E.7) yields

$$\ddot{\xi}_{m_0+2N_m} = - \sum_{m=0}^{2N_m-1} \ddot{\xi}_{m_0+m} \alpha_m + \dot{\xi}_{m_0+2N_m} \quad (\text{E.10})$$

with

$$0 \leq m_0 \leq M - 2N_m \quad (\text{E.11})$$

Relation (E.10) can now be used to determine the $2N_m$ coefficients α_m from R ($R \geq 2N_m$) successive samples, using the abridged equation

$$\dot{g}_p = \underline{J}_p \dot{g} + \dot{\xi}_p \quad (\text{E.12})$$

with

$$\underline{g}_p^T = [\underline{s}_{m_0+2N_m}^T \cdots \underline{s}_{m_0+R-1+2N_m}^T] \quad (\text{E.13})$$

$$\underline{\beta}_p^T = [\underline{\delta}_{m_0+2N_m}^T \cdots \underline{\delta}_{m_0+R-1+2N_m}^T]$$

$$\underline{\alpha}^T = [\alpha_0 \cdots \alpha_{2N_m-1}]$$

and

$$\underline{J}_p = \begin{vmatrix} \underline{s}_{m_0} & \underline{s}_{m_0+1} & \cdots & \underline{s}_{m_0+2N_m-1} \\ \underline{s}_{m_0+1} & & & \\ \vdots & & & \\ \underline{s}_{m_0+R-1} & & \cdots & \underline{s}_{m_0+R+2N_m-2} \end{vmatrix} \quad (\text{E.14})$$

(\underline{g}_p , $\underline{\beta}_p$, $\underline{\alpha}$ and \underline{J}_p are $(N \times R) \times 1$, $(N \times R) \times 1$, $2N_m \times 1$ and $(N \times R) \times 2N_m$ matrices, respectively).

From relation (E.12) a least squares estimate for the column $\underline{\alpha}$ can be obtained (which will not be provided with an additional index) by requiring the functional $F(\underline{\alpha})$

$$F(\underline{\alpha}) = \underline{\beta}_p^T \underline{\beta}_p = (\underline{g}_p - \underline{J}_p \underline{\alpha})^T (\underline{g}_p - \underline{J}_p \underline{\alpha}) \quad (\text{E.15})$$

to attain a stationary value, yielding

$$\underline{\alpha} = (\underline{J}_p^T \underline{J}_p)^{-1} \underline{J}_p^T \underline{g}_p \quad (\text{E.16})$$

With known coefficients $\underline{\alpha}$ the poles s_k ($k=1 \dots N_m$) can be determined from relations (E.5) and (E.6) (which requires extraction of the roots of the polynomial equation (E.5)).

Once the poles s_k have been determined the column matrices \underline{a}_k in relation (E.2) can be calculated. The column matrices \underline{a}_k are not independent however, as from relation (B.41) follows

$$\sum_{k=1}^{2N_m} \underline{A}_k \underline{f}_{e0}/f_{e0} = \sum_{k=1}^{2N_m} \underline{a}_k = \underline{0} \quad (\text{E.17})$$

The column matrices \underline{a}_k are complex quantities which can be written in terms of their real and imaginary part

$$\underline{a}_k = \underline{a}_k^r + j \underline{a}_k^i \quad (k=1 \dots N_m) \quad (\text{E.18})$$

A similar separation is handled for the complex quantities $s_k(P_k)_{m_0+m}$

$$s_k(P_k)^{m_0+m} = b_{k,m}^r + j b_{k,m}^i \quad (k=1 \dots N_m; m=0 \dots M-m_0) \quad (E.19)$$

Taking into account the occurrence of complex conjugate pairs of poles s_k and columns a_k , relation (E.2) can be written as

$$\begin{aligned} \bar{s}_{m_0+m} &= - \sum_{k=1}^{N_m} (b_{k,m}^r + j b_{k,m}^i)(a_k^r + j a_k^i) + \\ &\quad \sum_{k=1}^{N_m} (b_{k,m}^r - j b_{k,m}^i)(a_k^r - j a_k^i) + \varepsilon_{m_0+m} \\ &= -2 \sum_{k=1}^{N_m} (b_{k,m}^r a_k^r - b_{k,m}^i a_k^i) + \varepsilon_{m_0+m} \end{aligned} \quad (E.20)$$

For the constraint equation (E.17) holds with relation (E.18)

$$\sum_{k=1}^{N_m} a_k^r = 0 \quad (E.21)$$

The $N \times 1$ matrices a_k^r and a_k^i ($k=1 \dots N_m$) each contain N unknown parameters. From $R \geq 2N$ successive samples it follows in abridged notation

$$\underline{G}_r = \underline{J}_r \underline{B} + \underline{E}_r \quad (E.22)$$

with

$$\underline{G}_r^T = [\bar{s}_{m_0} \dots \bar{s}_{m_0+R-1}] \quad (E.23)$$

$$\underline{B}^T = [a_1^r \dots a_{N_m}^r \ a_1^i \dots a_{N_m}^i]$$

$$\underline{E}_r^T = [\varepsilon_{m_0} \dots \varepsilon_{m_0+R-1}]$$

$$\underline{J}_r = \left| \begin{array}{cccc} -2b_{1,0}^r & \dots & -2b_{N_m,0}^r & 2b_{1,0}^i & \dots & 2b_{N_m,0}^i \\ -2b_{1,1}^r & & & & & \\ \vdots & & & & & \\ & -2b_{1,R-1}^r & \dots & -2b_{N_m,R-1}^r & 2b_{1,R-1}^i & \dots & 2b_{N_m,R-1}^i \end{array} \right|$$

The constraint equation (E.21) can be written as

$$\underline{B}^T \underline{N}_c = 0 \quad (E.24)$$

with

$$\underline{N}_c^T = [1 \dots 1 \ 0 \dots 0] \quad (E.25)$$

Relations (E.22) and (E.24) must now be solved simultaneously. For the column \underline{b}_i ($i=1\dots N$) of the matrix \underline{B} and the corresponding columns \underline{g}_i and \underline{e}_i of the matrices \underline{G}_r and \underline{E}_r , respectively, it holds

$$\underline{g}_i = \underline{J}_r \underline{b}_i + \underline{e}_i \quad (i=1\dots N) \quad (E.26)$$

$$\underline{n}_c^T \underline{b}_i = 0 \quad (i=1\dots N) \quad (E.27)$$

Relations (E.26) and (E.27) can be solved using a least squares method in which the constraint equation (E.27) is taken into account by means of a Lagrange multiplier λ_i , to minimize the functional $F(\underline{b}_i, \lambda_i)$

$$F(\underline{b}_i, \lambda_i) = (\underline{g}_i - \underline{J}_r \underline{b}_i)^T (\underline{g}_i - \underline{J}_r \underline{b}_i) + 2\lambda_i \underline{n}_c^T \underline{b}_i \quad (E.28)$$

Requiring $F(\underline{b}_i, \lambda_i)$ to be stationary for infinitesimal small variations $\delta \underline{b}_i$ and $\delta \lambda_i$ of \underline{b}_i and λ_i , respectively, yields the following equations for estimates of the unknowns \underline{b}_i and λ_i (which are not indexed additionally to indicate that they must be considered as estimates)

$$(\underline{J}_r^T \underline{J}_r) \underline{b}_i = \underline{J}_r \underline{g}_i - \lambda_i \underline{n}_c \quad (i=1\dots N) \quad (E.29)$$

$$\underline{n}_c^T \underline{b}_i = 0 \quad (i=1\dots N) \quad (E.30)$$

Assuming that the matrix $\underline{J}_r^T \underline{J}_r$ is regular it follows

$$\underline{b}_i = (\underline{J}_r^T \underline{J}_r)^{-1} (\underline{J}_r \underline{g}_i - \lambda_i \underline{n}_c) \quad (i=1\dots N) \quad (E.31)$$

With relation (E.30) λ_i can be determined

$$\lambda_i = \frac{\underline{n}_c^T (\underline{J}_r^T \underline{J}_r)^{-1} \underline{g}_i}{\underline{n}_c^T (\underline{J}_r^T \underline{J}_r)^{-1} \underline{n}_c} \quad (i=1\dots N) \quad (E.32)$$

Relation (E.32) results in the Lagrange multiplier λ_i , which subsequently can be substituted in relation (E.31) to determine the column matrix \underline{b}_i (and thus the modal displacements \underline{g}_i).

References

- Ahmed, A.M. and Burke, D.L. (1983):
In vitro measurement of static pressure distribution in synovial joints - part I : tibial surface of the knee,
J. Biomech. Engng., 105, pp. 216-225.
- Ahmed, N. and Natarajan, T. (1983):
Discrete-time signals and systems,
Reston Publishing Company, Inc., Reston, Virginia (U.S.A.)
- Andrews, J.G. (1984):
On the specification of joint configurations and motions,
J. Biomech., 17, pp. 155 -158.
- Andriachi, T.P., Mikosz, R.P., Hampton, S.J. and Galante, O.J. (1983):
Model studies on the stiffness characteristics of the human knee joint,
J. Biomech., 16, pp. 23-29.
- Angeles, J. (1987):
Computation of rigid-body angular acceleration from point-acceleration measurements,
J. Biomech. Engng., 109, pp. 124-127.
- Antonsson, E.V. and Mann, R.W. (1985):
The frequency content of gait,
J. Biomech., 18, pp. 39-47.
- Armstrong, C.G. and Mow, V.C. (1980):
Friction, lubrication and wear of synovial joints.
In: Scientific foundations of orthopaedics and traumatology. Ed.: Owen, R., Goodfellow, J. and Bullough, P.. William Heinemann Medical Books Limited, London, pp. 223-232.
- Bendat, J. and Piersol A. (1980):
Engineering applications of correlation and spectral analysis,
John Wiley & Sons Inc.
- Brand, R.A. (1986):
Knee ligaments: a new view,
J. Biomech. Engng., 108, pp. 106-110.
- Brantigan, O.C. and Voshell, A.F. (1941):
The mechanics of the ligaments and the menisci of the knee joint,
J. Bone Jnt. Surg., 23, pp. 44-66.

Bullough, P.G., Munera, L., Murphy, J. and Weinstein, A.M. (1970):
The strength of the menisci of the knee as it relates to their fine structure,

J. Bone Jnt. Surg., 52-B, pp. 564-570.

Burstein, A.H., Shaffer, B.W. and Frankel, V.H. (1970):

Elastic analysis of condylar structures,

ASME publication 70-WA/BHF-1.

Butler, D.L., Noyes, F.R. and Grood, E.S. (1980):

Ligamentous restraints to anterior-posterior drawer in the human knee,

J. Bone Jnt. Surg., 62-A, pp. 259-270.

Chu, M.L., Yazdanu, S. Gradusar, I.A. and Askew, M.J. (1986):

An in vitro simulation of impulsive force transmission along the lower skeletal extremity,

J. Biomech., 19, pp. 979-987.

Cornelissen, P., Cornelissen, M. and Perre, G. van de (1986):

Assessment of tibial stiffness by vibration testing in situ - II.

Influence of soft tissues, joints and fibula.

J. Biomech., 19, pp. 551-561.

Crowninshield, R., Pope, M.H. and Johnson, R.J. (1976a):

An analytical model of the knee,

J. Biomech., 9, pp. 397-405.

Crowninshield, R., Pope, M.H., Johnson, M.R. and Miller, R.H. (1976b):

The impedance of the human knee,

J. Biomech., 9, pp. 529-535.

Dahhan, P., Delepine, G. and Larde D. (1981):

The femoropatellar joint,

Anat. Clin. 3, pp. 23-39.

Dickinson, J.A., Cook, S.D. and Leinhardt, T.M. (1985):

The measurement of shock waves following heel strike when running,

J. Biomech., 18, pp. 415-422.

Dortmans, L.J.M.G. (1983):

A model for the determination of positions of equilibrium of two rigid bodies which are coupled by means of passive elements and points of contact,

Report WFW 86.035, Eindhoven University of Technology, Eindhoven, The Netherlands.

Dortmans, L.J.M.G. and Kraker, A. de: (1987)
Numerieke analyse van een lineair systeem met discrete tijdreeksen
(Dutch),
Eindhoven University of Technology research reports/Department of
Mechanical Engineering, 86-WFW-029,
Eindhoven University of Technology, Eindhoven, The Netherlands.

Dowson, D. (1967):
Modes of lubrication in human joints,
In: Lubrication and wear in living and artificial human joints, Proc.
Instn. Mech. Engrs., 181, part 3J, pp. 45-54.

Ducheyne, P., Heymans, L., Martens, W., Aernoudt, E., Meester, P. de and
Mulier, J.C. (1977):
The mechanical behaviour of intracondylar cancellous bone at the
femur at different loading rates,
J. Biomech., 10, pp. 747-762.

Dijk, R. van, Huiskes, R. and Selvik, G. (1979):
Roentgenstereofotogrammetric methods for the evaluation of the
three-dimensional kinematic behaviour and cruciate ligament length
patterns of the human knee joint,
J. Biomech., 12, pp. 727-731.

Eijden, T.M.G.J. van (1985):
The mechanical behaviour of the patellofemoral joint,
Thesis University of Amsterdam, Amsterdam, The Netherlands.

Fukubayashi, T. and Kurosawa H. (1980):
The contact area and pressure distribution pattern at the knee,
Act. Orthop. Scan., 51, pp. 871-879.

Girgis, F.G., Marshall, J.L. and Monajem, A. Al (1975):
The cruciate ligaments of the knee joint,
Clin. Orthop., 106, pp. 216-231.

Günther, R. (1968):
Über Stosserschütterungen beim Gang des Menschen,
Int. Z. angew. Physiol., 25, pp. 130-141.

Hamer, A. (1982):
Het kniebelastingsapparaat (Dutch),
Report Eindhoven University of Technology, Faculty of Mechanical
Engineering, Eindhoven, The Netherlands.

Hayes, W.C., Swensson, L.W. and Schurman, D.J. (1978):
Axisymmetric finite element analysis of the lateral tibial plateau,
J. Biomech., 11, pp. 21-33.

Heck, J.G.A.M. van (1984):

On the dynamic characteristics of slideways,
Thesis Eindhoven University of Technology, Eindhoven, The
Netherlands.

Hsieh, H.-H. and Walker, P.S. (1976):

Stabilizing mechanisms of the loaded and unloaded knee joint,
J. Bone Jnt. Surg., 58-A, pp. 87-93.

Huiskes, R., Blankevoort, L., Dijk, R. van, Lange, A. de and Rens, Th.J.
de (1984):

Ligament deformation patterns in passive knee joint motions,
Proc. ASME. Winter annual meeting, Bioengineering symposium.

Jaspers, P. (1982):

De mechanische functie van de meniscus in het kniegewricht (Dutch),
Thesis University of Nijmegen, Nijmegen, The Netherlands.

Johnson, F., Scarrow, P. and Waugh, W. (1981):

Assessments of loads in the knee joint,
Med. & Biol. Eng. & Comput., 19, pp. 237-243.

Kampen, A. van (1987):

The three-dimensional tracking pattern of the patella,
Thesis University of Nijmegen, Nijmegen, The Netherlands.

Kennedy, J.C., Hawkins, R.J., Willis, R.B. and Danylchuk, K.D. (1976):

Tension studies of human knee ligaments,
J. Bone Jnt. Surg., 58-A, pp. 350-355.

Kettelkamp, D.B. and Jacobs, A.W. (1972):

Tibiofemoral contact area - determination and implications,
J. Bone Jnt. Surg., 54-A, pp. 349-356.

Krause, W.R., Pope, M.H., Johnsson, R.J. and Wilder, D.G. (1976):

Mechanical changes in the knee after meniscectomy,
J. Bone Jnt. Surg., 58-A, pp. 599-604.

Krstic, R.V. (1978):

Die Gewebe des Menschen und der Säugetiere,
Springer Verlag, Berlin (F.R.G.).

Lakes, R.S., Katz, J.L. and Sternstein, S.S. (1979):

Visco-elastic properties of wet cortical bone,
J. Biomech., 12, pp. 657-698.

Lewis, J.L. Lew, W.D. and Schmidt, J. (1982):

A note on the application and evaluation of the buckle transducer for
knee ligament force measurement,
J. Biomech. Engng., 104, pp. 125-128.

Mak,A.F. (1986):

The apparent viscoelastic behavior of articular cartilage-The contributions from intrinsic matrix viscoelasticity and interstitial fluid flows,

J. Biomech. Engng., 108, pp. 123-130.

Markolf,K.L., Mensch,J.S. and Amstutz,H.C. (1976):

Stiffness and laxity of the knee - the contributions of the supporting structures,

J. Bone Jnt. Surg., 58-A, pp. 583-593.

Markolf,K.L., Graff,A. and Amstutz,H.C. (1978):

In vivo knee stability,

J. Bone Jnt. Surg., 60-A, pp. 664-674.

Markolf,K.L., Barger,W.L. Shoemaker,S.C. and Amstutz,H.C. (1981):

The role of joint load in knee stability,

J. Bone Jnt. Surg., 63-A, pp. 570-585.

McCutchen,C.W. (1967):

Physiological lubrication,

In: Lubrication and wear of living and artificial human joints,

Proc. Instn. Mech. Engrs., 181, part 3J, pp. 55-62.

Mergeay,M. (1980):

Theoretical background of curve-fitting methods used by modal analysis,

Seminar on modal analysis, University of Leuven (Belgium).

Moehnzadeh,M.H., Engin,A.E. and Akkas,N. (1983):

Two-dimensional dynamic modelling of human knee joint,

J. Biomech., 16, pp. 253-264.

Moffatt,C.A., Harris,E.H. and Haslam,E.T. (1969):

An experimental and analytic study of the dynamic properties of the leg,

J. Biomech., 2, pp. 373-387.

Morrison,J.B. (1968):

Bio-engineering analysis of force actions transmitted by the knee joint,

Biomed. Engng., 3, pp. 164-170.

Mow,V.C., Holmes,M.H. and Lai,W.M. (1984):

Fluid transport and mechanical properties of articular cartilage: a review,

J. Biomech., 17, pp. 377-394.

Natke, H.G. (1983):

Einführung in Theorie und Praxis der Zeitreihen- und Modalanalyse:
 Identification schwingungsfähiger elastomechanischer Systeme,
 Vieweg, Braunschweig (F.R.G.).

Nokes, L., Fairclough, J.A., Mintow, J.A., Mackie, I. and Williams, J.
 (1984):

Vibration analysis of the human tibia: the effect of soft tissue on
 the output from skin-mounted accelerometers,
 J. Biomed. Engng., 6, pp. 223-226.

Oomens, C.W.J., Campen, D.H. van, Grootenboer, H.J. (1987):

In vitro compression of a soft tissue layer on a rigid foundation
 J. Biomech., 20, pp. 923-935

Padgaonkar, A.J., Krieger, K.W., King, A.I. (1975):

Measurement of angular acceleration of a rigid body using linear
 accelerometers,
 J. Applied Mech., pp. 552-556.

Peters, G.W.M. (1987):

Tools for the measurement of stress and strain fields in soft tissue,
 Thesis University of Limburg, Maastricht, The Netherlands.

Piziali, R.L., Rastegar, J.C. and Nagel, D.A. (1977):

Measurement of the nonlinear, coupled stiffness characteristics of
 the human knee,
 J. Biomech., 10, pp. 45-51.

Piziali, R.L., Seering, W.P., Nagel, D.A. and Schurman, J. (1980):

The function of the primary ligaments of the knee in anterior-
 posterior and medial-lateral motions,
 J. Biomech., 13, pp. 777-784.

Pope, M.H., Crowninshield, R., Miller, R. and Johnsson, R. (1976):

The static and dynamic behaviour of the human knee in vivo,
 J. Biomech., 9, pp. 449-452.

Pugh, J.W., Rose, R.M. and Radin, E.L. (1973):

Elastic and visco-elastic properties of trabecular bone: dependence
 on structure,
 J. Biomech., 6, pp. 475-485.

Radin, E.L. and Paul, I.L. (1971):

Response of joints to impact loading - I: in vitro wear,
 Arth. Reumat., 14, pp. 356-362.

Radin, E.L. and Paul, I.L. (1972):

A consolidated concept of joint lubrication,
 J. Bone Jnt. Surg., 54-A, pp. 607-616.

- Reilly,D.T. and Burstein,A.H. (1975):
The elastic and ultimate properties of compact bone tissue,
J. Biomech., 8, pp. 393-405.
- Renterghem,R.J. van (1983):
Aortic valve geometry during the cardiac cycle,
Thesis University of Limburg, Maastricht, The Netherlands.
- Roddeман,D.G. (1988):
Force transmission in wrinkling membranes,
Thesis Eindhoven University of Technology, Eindhoven, The Netherlands
(to be published january 1988).
- Rousseau,E.P.M. (1985):
Mechanical specifications for a closed leaflet valve prosthesis,
Thesis Eindhoven University of Technology, Eindhoven, The
Netherlands.
- Sauren,A.A.H.J. (1981):
The mechanical behaviour of the aortic valve,
Thesis Eindhoven University of Technology, Eindhoven, The
Netherlands.
- Sauren,A.A.H.J., Huson,A. and Schouten,R.Y. (1984):
An axisymmetric finite element analysis of the mechanical function of
the meniscus,
Int. J. Sports Med., 5, pp. 93-95.
- Schultz,R.A., Miller,D.C., Kerr,C.S. and Micheli,L. (1984):
Mechanoreceptors in human cruciate ligaments,
J. Bone. Jnt. Surg., 66-A, pp. 1072-1076.
- Seering,W.P., Piziali,R.L., Nagel,D.A. and Schurman,D.J. (1980):
The function of the primary ligaments of the knee in varus-valgus and
axial rotation,
J. Biomech, 13, pp. 785-794.
- Seireg,A. and Arvikar,R.J. (1975):
The prediction of muscular load sharing and joint forces in the lower
extremities during walking,
J. Biomech., 8, pp. 89-102.
- Shoemaker,S.G. and Markolf,K.L. (1985):
Effects of joint load on the stiffness and laxity of ligament-
deficient knees,
J. Bone Jnt. Surg., 67-A, pp. 136-146.

Simon, S.R., Radin, E.L., Paul, I.L. and Rose, M.R. (1972):
The response of joints to impact loading - II: in vivo behaviour of
subchondral bone,
J. Biomech., 5, pp. 267-272.

Sokoloff, L. (1978):
The joints and synovial fluid,
Vol. II. Ed.: L. Sokoloff,
Academic Press.

Sol, E.J. (1983):
Kinematics and dynamics of multibody systems,
Thesis Eindhoven University of Technology, Eindhoven, The
Netherlands.

Spoor, C.W. and Veldpaus, F.E. (1980):
Rigid body motion calculated from spatial coordinates of markers,
J. Biomech., 13, pp. 391-393.

Steenhoven, A.A. van (1979):
The closing behaviour of the aortic valve,
Thesis Eindhoven University of Technology, Eindhoven, The
Netherlands.

Trent, P.S., Walker, P.S. and Wolf, B. (1976):
Ligament length patterns, strength and rotational axes of the knee
joint,
Clin. Orthop., 117, pp. 263-270.

Uezaki, N., Kobayashi, A. and Matsushige, K. (1979):
The visco-elastic properties of the human semilunar cartilage,
J. Biomech., 12, pp. 65-73.

Voloshin, A. and Wosk, J. (1983):
Shock absorption in meniscectomized and painful knees: a comparative
in vivo study,
J. Biomech. Engng., 5, pp. 157-161.

Walker, P.S., Dowson, D., Longfield, M.D. and Wright, V. (1968):
"Boosted lubrication" in synovial joints by fluid entrapment and
enrichment,
Ann. Rheum. Dis., 27, pp. 512-520.

Walker, P.S. and Hajek, J.V. (1972):
The load-bearing area in the knee joint,
J. Biomech., 5, pp. 581-589.

Wang, C. and Walker, P.S. (1974):
Rotatory laxity of the human knee joint,
J. Bone Jnt. Surg., 56-A, pp. 161-170.

Wisnans, J., Veldpaus, F., Janssen, J., Huson, A., and Struben, P. (1980):

A three-dimensional mathematical model of the human knee joint, J. Biomech., 13, pp. 677-685.

Wittenburg, J. (1977):

Dynamics of systems of rigid bodies, B.G. Teubner, Stuttgart (F.R.G.)

Woltring, H.J., Huiskes, R., Lange, A. de and Veldpaus, F.E. (1985):

Finite centroid and helical axis estimation from noisy landmark measurements in the study of human joint kinematics, J. Biomech., 18, pp. 379-389.

Wongchaisuwat, C., Hemami, H. and Buchner, H.J. (1984):

Control of sliding and rolling at natural joints, J. Biomech. Engng., 106, pp. 368-375.

Woo, S.L.-Y. (1982):

Mechanical properties of tendons and ligaments, Biorheology, 19, pp. 385-396.

Wosk, J. and Voloshin, A. (1981):

Wave attenuation in skeletons of young healthy persons, J. Biomech., 14, pp. 261-267.

Wright, V. (1981):

The structure, friction and wear of natural joints. In: Tribology of natural and artificial joints. Ed.: Dumbleton J.H., Tribology series, 3, Elsevier Scientific Publishing Company, Amsterdam, pp. 23-46.

Ziegert, J.C. and Lewis, J.L. (1979):

The effect of soft tissue on measurements of vibrational bone motion by skin-mounted accelerometers, J. Biomech. Engng., 101, pp. 218-220.

SAMENVATTING

Het in dit proefschrift beschreven onderzoek heeft tot doel het inzicht te vergroten in het dynamisch gedrag van het menselijk kniegewricht. De nadruk ligt hierbij op ontwikkeling en toepassing van een experimentele methode ter bepaling van de relevante karakteristieken en parameters voor de beschrijving van het gedrag van het gewricht onder dynamische belasting in post-mortem experimenten. Een samenvatting van beschikbare literatuur leert dat zowel via experimenten als theoretische modellen het gedrag van het gewricht onder (quasi-)statische en dynamische belastingen geanalyseerd is. Desondanks is er een gebrek aan kennis op 3 belangrijke punten: feitelijk inzicht in het dynamisch gedrag van het gewricht ontbreekt, het constitutief gedrag van weke delen in het gewricht is slechts in beperkte mate bekend en evenzo is weinig informatie beschikbaar over de belastingen die in vivo op het gewricht als geheel of de gewrichtselementen afzonderlijk uitgeoefend worden. Omdat een analyse van het gedrag van het gewricht door middel van in vivo of post-mortem experimenten slechts beperkte mogelijkheden biedt, is een mathematisch model van het gewricht onontbeerlijk. De ontwikkeling van zo'n model moet gebaseerd zijn op enige basiskennis omtrent het gedrag van het gewricht. Om deze reden wordt een experimentele methode besproken die moet leiden tot richtlijnen voor het ontwikkelen van een theoretisch model. Gezien het verwachte niet-lineaire gedrag van het gewricht, is een methode gekozen waarbij geometrische niet-lineariteiten geen rol van betekenis spelen. Het gedrag van het gewricht wordt hierbij geanalyseerd voor kleine trillingen rond een statische evenwichtsstand. Hierbij wordt er vanuit gegaan dat deze linearisatie-procedure ook leidt tot linearisatie van de fysische niet-lineariteiten. De linearisatie-procedure leidt tot een beschrijving van het gewricht door een lineair systeem met systeemparameters die afhangen van een gekozen statische evenwichtsstand, de grootte van de krachten die uitgeoefend worden op spierpezen om deze statische evenwichtsstand te creëren en de mate waarin gewrichtselementen beschadigd zijn. Op basis van experimenten met random excitatie konden enige belangrijke conclusies getrokken worden: het creëren van een stabiele, statische evenwichtsstand van het gewricht door het uitoefenen van krachten op een drietal spierpezen is mogelijk, terwijl beschrijving van het dynamisch gedrag van het gewricht met behulp van transfer-functies de mogelijkheid geeft om de invloed van de statische evenwichtsstand, de grootte van de krachten op de spierpezen en het beschadigen van gewrichtselementen vast te leggen. De linearisatie-procedure blijkt strikt genomen niet toepasbaar te zijn vanwege het essentiële niet-lineaire gedrag van het gewricht. Deze niet-lineariteit kan echter in rekening gebracht worden door de systeemparameters voor het best-passende lineaire systeem afhankelijk te maken van de grootte van de aangebrachte belasting. Deze methode is toegepast voor stapvormige excitatie. Het effect van het beschadigen van de menisci en de voorste kruisband kan goed worden vastgelegd. Interpretatie van de resultaten wordt vooreerst bemoeilijkt door het ontbreken van een adequaat numeriek model van het gewricht.

Curriculum vitae

29 april 1959 Geboren te Eindhoven

1971-1977 VWO (Lyceum Augustinianum) te Eindhoven

1977-1983 Technische Universiteit Eindhoven,
Faculteit Werktuigbouwkunde

1983-1987 Wetenschappelijk assistent aan de Technische
Universiteit Eindhoven, Faculteit Werktuigbouwkunde

21-10-1987 In dienst getreden van de Technisch Fysische
Dienst TNO-TH in het kader van het IOP Technische
Keramik.

Op deze plaats een hartelijk woord van dank aan eenieder die met raad en daad steun gegeven heeft bij het in dit proefschrift beschreven onderzoek.

Stellingen

- 1 Lineaire modellen voor het beschrijven van het dynamisch gedrag van het menselijk kniegewricht zijn een foutieve simplificatie van de werkelijkheid.
 - Dit proefschrift, hoofdstukken 4 en 5.
- 2 De door Mergeay voorgestelde methode voor het bepalen van modale parameters uit gemeten impulsresponsies houdt geen rekening met de afhankelijkheid van de residuematrices en kan daarom leiden tot foutieve resultaten.
 - Mergeay, M. (1980):
Theoretical background of curve-fitting methods used by modal analysis, Seminar on modal analysis, Universiteit van Leuven (Belgie).
 - Dit proefschrift:
hoofdstukken 4 en 5.
- 3 Het ontwikkelen van gereedschap om op systematische wijze de aard van geconstateerde niet-lineariteiten in mechanische systemen te bepalen is van belang bij verder onderzoek naar het dynamisch gedrag van het kniegewricht en van werktuigkundige verbindingen.
 - Heck, J.G.A.M. van (1984):
On the dynamic characteristics of slideways, Dissertatie Technische Universiteit Eindhoven.
 - Dit proefschrift:
hoofdstukken 4 en 5.
- 4 Bij de toepassing van geavanceerde computertechnologie is de letterlijke betekenis van "Schnittstelle" helaas vaak beter dan die van "interface".
 - Handbuch Klein-computer und Mikroprozessoren in der Mess- und Versuchstechnik, VDI/VDE-Gesellschaft Mess- und Regelungstechnik, VDI-Bildungswerk, Dusseldorf (BRD).
- 5 Autolyse is een onvermijdelijk probleem bij post-mortem onderzoek naar het mechanisch gedrag van het kniegewricht. De ontwikkeling van een algemeen aanvaard (fysisch) model van het kniegewricht moet daarom meer aandacht krijgen.
- 6 Gezien de beschikbare middelen is concentratie van het onderzoek op het gebied van de toepassing van technische keramiek in Nederland essentieel.
 - With, G. de (1986):
"Een nieuw stenen tijdperk?", Intreerede Technische Universiteit Eindhoven.

- 7 In het basis-curriculum voor werktuigkundig ingenieur moet veel meer aandacht besteed worden aan het mechanisch gedrag van niet-metallische materialen.
- Nota materialenbeleid van de Ministeries van Onderwijs en Wetenschappen en Economische Zaken. Werkgroep Materialennota (1986).
- 8 Als het niet lukt om het ontwerpen met "nieuwe materialen" systematisch te ontwikkelen (inclusief de bepaling van relevante eigenschappen en de ontwikkeling van het noodzakelijke analyse-gereedschap) zal in 1998 geconstateerd worden dat de "nieuwe materialen" de verwachtingen van 1988 in het geheel niet waargemaakt hebben.
- "Wissel tussen kennis en markt", Rapport van de adviescommissie voor de uitbouw van het technologiebeleid, 's Gravenhage 1987.
 - PT|Werktuigbouw 42 (1987), no. 2.
- 9 De werktuigkunde en de werktuigbouwkunde kunnen heel veel leren van de wijze van functioneren van het spier-skeletstelsel. Daarom zou functionele anatomie een basisvak voor de opleiding tot werktuigkundig ingenieur kunnen zijn.
- 10 Beter een gezond gebrek aan organisatie dan een gebrek aan gezonde organisatie.
- Deelder, J. (1987): "Boulevarddeel".